DUAL-FUNCTIONALIZED LIPOSOMES FOR GENE DELIVERY TO BRAIN TO PREVENT AND TREAT ALZHEIMER'S DISEASE

A Dissertation
Submitted to the Graduate Faculty
of the
North Dakota State University
of Agriculture and Applied Science

By

Bruna dos Santos Rodrigues

In Partial Fulfillment of the Requirements
for the Degree of
DOCTOR OF PHILOSOPHY

Major Department:
Pharmaceutical Sciences

July 2019

Fargo, North Dakota

North Dakota State University
Graduate School

Title

DUAL-FUCNTIONALIZED LIPOSOMES FOR GENE DELIVERY TO BRAIN TO PREVENT AND TREAT ALZHEIMER'S DISEASE

By

Bruna dos Santos Rodrigues

The Supervisory Committee certifies that this ***disquisition*** complies with North Dakota State University's regulations and meets the accepted standards for the degree of

DOCTOR OF PHILOSOPHY

SUPERVISORY COMMITTEE:

Dr. Jagdish Singh
Chair

Dr. Chengwen Sun

Dr. Sathish Venkatachalem

Dr. Megan Orr

Dr. John Ballantyne

Approved:

7/30/2019
Date

Dr. Jagdish Singh
Department Chair

ABSTRACT

Alzheimer's disease (AD) is the most common age-related neurodegenerative disorder which lacks effective disease-modifying therapies. We have investigated the therapeutic potential of pDNA encoding apolipoprotein E2 (ApoE2), or nerve growth factor (NGF) by transporting pDNA across the blood brain barrier (BBB) and expressing the ApoE2 or NGF into brain, using brain-targeted liposomal nanoparticles for treatment of AD. We explored the neuroprotective functions of ApoE2 and survival-promoting properties of NGF through gene therapy as potential disease-modifying therapies for AD. We designed brain-targeted gene delivery systems with prolonged systemic circulation and enhanced cellular penetration by conjugating transferrin (Tf) ligand and cell-penetrating peptide (CPP) to liposome *via* DSPE-PEG phospholipid. *In vitro* characterization studies showed that the nanoparticles had homogeneous particle size, positive zeta potential and protected plasmid DNA against enzymatic degradation. Additionally, they exhibited low hemolytic potential and low cytotoxicity. Cellular uptake occurred in a time-dependent manner through multiple endocytosis pathways. Reporter gene transfection and consequent protein expression in different cell lines were significantly higher using CPP-Tf-liposomes compared to single modified liposomes. The ability of these liposomes to escape from endosomes can be an important factor which may have likely contributed to the high transfection efficiency observed. *In vivo* brain targeting efficiency of designed liposomes was evaluated using *in vitro* triple co-culture BBB model. Dual-modified liposomes efficiently crossed *in vitro* BBB and, subsequently, transfected primary neuronal cells. Increasing NGF expression in primary neuronal cells following treatment with liposomes increased the levels of pre-synaptic marker synaptophysin *in vitro*. PenTf-liposomes containing pDNA efficiently induced protein expression in the brain of mice. A dose response study was performed in order to select the appropriate dose of pNGF to induce

significant NGF expression and, consequently, a therapeutic effect. Administration of PenTf-liposomes containing pNGF to APP/PS1 mice (aged 3 months) for four weeks (one injection per week) decreased the levels of toxic soluble and insoluble Aβ peptides. Additionally, the treatment stimulated cell proliferation and increased the levels of synaptic markers, synaptophysin and PSD-95. These data suggest the therapeutic potential of PenTf-liposome-mediated NGF gene therapy which can be considered as a candidate for treatment of AD.

ACKNOWLEDGEMENTS

I would like to express my sincere gratitude towards my advisor Dr. Jagdish Singh for providing me the opportunity to be part of his research group. His constant support and guidance throughout my graduate studies helped me in my professional development.

I would like to extend my genuine thanks to my graduate advisory committee members, Dr. Megan Orr, Dr. Chengwen Sun, Dr. Sathish Venkatachalem and Dr. John Ballantynes for their valuable suggestions, guidance and motivation.

I would like to thank Dr. Hiroshi Oue and Dr. Takahisa Kanekiyo from Mayo Clinic for important contribution to this study. I would like to thank Dr. Amrita Banerjee for her guidance and help. I would also like to extend sincere thanks to Dr. Sushant Lakkadwala, Dr Lindsey Lipp, Divya Sharma. Sanjay Arora, Riddhi Trivedi, Richard Ni Lamptey and Bivek Chaulagain for being excellent lab mates. I would like to acknowledge Janet Krom, Diana Kowalski and Tiffany Olson for their help and assistance throughout my graduate studies. I would like to acknowledge also all the faculty, students and staff of Department of Pharmaceutical Sciences for helping me directly or indirectly during my research.

I gratefully acknowledge the financial support from National Council for Scientific and Technological Development (CNPq, Brazil), and the National Institute of Health (NIH).

I would like to thank my parents, family and friends for their support, patience and understanding during my entire graduate studies.

DEDICATION

Dedicated to my parents,

Paulo Afonso and Cilene,

For all love, support,

Upbringing and dedication,

For everything that I am.

TABLE OF CONTENTS

LIST OF TABLES

LIST OF FIGURES

1. INTRODUCTION

Alzheimer's disease (AD) has emerged as the most common form of dementia in late-life. This disease currently affects more than 5.7 million Americans of all ages. This number is predicted to increase to 13.8 million by 2050. The total cost in 2018 of AD or other dementias in the United States was estimated at $277 billion [1,2], which constitutes a growing public health threat overwhelming the health care system [3]. AD is an age-dependent neurological disorder characterized by a global and progressive disruption of neuronal communications involving multiple transmitter systems. The major features of AD pathogenesis is the presence of extracellular amyloid plaques composed of amyloid-β (Aβ) and intracellular neurofibrillary tangles [4,5]. Mounting evidence supports a role of Aβ aggregation and accumulation as early trigger of a toxic cascade leading to synaptic dysfunction, neurodegeneration and cognitive impairment in the etiology of AD [6,7].

Multiple genetic and environmental risk factors are involved in late onset AD pathogenesis. Impairment of Aβ clearance is probably a major contributor to disease development, while the ε4 allele of APOE gene is the strongest genetic risk factor amongst its three polymorphic alleles (ε2, ε3 and ε4), whereas the ε2 allele had demonstrate to have protective effects [8–10]. Many lines of evidence have shown that the risk factors of AD (aging and APOE ε4) accelerate accumulation of Aβ prior to the development of the disease. The apolipoprotein E (ApoE), in the central nervous system (CNS), transports cholesterol from astrocytes to neurons through cell surface receptors, including the low density lipoprotein receptor (LDLR) and LDLR-related protein 1 (LRP1) [11,12]. Consequently, ApoE contributes to synaptic plasticity and neuronal function by controlling cholesterol homeostasis with ApoE3 and ApoE2 alleles having superior function than ApoE4 [13].

Although most of research has been focused on the development of therapies to delay or halt the progression of AD, currently there is no approved disease-modifying therapies [14]. A combination of factors lead to high rate of negative clinical trials in AD drug development such as complexity of AD etiopathology, lack of biomarkers and surrogate markers to predict clinical outcomes and accelerate the drug development, and even challenges in the recruitment of participants, for example [14–16]. The greatest need in the development of AD treatment continues for disease-modifying therapies that will delay or slow the clinical course of the disease by intervening in the processes leading to cell death.

Therapies with neurotrophins have shown intervention in AD pathology with improvement in memory as well as behavioral function in AD animal models [17–20]. Since the discovery of nerve growth factor (NGF) in 1951 [21], it has demonstrated particular importance for treatment of AD by reversing atrophy, preventing degeneration and stimulating the function of basal forebrain cholinergic neurons [22–24]. The growth and survival-promoting properties of NGF have been observed in the ability to prevent the death and stimulate forebrain cholinergic neurons that undergo early and prominent degeneration in AD. It is important to note that NGF levels in the basal forebrain region decline in patients with AD. Although NGF therapy seems promising, the peripheral administration of this neurotrophin in a safe manner is limited by enzymatic degradation and, its inability to cross blood brain barrier (BBB) [25,26]. Moreover, the intolerable side effects of NGF from its broad distribution prevents it from clinical use [27]. For clinical application, sufficient amount of NGF must be delivered to target degenerative neurons for not only to avoid adverse effects of unspecific distribution, but also to generate effective stimulation. Gene therapy is an alternative means of introducing NGF into the CNS in a localized and targeted-manner [17,28].

Another potential therapeutic approach in the development of disease-modifying therapies for AD considers the neuroprotective functions of APOE ε2 allele. It has been suggested that ApoE2 isoform may differentially regulate Aβ in the brain, which could be attributed to its distinguished features such as higher conformational stability, lower binding affinity to LDLRs, and greater affinity to bind to Aβ as compared to E3 and E4 isoforms [13,29,30]. Therefore, expression of ApoE2 isoform through gene therapy may help in establishing ApoE-based targeted therapy for AD prevention and treatment. However, the progression of gene therapy largely depends on the development of safe and effective vectors to improve membrane permeability and half-life of therapeutic genes [31,32]. To this end, the vector should overcome extracellular and intracellular barriers, ensuring that DNA is delivered to the nucleus, where it can be transcribed and translated into a therapeutic protein [33]. Several researchers have focused on the development of effective non-invasive delivery systems with targeting properties that are able to reach brain parenchyma at therapeutic doses [34–38]. Non-viral vectors, such as liposomes, have attracted much attention due to their favorable characteristics over viral vectors such as safety, ease of preparation, low immunogenicity, low cost and ability to deliver a wide range of plasmid sizes [33,39]. These nanoparticles have also shown to protect plasmid DNA (pDNA) from DNase degradation, ability to pass through BBB *via* transcytosis and internalize into brain cells using various endocytotic pathways [40,41].

Some transport mechanisms are present on BBB that enable nanoparticles transport into brain, amongst which receptor-mediated transcytosis is most commonly used in many platforms for brain delivery [42]. The high endocytotic potential of Transferrin receptor (TfR) makes it an interesting choice for targeted delivery to the brain [43,44]. TfR are expressed in different types of tissues in the body [45] and the brain possesses high densities of TfR localized in the brain

endothelium and neurons [46,47]. Liposome surface modification with 80 kDa Tf protein have been used as targeting ligand for BBB, leading to their sequential uptake and presentation of therapeutic molecule to the neurons [48]. Receptor-mediated transcytosis is normally a saturable process and dual targeting has become a strategy to overcome receptor saturation and provide efficient carrier delivery [49,50]. For this purpose, protein-transduction domains, also known as cell-penetrating peptides (CPP) that are small sequences of peptides ranging from 5-30 amino acids long, have demonstrated ability to transport cargo into cells in a non-invasive manner. These peptides have been widely used in the delivery of a variety of molecules across the cell membrane [51,52]. Different studies have reported successful delivery of therapeutic molecules into the brain using receptor-targeted liposomes conjugated to CPP [53,54]. This dual targeting design of liposomes is intended to achieve a high degree of internalization and accumulation in the target site for therapeutic function.

1.1. Targeting ligands for gene delivery to brain

A significant number of treatment opportunities for CNS diseases have failed due to the restrictive permeability of BBB. This leads to reduced uptake of therapeutics and subsequent inability to undergo transport into brain parenchyma. Many brain carriers take advantage of endogenous transport systems on BBB to enable their access to brain [55–57]. Receptor-mediated transcytosis (RMT) has been explored through conjugation of carrier to specific ligand for targeting RMT systems such as TfR, LDLR, or insulin receptors. Carrier-mediated transcytosis (CMT) has increasingly been recognized as important entry route to brain and this includes glucose transporters at the BBB [58,59].

1.1.1. Transferrin receptors

Transferrin receptor (TfR), a 90 kDa transmembrane glycoprotein homodimer, has been actively explored as a potential transport system to deliver therapeutic molecules into the brain. It is constituted of two identical monomers linked by two disulfide bonds at Cys89 and Cys98 [60]. Each subunit has three domains: a large extracellular C-terminus (globular extracellular portion), a hydrophobic intramembranous (α-helix) part and short intracellular N-terminus (61 residues) [61]. The C-terminus contains the binding site for transferrin. It comprises one O-linked site and three N-linked glycosylation site, which are important for folding and protein function [61–63].TfR is expressed in most active cell types and serves as the main port of entry for iron bound to Tf into cells [43,45]. The expression is regulated by changes in intracellular iron concentrations, following the iron responsive elements/iron regulatory proteins (IRE/IRP) system [64–66].

Tf glycoprotein is a homologous group of nonheme iron-binding proteins of approximately 80 kDa which plays a central role in iron metabolism. Tf is found in the human plasma at concentration range of 170-370 mg/dl and binds up to two atoms of elemental iron in the form of ferric iron (Fe^{3+}) [65,67,68]. Each monomer of TfR may bind to a molecule of Tf, allowing up to four iron atoms to be transported into a cell by one Tf-TfR complex. TfR cycle into acid endosomes into cells in a clathrin/dynamin dependent manner. Iron is delivered into cells and TfR is recycled back to cell surface [69,70].

The most common strategies for delivery of therapeutics to the brain through targeting TfR have focused on the natural ligand Tf or monoclonal antibodies or their fragments [48]. Studies with liposomal drug delivery systems targeting TfR have demonstrated larger uptake into brain capillary endothelial as compared to attempts focused on receptors such as the low-density lipoprotein receptor (LDLR), LDLR-related protein, glucose transporter 1, or insulin-like growth

factor receptor [71–73]. Recently, dual-functional systems which combine Tf-targeting with an additional active moiety have been designed as a new approach for effective targeted liposomal gene therapy to the brain [74]. Investigation of Tf-targeting delivery of immunoliposomes and their encapsulated cargo to the brain *via* TfR has shown that full transcytosis of nanomedicine seems unlikely [75]. The nanoparticles showed to accumulate in the brain capillary endothelial cells and increase the transport of encapsulated cargo into the brain. Although other studies using Tf-conjugated nanoparticles have not addressed this parameter, their findings strongly suggest that this is a relevant strategy for delivery of therapeutics to the brain [75–78].

1.1.2. Low density lipoprotein receptors

Various members of low-density lipoprotein receptor (LDLR) family, including LDLR, LRP1 and LRP2, have been implicated in mediating apoE-independent or apoE-dependent clearance across the BBB. They are single transmembrane glycoprotein expressed in brain capillary endothelial cells and regulates brain to blood cholesterol levels through RMT [79–81]. Delivery of therapeutic molecules to the brain *via* low LDLR family have demonstrated significant potential due to the potentially higher transcytosis of these receptors compared to other RMT systems such as TfR. Although monoclonal antibodies have not been successfully engineered against LDLR family, there are ligands with demonstrated ability to target these receptors and facilitate RMT [56]. The ability of nonionic surfactant PS 80 to mediate BBB transport has been suggested by studies conducted with PS 80-coupled nanoparticles. The nanoparticles could adsorb apolipoproteins such as ApoE which in turn interacted to LDLR expressed in BBB and triggered RMT [82].

Angiopep-2 is a LRP1 ligand which was discovered through screening designed peptides based on a conserved LDLR family-biding domain. When conjugated on the surface of

nanoparticles, Angiopep-2 facilitated carrier transport through LRP1 and displayed higher transcytosis capacity *in vitro* and *in vivo* compared to other ligands such as lactoferrin, transferrin and avidin [83,84]. LDLR family are ubiquitously expressed in the body, therefore unspecific distribution of the systems targeting LDLR needs to be addressed to improve the applications of BBB targeting through LDLR.

1.1.3. Insulin receptor

The insulin receptor, a receptor tyrosine kinase, is a disulfide-linked heterotetrametric glycoprotein consisting of two α-subunits and two β-subunits which mediates metabolic regulation [85]. The insulin binding sites present on brain endothelial cells can transport insulin across BBB and activate insulin receptors. The transport of insulin to CNS occurs through RMT *via* the signaling-related insulin receptor [84]. This is a highly regulated saturable process and it may alter in a number of states such as diabetes, obesity, starvation, hyperglycaemia and Alzheimer's disease [86]. Monoclonal antibodies against insulin receptors have been engineered for brain delivery. Engineered chimeric monoclonal antibodies have shown promising clinical applications after tests performed on Rhesus monkeys [87]. Although the monoclonal antibodies can be designed by binding to different epitope of insulin receptor with higher affinity, there are still limitations imposed by competition between the endogenous ligands and the monoclonal antibody conjugates.

1.1.4. Glucose transporter

Glucose transporters at the BBB have been recognized as potential therapeutic targets for treatment of hypoglycemic, hyperglycemic conditions and post-ischemia treatment [88]. In addition, glucose transporters at the BBB are potential routes of entry for delivery of therapeutic molecules into the CNS. GLUT1 is a Na^+-independent glucose transporter at BBB which facilitates the transport of hexoses and it is expressed ubiquitously. GLUT3 is the major glucose transporter

in neurons. This transporter is expressed on neurons, brain capillary endothelial cells, sperm, preimplantation embryos and circulating white blood cells [88,89]. Despite GLUT1 is widely distributed in the body, this transporter has been explored as specific targeting transporter for delivery of therapeutics into the brain. Due to specific expression of GLUT3 in neuronal cells, this transporter has been recently investigated as new strategy for targeted delivery to neurons [90]. Studies with glucose-modified liposomes reported this system easily crossed BBB through glucose transporters and was considered as a potential strategy for delivery of drugs to brain [91]. These receptors need to be more studied consistently as transporters at BBB for understanding their clinical implications and further applications.

1.2. Cell-penetrating peptide

Opportunities to improve the delivery of a variety of bioactive entities into cells have arisen with the discovery of shuttling properties of specific sequences of peptides. Cell penetrating peptides (CPPs) were discovered more than 30 years ago [92,93]. Since then, several sequences have been studied and characterized, moreover, demonstrating unique properties such as endosomal escape, resist enzymatic degradation and show high affinity for specific cell type or intracellular destination. The CPP can interact electrostatically to payload or covalently conjugate to payloads or even enhance the delivery properties of other carriers such as polymers, nanoparticles or viral vectors [94,95].

Several criteria have been proposed for the classification of CPPs based on their origin, sequence, physicochemical properties, function or mechanism of uptake [96]. According to their origin, CPPs are classified as protein-derived peptides, which are from the short stretches of the protein domain that are primarily responsible for cellular internalization ability; chimeric CPP such

as Transportan derived from the binding of the neuropeptide galanin N-terminus to the Mastoparan toxin [97]; and synthetic CPP, comprising oligoarginines and numerous peptide nucleic acids (PNAs) formed by synthetic nucleic acid analogues bound to pseudopeptide backbone. Examples of protein-derived peptides include Tat peptide derived from HIV protein Tat [98], penetratin derived from homeodomain of *Drosophila* Antennapedia [99], and pVec derived from vascular endothelial-cadherin protein [100]. Based on their physicochemical properties, CPPs are classified into three major classes: cationic, amphiphilic and hydrophobic [95].

Cationic CPPs are characterized by high positive net charge at physiological pH and 3D arrangement does not form an amphipathic helix. They are primarily originated from the basic short strands of arginines and lysines [51,101]. This class is represented by Tat, penetratin and poly-arginines. Studies on Tat derivatives and polyarginines (R5-R12) have determined the structural requirements for cellular uptake of cationic CPP [102,103]. These reports proposed that the number and order of amino acids in the peptide sequence is important for translocation properties of CPP. Additionally, arginine residues contribute more to cellular internalization compared to lysine residues [103,104].

A special group of short cationic peptides called nuclear localization sequences (NLS) have attracted attention due to their ability to be transported to the nucleus through the nuclear pore complex [104]. NLS constitutes lysine-, arginine- and proline-rich motifs having one (monopartite) or two clusters (bipartite) of basic amino acids separated by a 9–12 amino acid linker [96]. Examples of NLS include TFIIE-beta (SKKKKTKV), Oct-6 (GRKRKKRT), HATF-3 (ERKKRRRE), and SDC3 (FKKFRKF) [105,106]. NFL has reduced application as CPP due to inferior delivery properties caused by low net charge (below 8). On the other hand, conjugation of

NFL to hydrophobic peptide sequence forming an amphipathic peptide has shown enhancement of cellular uptake [96].

Amphipathic CPP contain both hydrophobic and hydrophilic domains of amino acids. They are generally classified into primary, secondary and proline-rich CPPs. NFL conjugated to hydrophobic peptide sequence is part of primary amphipathic CPP [94,96]. For instance, MPG and Pep1 generated by fusing of SV40 NLS (PKKRKV) to the HIV glycoprotein 41 and the tryptophan-rich cluster, respectively, through the linker domain WSQP [107]. Other primary amphipathic CPPs are originated from natural proteins, such as pVec derived from VE-cadherin protein [100]; ARF (1-22) derived from N-terminal domain of p14ARP protein [108]; and BPrPr (1-28) derived from N-terminus of unprocessed bovine prion protein [109]. Secondary amphipathic CPPs assume α-helix conformation with hydrophilic and hydrophobic residues grouped on different sides of the helix. Examples include Transportan [97], azurin-derived 28 peptide and MAP [110]. Alternatively, secondary amphipathic CPPs can present their amino acid sequence in a β-sheet structure on interaction with a phospholipid membrane. Cellular uptake studies on VP5 showed that β-sheets were essential for internalization. The proline-rich CPP bactenecin-7 has demonstrated cell permeability and antibacterial activity which co-localized at the N-terminal 24 residues [111].

Hydrophobic CPPs contain mainly nonpolar residues, resulting in a low net charge. The affinity of hydrophobic residues of CPP to hydrophobic domain of plasma membrane are crucial for cellular uptake [95,106]. Differently than the other classes of CPPs, it has been proposed that hydrophobic CPPs can spontaneously internalize into cells in an energy-independent process. C105Y [112], PFVYLI [112], Pep-7, and the pentapeptides QLPVM, VPTLK and KLPVM [113] are examples of hydrophobic CPPs.

Table 1 contains some examples of CPPs, their sequence, origin and physicochemical properties.

Table 1. Examples of CPPs, their sequence, origin and physicochemical properties

CPP	Sequence	Origin	Class	Ref.
Penetratin	RQIKIWFQNRRMKWKK	Antennapedia homeodomain	Cationic	[99]
TAT	YGRKKRRQRRR	HIV-1 TAT protein	Cationic	[98]
R9F2	RRRRRRRRRFF	Chemically synthesized	Cationic	[114]
Oct4	DVVRVWFCNRRQKGKR	Oct4 protein	Cationic	[101]
Melittin	GIGAVLKVLTTGLPALISWIKRKRQQ	Bee venom	Amphipathic	[115]
pVec	LLIILRRRIRKQAHAHSK	VE-cadhein	Amphipathic	[116]
MPG	GALFLGFLGAAGSTMGAWSQPKKKRKV	HIV glycoprotein 41/ SV40 T antigen NLS	Amphipathic	[107]
PasR8	FFLIPKGRRRRRRRRG	Chemically synthesized	Amphipathic	[117]
MAP	KLALKLALKALKAALKLA	Chemically synthesized	Amphipathic	[110]
kFGF	AAVALLPAVLLALLAP	Kaposi fibroblast growth factor	Hydrophobic	[118]
C105Y	CSIPPEVKFNKPFVYLI	α1-antitrypsin	Hydrophobic	[119]
PFVYLI	PFVYLI	Synthetic C105Y	Hydrophobic	[112]
QLPVM	QLPVM	Bax-binding domain of Ku-70 protein	Hydrophobic	[120]
Transportan	GWTLNSAGYLLGKINLKALAALAKKIL	Chimeric galanin–mastoparan	Amphipathic	[97]

1.2.1. Penetratin

Penetratin (Pen, RQIKIWFQNRRMKWKK) is a CPP derived from Antennapedia homeodomain, which correspond to the third helix of the homeodomain deleted of its N-terminal

glutamate. C-terminal region and the third helix are responsible for the capability of translocating through plasma membrane. Pen has been widely used for intracellular delivery of a variety of molecules and presents the advantage of the absence of saturable transport [121–123]. Researchers have demonstrated particular interest in Pen for delivery of cargo to the brain due to its endosomal escape properties and ability to penetrate neurons and accumulate in the nucleus [101,124,125]. The cationic-amphiphilic character of Pen is involved in interaction with lipid components of cellular membrane and subsequent internalization into the cell [51,52]. Numerous studies have demonstrated the enhanced drug delivery abilities of Pen-modified liposomes [126,127]. Therefore, modification of liposomes with Pen may enhance transfection efficiency and neuronal targeting of our gene carrier.

1.2.2. Melittin

Melittin (Mel, GIGAVLKVLTTGLPALISWIKRKRQQ) is a 26 amino acid-long peptide derived from bee venom and presents strong interaction with plasma membrane promoting its rearrangement with subsequent formation of transmembrane pores, which facilitate the transport of cargo into the cell [128–130]. Mel structure is composed of a bent α-helical rod attached to a charged C-terminus. The amphiphilic structure facilitates the insertion of Mel into cell membranes, and consequently promoting cargo internalization. Mel derivatives have shown to enhance intracellular delivery of therapeutic macromolecules [115]. Hence, conjugation of Mel to liposomes can be a strategy to improve the internalization of the system into the cells and, consequently, promote the transfection.

1.2.3. pVec

The CPP pVec (LLIILRRRIRKQAHAHSK) is an 18-amino acid peptide derived from murine vascular endothelial-cadherin protein which mediates physical contact between adjacent

cells by homophilic dimerization. Amphipathic CPP such as pVec is characterized by hydrophobic and hydrophilic regions in opposite directions. The charged region interacts with cell membrane, while the hydrophobic region causes membrane perturbation enabling the translocation across plasma membrane [95,96]. This CPP has shown ability to transport a variety of proteins into the cells. Additionally, it has the ability to effectively reach brain parenchyma without significant efflux out of the brain [131]. Therefore, the strategy of coupling pVec to liposomes can provide high translocation of nanoparticles across BBB avoiding their efflux from brain which consequently can reflect on enhanced transfection.

1.2.4. TAT

The first characterized CPP was TAT (YGRKKRRQRRR), a cationic peptide derived from the trans-activating protein of the human immunodeficiency virus type-1 [92,93]. TAT is a class of immediate early viral proteins that can *trans*-activate the expression of specific viral and/or cellular genes, however it is not involved in initial viral infection event. Studies with TAT protein have demonstrated that TAT derived segments conjugated to exogenous proteins promote their internalization into cells [92,93,132]. The arginine-rich segment in TAT protein (GRKKRRQRRRPPQ), positions 48-60, has been reported to be critical for internalization properties of the protein [133]. The transduction ability of TAT is facilitated by the interaction of their positive charges with the negatively charged glycosaminoglycans on the cell surface [101,132]. The carrier properties of TAT has been extensively explored, including surface modification of liposomal formulations for enhanced BBB permeation [98,134,135]. We hypothesize that TAT and Tf modification will enhance liposome permeability across BBB and delivery of plasmid DNA into brain cells.

1.2.5. R9F2

Cationic CPPs have been extensively employed as delivery carriers for a variety of macromolecules. Studies of the cellular mechanisms of cationic CPP demonstrated that the number and order of arginine residues within the peptide sequence are determinant factors of CPP internalization properties [95,136]. Although nona-arginine (R9) peptides have reported better cellular internalization when compared to analogs of TAT and polyarginines [103,137,138], conjugation of two phenylalanine to C-terminus of R9 peptide increased the hydrophobicity of the peptide and allowed better interaction with cell membrane and improved uptake of the cargo. R9F2 has shown strong cellular internalization with enhanced delivery properties as compared to other rich-arginine peptides such as R9, R8 and TAT [114,139]. Conjugation of R9F2 to our designed liposomes attempted to enhance permeation across BBB and internalization of the nanoparticles into brain cells.

1.2.6. PasR8

The integration of hydrophobic CPPs to either N- or C-terminus of other cationic CPP has shown to enhance the cellular uptake and delivery capacity of the original cationic CPP [140]. Regarding the latter, the improvement of carrier effectiveness of an octaarginine (R8) peptide was planned with the addition of a hydrophobic sequence derived from a lysosomal enzyme, cathepsin D. The hydrophobic FFLIPKG sequence, known as penetration accelerating sequence (Pas), provided enhancement of cellular penetration and endosomal escape properties for the new formed CPP in the presence of serum [117]. As a result, Pas conjugation to R8 formed the hybrid PasR8 and revealed to improve not only the carrier abilities but also facilitated the escape from endocytic lysosomes. The efficient translocation was suggested to be attributed to local and temporal destabilization of plasma membrane during early stages of endocytosis [141,142]. Considering the

improved aspects of PasR8 peptide, we expect that PasR8-modified liposomes will provide efficient brain internalization and delivery of pDNA into the cells.

1.2.7. kFGF

Hydrophobic sequences such as Kaposi fibroblast growth factor (kFGF) (AAVALLPAVLLALLAP) have been reported relevant for intracellular delivery of nucleic acids, providing stable non-covalent DNA complexation and protection against nucleases [143,144]. With half-life of ~48 h, this CPP has a hydrophobic stretch of residues necessary for internalization into cells. This process depends on its interaction to cells membrane and likely occur through energy-independent pathways [145–147]. Conjugation of kFGF to CBD3, peptide which mediates inhibition of NMDA receptors, conferred long-term neuroprotection in a toxic glutamate challenge probably as a result of increased internalization and reduced efflux of kFGF-CBD3 as compared to TAT- CBD3 conjugates [148]. Therefore, conjugation of kFGF to our designed liposomes intend to enhance transfection of pDNA in brain cells.

1.2.8. PFVYLI

The sequence PFVYLI (PF) is a known hydrophobic CPP derived from α1-antitrypsin that has the ability to enhance targeting and delivery properties of liposomes encapsulating therapeutics molecules, imaging agents and fluorescent probes both *in vitro* and *in vivo* [112,149]. The α1-antitrypsin can mediate binding to the serpin enzyme complex receptor and promote its uptake when complexed to elastase. The synthetic PF showed to be able to compete with the natural ligand for binding to the serpin receptor and provided gene transfer to cells when complexed to nucleic acid. Additionally, PF consistently increased the intensity and duration of reporter gene expression *in vitro* [150,151]. Conjugation of PF to nanoparticles showed to facilitate cell internalization and rapid nuclear localization of DNA-loaded nanoparticles leading to enhancement of gene

expression [119]. Considering the delivery properties of this CPP, liposomes were modified with PF aiming the delivery of pDNA to brain cells and enhancement of gene expression.

1.2.9. QLPVM

The hydrophobic QLPVM (QL) is part of the group of penta-peptides derived from Bax-binding domain of Ku-70 protein and they are also known as cell-penetrating pentapeptide. These group of pentapeptides have reported cell permeability and cell death inhibition properties [113,152,153]. QL has shown to enhance i*n vitro* and *in vivo* delivery properties of QL-modified liposomes and facilitated drug release into desired cell [120]. Additionally, the category of hydrophobic peptides have a low global net charge, which could be associated to their exhibited low toxicity. The hydrophobic motif is crucial for uptake assisting the peptide direct translocation through the cell membrane. This could be advantageous due to their immediate availability in cytosol removing the issues of endosomal entrapment and degradation [96,113]. We investigated the role of QL in enhancing the delivery and transfection properties of designed liposomes.

1.2.10. RVG

Rabies virus glycoprotein peptide (RVG) is a 29-amino acid peptide that has been considered as attractive approach for targeted-delivery of therapeutics to brain [154–156]. This peptide derives from the 189-214 amino acid sequence of rabies virus glycoprotein and it has shown to specifically target neuronal cells expressing nicotinic acetylcholine receptors (nAchR), mediate the retrograde axonal transport and facilitate the propagation of viral vector in the brain [154,157]. Especial interest for brain gene delivery has increased due to the ability demonstrated by RVG-conjugated nanoparticles to overcome the BBB through nAchR-mediated endocytosis and promote preferential accumulation of loaded nucleic acid in neuronal cells [157–162]. RVG

was conjugated to our designed liposomes as a strategy for effective brain targeting across BBB and delivery of pDNA.

The selection of CPPs in this study was based on their physicochemical properties and reported ability to improve the delivery properties of conjugated drug/gene carriers. Here we investigated the efficiency of liposomal nanoparticles modified with Tf and CPP as potential brain-targeted gene delivery systems.

1.3. Statement of problems and research objectives

Alzheimer's disease (AD) is the most common form of dementia, affecting approximately 5.7 million individuals in United States of all ages. The current available treatments for AD only provide symptomatic relief and are unable to halt the progression of the disease and restore normal neurological function [2,14]. Gene therapy is a promising tool for the treatment of neuro disorders such as AD, however, the therapeutic genes are unable to surpass the natural CNS protective barriers, which is mainly represented by BBB, and reach brain cells. The success of gene therapy relies on the development of a safe gene vector with specific transgene delivery and long-expression properties [163].

Non-viral vectors, such as liposomes, have attracted much attention due to their favorable characteristics over viral vectors such as safety, ease of preparation, low immunogenicity, low cost and ability to deliver a wide range of plasmid sizes [33,39], as well as to protect plasmid DNA (pDNA) from DNase degradation [40,41]. Effective delivery of liposomes to target cells can be achieved by decorating liposomal surface with ligands of specific receptors present on surface of tissues, which afford strategic targeted delivery [74]. Transferrin receptor (TfR), transmembrane protein overexpressed on brain endothelial cells, has been extensively explored for delivery of

therapeutics to the brain. Nevertheless, targeting *via* TfR presents a high degree of internalization, but receptor saturation can be a drawback [49]. The capacity of CPP in translocating a variety of cargo into the cell in a non-invasive manner without the use of receptors might be an additional strategy to enhance carrier internalization. We hypothesized that a combination of these two ligands on near-neutral PEGylated liposomes will enhance their ability to penetrate the BBB and transfect the desired cells *via* receptor targeting and enhanced cell penetration. Our primary aims are: (I) to synthesize and evaluate near neutral PEGylated liposomal delivery system, surface modified with transferrin and cell penetrating peptide (Tf-CPP-liposomes) *in vitro*, (II) to evaluate the ability of liposomal formulations to overcome an *in vitro* BBB model followed by transfection of primary neuronal cells, (III) to investigate the biodistribution, transfection and biocompatibility of the dual-modified delivery system *in vivo*, and the effects of CPP-Tf-liposome-mediated gene therapy on amyloid AD mouse model.

The long term goal of our research is to design a liposomal gene delivery system for efficient delivery of Nerve Growth Factor (NGF) into brain of AD mice for prevention and treatment of AD. Our research work focused on brain-targeted liposomes combining Tf receptor targeting and enhanced cell penetration utilizing cell-penetrating peptide for NGF-mediated gene transfer for treatment of AD. The high rate failure of clinical trials in AD reflects the complexity of this disease, and emphasizes the urgent need for approval of early-stage disease therapies and disease-modifying therapies. Therefore, the development of efficient brain targeted therapies for prevention and treatment of AD are significantly important.

1.3.1. Specific aim 1: Synthesize and characterize Tf and CPP coupled liposomes loaded with chitosan-pDNA polyplexes

Liposomes nanoparticles were prepared using thin lipid film hydration technique while dual-functionalized liposomes preparation involved the incorporation of Tf-micelles into CPP-liposomes by post-insertion technique. We proposed different types of CPPs (Penetratin, Melittin, pVec, TAT, R9F2, PasR8, kFGF, PFVYLI, QLPVM and RVG). The genes of interest (pGFP, pβgal, pNGF and pApoE2) were complexed to chitosan and loaded into liposomes to improve liposome transfection properties. Liposomal formulations were evaluated for particle size, zeta potential, morphology, encapsulation efficiency, chitosan-pDNA binding affinity, liposome-pDNA enzymatic protection, *in vitro* release, blood compatibility, cytotoxicity, cell uptake and uptake mechanism(s), transfection efficiency, endosomal escape, and effect of PenTf-liposomes containing chitosan-pNGF on formation of new synaptic vesicles in primary neuronal cells.

1.3.2. Specific aim 2: Design an *in vitro* 2-Dimentional (2D) BBB model to study the transport efficacy of liposomes across the barrier layer and evaluate the transfection efficiency in primary neuronal cells

The transport efficacy of liposomes were evaluated across 2D BBB model designed by co-culture of brain endothelial cells and glial cells on the inner and bottom side of culture inserts, respectively. The stablished *in vitro* BBB co-culture model has been recognized as a good model for screening of formulations with better brain penetration due to the high correlation demonstrated with the permeability of *in vivo* BBB [164,165]. The transfection efficiency of liposomes loading pGFP, pNGF or pApoE2 in primary neuronal cells after crossing the 2-D BBB model were also evaluated.

1.3.3. Specific aim 3: To assess the distribution and transfection efficiency of CPP-Tf-liposomes *in vivo* and investigate effects of CPP-Tf-liposome-mediated gene therapy in amyloid AD mouse model

Gene therapy has potential as a novel strategy to treat neurodegenerative disorders including AD. To establish successful gene therapies for AD, we validated CPP-Tf-liposomes obtained through above aims for their biodistribution, biocompatibility and transfection efficiency into mice brains through tail vein injection. Finally, we examined effects of NGF gene therapy through CPP-Tf-liposomes on amyloid pathology and neurogenesis in amyloid model APP/PS1 mice.

2. MATERIAL AND METHODS

2.1. Material

The phospholipids, Dioleoyl-3-trimethylammonium-propane chloride (DOTAP) and Dioleoyl-sn-glycero-3-phosphoethanolamine (DOPE) were purchased from Avanti Polar Lipids (Birmingham, AL, USA). The phospholipid DSPE–PEG_{2000}–NHS was purchased from Biochempeg Scientific Inc (Watertown, MA, USA). Cholesterol, 4-(2-hydroxyethyl)-1-piperazineethanesulfonic acid (HEPES), Ethylenediaminetetraacetic acid (EDTA), Hoechst 33342 and Triton™ X-100 were obtained from Sigma–Aldrich (St. Louis, MO, USA). Chitosan (MW 30 kDa) was purchased from Glentham Life Sciences (Corsham, UK). The cell-penetrating peptides Penetratin (RQKINFQNRRMKWKK), Melittin (GIGAVLKVLTTGLPALISWIKRKRQQ), pVec (LLIILRRRIRKQAHAHSK), PFVYLI, QLPVM, Kaposi fibroblast growth factor (AAVALLPAVLLALLAP), TAT (YGRKKRRQRRR), PasR8 (FFLIPKGRRRRRRRRGC) and R9F2 were purchased from Ontores Biotechnologies (Zhejiang, China). Plasmid DNA encoding beta-galactosidase (gWiz-βGal) and plasmid DNA encoding Green Fluorescent Protein (gWiz-GFP) were purchased from Aldevron LLC (Fargo, ND, USA). Plasmid DNA encoding ApoE2 was purchased from Addgene (Watertown, MA, USA). Human NGF ORF mammalian expression plasmid, C-HA tag, and NGF ELISA kit were purchased from Sino Biological (Wayne, PA, USA). Dulbecco's Modified Eagle Medium (DMEM), and phosphate buffered saline (PBS) were purchased from Corning Incorporated (Corning, NY, USA). Fetal bovine serum (FBS) was purchased from Omega Scientific (Tarzana, CA, USA). Lipofectamine 3000, RIPA buffer, BCA protein assay, Apolipoprotein E human ELISA kit and protease and phosphatase inhibitors were purchased from ThermoFisher Scientific (Waltham, MA, USA). Beta-Galactosidase Enzyme Assay kit with reporter lysis buffer was supplied by Promega (Madison, WI, USA). Sensolyte anti-

mouse β-amyloid (1-42) and (1-40) quantitative ELISA were purchased from AnaSpec (Fremont, CA, USA).

2.2. Synthesis of CPP-PEG$_{2000}$-DSPE and Tf-PEG$_{2000}$-DSPE

In order to prepare CPP-liposomes with stealth properties, CPPs and Tf were conjugated to NHS activated PEG$_{2000}$-DSPE, separately. Briefly, CPP and NHS-PEG$_{2000}$-DSPE at molar ratio of 1:5 were dissolved in anhydrous dimethylformamide (DMF), after adjusting the pH to 8.0-9.0 with trimethylamine [112,166]. The reaction was conducted for 120 h at room temperature under moderate stirring. The resultant reaction mixture was dialyzed (molecular weight cut-off of 3500 Da) in deionized water for 48 h to remove uncoupled CPP. The dialysate was lyophilized and stored at -20 °C until use. Holo-Tf and DSPE-PEG$_{2000}$-NHS (125 µg Tf/µM phospholipid) were dissolved in anhydrous DMF, after adjusting pH to 8.0-9.0 with trimethylamine, and stirred for 24 h at room temperature [76,166,167]. The product were passed through Sephadex G-100 column to removed unbound protein. Coupling efficiencies of both reactions were determined using BCA protein assay.

2.3. Preparation and characterization of liposomal formulations

Liposomes preparation was performed using thin lipid film hydration technique while dual-functionalized liposomes preparation involved the incorporation of Tf-micelles into CPP-liposomes by post-insertion technique [26]. CPP-PEG-lipid (4 mol %) was combined with DOPE/DOTAP/Cholesterol (45:45:2 mol %) in chloroform:methanol (2:1, v/v) and dried to form a lipid film, which was hydrated using HEPES buffer (pH 7.4). CPP-liposomes were stirred overnight with Tf-micelles (4 mol %) to form CPP-Tf-liposomes. Free Tf-micelles were separated

from liposomal formulations by passing through Sephadex G-100 column. Chitosan-plasmid GFP, plasmid βgal, plasmid NGF and plasmid ApoE2 polyplexes were added to hydration buffer at N/P ratio of 5 for incorporation into liposomes. Liposomes were characterized for hydrodynamic size and zeta potential using dynamic light scattering method on Zetasizer Nano ZS 90 (Malvern Instruments, Malvern, UK) at 25 °C. Morphology of liposomes was evaluated using transmission electron microscopy (TEM, JEM-2100, JEOL) after the samples were stained with 1% phosphotungstic acid aqueous solution. The percent of chitosan-plasmid DNA complexes encapsulated into liposomes was calculated as the fluorescence signal Hoechst 33342 divided by the fluorescence following the addition of Triton X-100 using Spectra Max M5 spectrophotometer (Molecular Devices, Sunnyvale, CA, USA) at excitation/emission wavelengths: 354/458 nm, respectively.

2.4. Chitosan-pDNA binding ability

The optimal chitosan-pDNA N/P ratio (molar ratios of the amine groups in chitosan and phosphate groups in DNA) was monitored by EtBr exclusion assay and agarose gel electrophoresis [168]. Naked pDNA was used as a positive control. The complexes containing 1 µg of pDNA at different chitosan weight ratios were stained with EtBr (0.5 µg) for 5 min and the fluorescence intensity was measured using a spectrophotometer (excitation/emission wavelengths: 260/600 nm, respectively). Relative fluorescence intensity of EtBr solution in the presence of free plasmid corresponded to 0% condensation while fluorescence intensity without plasmid corresponded to 100% condensation. For agarose gel electrophoresis, the complexes (1 µg pDNA at different chitosan weight ratios) were loaded in 0.8% w/v agarose gel stained with EtBr (0.5 µg/mL) and

electrophoresed at 80 V in 0.5X Tris-acetate-EDTA (TAE, Bio-Rad, CA, USA) buffer for 80 min. The pDNA migration was thereafter recorded.

2.5. DNase protection assay

Protection of chitosan-pDNA encapsulated into liposomal formulations against enzymatic degradation was examined by DNase I protection assay [27]. Liposomal formulations containing 1 µg chitosan-pDNA complexes were incubated for 60 min at 37 °C with 1 unit DNase I. Free pDNA was used as a negative control and pDNA with DNase I was used as a positive control. After incubation the reaction was stopped by adding 5 µl of EDTA (100 mM). Subsequently, 20 µl of heparin (5 mg/mL) was added and incubated for 2 h at 37 °C to release the pDNA from the complex. The released pDNA samples were subjected to agarose gel electrophoresis 0.8% (w/v) for 80 min at 80 V.

2.6. *In vitro* release

Liposomal formulations containing 50 µg of pDNA were dispersed in 10 mL of PBS (pH 7.4) and incubated at 37 °C under constant shaking at 50 rpm. At predetermined time intervals, 300 µL of the suspension was withdrawn and centrifuged at 5,000 rpm, 4 °C, for 30 min. After staining with Hoechst 33342 (0.15 µg/mL), the content of pDNA was determined using fluorescence spectrophotometer (excitation/emission wavelengths: 354/458 nm, respectively) [54,166]. The cumulative amount of released pDNA from the liposomes was then calculated.

2.7. Cell culture and animals

Primary cultures were obtained from brain of 1-day-old rats [28]. Briefly, meninges and vessels were removed from dissected brains. Brains were minced and incubated with DMEM containing 0.25% trypsin and DNase I (8 µg/mL) at 37 °C. Astrocytes obtained from the dissociated cells were cultured in DMEM containing 10% v/v FBS and 1% v/v antibiotics. The purity of astrocytes was checked by immunostaining for glial fibrillary acidic protein (GFAP) antibody. Primary neuronal cells were obtained by treating the dissociated cells with 10 µM cytosine arabinoside at day 3, they were cultured in Neurobasal media with 10% v/v plasma-derived horse serum, B-27 supplements, L-Glutamate (25mM) and 1% v/v antibiotics. The purity of neuronal cultures was checked by immunostaining for anti-MAP2 antibody. Mice brain endothelial bEnd.3 cells, obtained from ATCC (Manassas, VA, USA), were cultured in DMEM 10% FBS and 1% v/v antibiotics. Cells were incubated in atmosphere of 5% of CO_2 at 37 ºC.

All procedures and handling of rats and mice were conducted in accordance with the protocols approved by the Institutional Animal Care and Use Committee (IACUC) at North Dakota State University. Animals were maintained under standard housing conditions with free access to food and water and exposed to 12 h light-dark cycle. Sprague Dawley (male/female) rats were purchased from Charles River Laboratories (Wilmington, MA, USA), C57BL/6 (male/female) and B6C3-Tg(APPswe,PSEN1dE9)85Dbo/Mmjax (APP/PS1) (male/female) mice were purchased from Jackson Laboratories (Bar Harbor, ME, USA).

2.8. *In vitro* cytotoxicity assay

Cell viability was evaluated in bEnd.3, primary astrocytes and primary neuronal cells after treatment with liposomal formulation at 100, 200, 400 and 600 nM phospholipid concentration

using MTT assay [166,167]. All cell lines ($1x10^4$ cells/well) were plated on 96-well plate 24 h prior to perform the assay and exposed to liposomal formulations in serum free media during 4 h. Thereafter, media was replaced, and cells incubated for 48 h. MTT (5 µg/well) was added to each well for 3 h. Subsequently, MTT solution was removed and the formazan crystals solubilized using DMSO. Absorbance was measured at 570 nm, control group consisted of untreated cells and cell viability was expressed as percentage of control.

2.9. Cellular uptake and internalization mechanisms

2.9.1. Cellular uptake study

Cellular uptake of DiI-labeled liposomes was evaluated in bEnd.3, primary astrocytes and primary neuronal cells. About $1x10^5$ cells/well were seeded in 24-well plates, 24 h prior to uptake analysis. Cells were incubated with liposomal formulation (100 nM) and the uptake was investigated at different time intervals [166,167]. Quantitative estimation of liposomal uptake was performed by lysis of cells in 0.5% Triton-X 100 followed by extraction of fluorescent dye in methanol. Fluorescence intensity was measured using spectrophotometer (excitation wavelength: 553 nm, emission wavelength: 570 nm).

2.9.2. Uptake mechanism

In order to elucidate the mechanisms associated with cellular uptake, the aforementioned cells were seeded in 24-well plates ($1x10^5$ cells/well), 24 h prior to the experiment. Cells were treated with well-known endocytosis inhibitors such as sodium azide (10 mM) to inhibit all energy-dependent endocytosis, chlorpromazine (10 µg/mL) to block clathrin-mediated endocytosis, colchicine (100 µg/mL) to inhibit lipid/raft caveolae or amiloride (50 µg/mL) to inhibit

macropinocytosis for 30 min at 37 °C before application of DiI-labeled liposomes (100 nM) [27]. Following 4 h of uptake process, fluorescence intensity was measured using spectrophotometer (excitation/emission wavelength: 553-570 nm).

2.10. *In vitro* transfection efficiency

Transfection efficiency of liposomal formulations was investigated in bEnd.3, primary astrocytes and primary neuronal cells. About $1x10^6$ cells/well were seeded in 6-well plates, 24 h prior to transfection analysis. Cells were treated with Lipofectamine 3000 and liposomal formulations (100 nM) containing either pGFP, or pβgal, pNGF or pApoE2 complexes, in serum-free medium, during 4 h [166,167]. Thereafter, cells were rinsed with PBS and incubated for 48 h. For pGFP transfection, GFP expression was analyzed using fluorescence microscope, and quantitative evaluation was performed using FACS analysis- BD Accuri C6 flow cytometer (Ann Arbor, MI, USA) laser excitation wavelength 488 nm, emission detection wavelength using optical filter FL1 533/30 nm.

For β-galactosidase expression, cells were washed with PBS (pH 7.4), and lysed using βgal assay buffer. β-galactosidase enzyme activity was quantified using β-galactosidase reagent assay at 420 nm. Measured values were normalized by total protein levels in the samples, which were determined by BCA protein assay.

NGF expression was quantified using NGF ELISA kit. Supernatant and cell lysates were incubated for 2 h in 96-well plates pre-coated with primary anti-NGF antibody. Subsequently, a detection antibody was incubated 1 h, and developed with 3,3',5,5'-tetramethylbenzidine substrate, followed by colorimetric measurement at 450 nm. Measured values were normalized by total protein levels in the samples, which were determined by BCA protein assay.

ApoE expression was quantified using ApoE ELISA kit. Supernatant and cell lysates were incubated for 2.5 h in 96-well pre-coated plates. Biotinylated antibody was added and incubated for 1 h. HRP reagent was incubated 45 min. Subsequently, TMB substrate was incubated for 30 min, the reaction was stop with stop solution followed by colorimetric measurement at 450 nm and 550 nm. Subtraction of 550 nm values from 450 nm values corrected the optical imperfections in the plate. Measured values were normalized by total protein levels in the samples, which were determined by BCA protein assay.

2.11. Endosomal escape

Enhancement in transfection efficiency due to endosomal escape was evaluated in bEnd.3 cells. About $5x10^5$ cells/well were seeded in 24 well-plates, 24 h prior to the assay. Thereafter, cells were treated with 50 mM sucrose (a lysosomotropic agent) and liposomal formulations containing 1 µg pGFP [169]. After a 4 h incubation, the media was replaced and cells were incubated for a total of 48 h. Cellular GFP expression was analyzed using fluorescence microscope and flow cytometer.

2.12. Effect of PenTf-liposomes containing chitosan-pNGF on formation of new synaptic vesicles in primary neuronal cells

Primary neuronal cells ($1x10^6$ cells/well) seeded on 6-well plate were treated with PenTf-liposomes containing chitosan-pNGF complexes (1µg of pDNA) for 4 h. Media was replaced and formation of new vesicles was observed after 12 h, 24 h, 48 h, 72 h, 7 days and 14 days of the treatment. Cells were fixed with 4% neutralized buffer formalin for 15 min, followed by membrane permeabilization with 0.3% Triton X-100 in PBS for 1 min. Cells were incubated 4 °C overnight

with primary antibody (NeuN rabbit IgG or Synaptophysin mouse IgG1) followed by secondary antibody (Alexa Fluor 647 goat anti-rabbit IgG or Alexa Fluor 488 goat anti mouse IgG) for 2 h at room temperature. The cells were observed under Leica DMi8 fluorescence microscope. Synaptophysin levels were quantified using Synaptophysin ELISA kit (Boster Biological Technology, Pleasanton, CA, USA). Measured values were normalized by total protein levels in the samples, which were determined by BCA protein assay.

2.13. Design of *in vitro* co-culture BBB model

The *in vitro* BBB model was designed combining bEnd.3 and primary astrocyte cell cultures [29,30]. Primary astrocytes ($1.5x10^4$ cells/cm^2) were seeded on the bottom side of transwell inserts (BD Biosciences, NC, USA) with 0.4 µm pore size and effective growth area 0.33 cm^2 in DMEM with 20% v/v FBS, overnight incubation. About $1.5x10^4$ cells/cm^2 bEnd.3 cells were seeded on upper side of culture inserts that were placed in 24-well plates (DMEM 20% v/v FBS). Formation of tight junctions was assessed measuring transendothelial electrical resistance (TEER) values using $EVOM^2$ (World Precision Instruments, Sarasota, FL, USA). Inserts containing only bEnd.3 cells on the upper side and inserts only with glial cells on the underside were also constructed and maintained similarly.

2.14. Transport across *in vitro* BBB model

Transport of labeled liposomal formulations was measured across the *in vitro* BBB model according to a modified method [26]. Liposomal suspensions (100 nM) were added into inserts, which were placed in 24-well plates containing 0.5 mL PBS with 10% v/v FBS. After 0.25 h, 0.5 h, 1 h, 2, 4 and 8 h, the inserts were transferred to new wells with serum-PBS. Concentrations of

fluorescent-labeled liposomes in the upper and the lower compartments were determined using spectrophotometer (excitation/emission wavelengths: 568/583 nm, respectively). Sodium fluorescein (NA-Fl) was used as a small molecular sized marker to test BBB permeability. Intactness of the barrier layer was evaluated measuring TEER before and after (8 h) liposome transport across *in vitro* BBB using EVOM^2. The permeability of the endothelial barrier was calculated using the following equation:

$$1/Pe = 1/Pt - 1/Pf \text{ (cm/sec)}$$

where Pt is the permeability coefficient of the total system (in vitro model) and Pf is the permeability coefficient across cell free inserts. Permeability coefficient for each liposomal formulation dividing the amount of liposomes transported per min (µg/min) through total system (Pt) or cell free insert (Pf) by the surface area of the transwell membrane (cm^2), by the initial concentration of liposomes (µg/mL) and by 60 (conversion factor from min to sec).

2.15. Transfection efficiency in primary neuronal cells after liposome transport across *in vitro* BBB model

Primary neuronal cells were seeded in 24-well plates. Culture inserts containing the *in vitro* BBB model were placed in the same well containing primary neuronal cells [31]. Liposomal suspensions (100 nM) encapsulating either pGFP, pNGF or pApoE2 (1 µg) were added to the upper compartment of inserts and incubated for 8 h. Thereafter, the inserts were removed and the media was replaced for fresh media. After 48 h incubation, GFP expression was analyzed using flow cytometer and fluorescence microscopy. The amount of NGF or ApoE produced by primary neuronal cells was determined by NGF ELISA kit or ApoE ELISA kit, respectively, as described

previously. Measured values were normalized by total protein levels in the samples, which were determined by BCA protein assay.

2.16. Blood compatibility

Blood was freshly harvested from Sprague Dawley rats into EDTA containing tubes and centrifuged three times at 1500 rpm for 10 min in PBS, pH 7.4, 10 mM $CaCl_2$. Erythrocytes solution containing 1.5 x 10^7 cells was exposed to negative control (PBS), positive control (Triton X-100 1% v/v) and liposomal formulations in different phospholipid concentrations (31.25-1000 µM) for 1 h at 37 ºC, 5% CO_2. After incubation, cell suspension was centrifuged at 1500 rpm for 10 min. The supernatant was removed, and absorbance of released hemoglobin was measured using spectrophotometer at 540 nm [54,76,166,170]. Percent hemolysis was calculated by considering absorbance in presence of Triton X-100 as 100% hemolysis.

2.17. *In vivo* biodistribution in wild type mice

C57BL/6 mice were randomly divided into three groups consisted of 6 animals each (3 male and 3 female). Each group was injected with either PBS, CPP-liposomes and CPPTf-liposomes administered via tail vein at a dose of ~15.2 µmoles phospholipid/kg body weight [54,76]. Quantification of liposomes were performed in brain, liver, kidneys, lungs, heart, spleen and blood after 24 h of administration. The tissues were weighted, homogenized with PBS and fluorescent dye extracted in chloroform:methanol (2:1, v/v). The fluorescence intensity was measured by spectrophotometer at λex 560 nm and λem 580 nm. Data were normalized with the negative control (PBS).

2.18. *In vivo* gene transfection efficiency of liposomal formulations containing chitosan-pDNA and biocompatibility in wild type mice

Six C57BL/6 mice were injected with single dose of liposomal formulations (~15.2 μmoles phospholipids/kg body weight) encapsulating pβgal (1 mg pDNA/kg body weight), or pβgal in buffer or buffer alone. After 5 days, different organs (brain, liver, kidneys, heart, lungs, spleen and blood) were removed, weighed, transferred to tissue lysis/protein extraction buffer (200 μl), homogenized and centrifuged at 4,000 rpm, 4 °C for 15 min. The supernatant was extracted with an equal volume of pβgal assay buffer containing the substrate, o-nitrophenyl-β-D-galactopyranoside (ONPG) and incubated at 37 °C for 60 min. Addition of sodium carbonate stopped the reaction and the absorbance was measured at 420 nm. Tissue samples from control mice (PBS administration) were similarly processed to quantify the endogenous βgal activity of individual organs. Measured values were normalized by total protein levels in the correspondent samples, which were determined by BCA protein assay.

Six C57BL/6 mice were injected with single dose of Plain-lip or PenTf-liposomes (~15.2 μmoles phospholipids/kg body weight) encapsulating either 4 μg, 20 μg or 40 μg pNGF/100g body weight. After 5 days of liposomal administration, transfection in different tissues (brain, liver, kidneys, heart, lungs, spleen and blood) was quantified using NGF ELISA kit. Transfection efficiency of PenTf-liposomes containing 40μg pNGF/100g body weight was also analyzed after 15 days of liposome administration. Organs were removed, weighed, homogenized in RIPA buffer containing proteinase and phosphatase inhibitor cocktail and centrifuged at 4,000 rpm, 4 °C for 15 min. NGF levels in the samples were quantified using NGF ELISA kit as previously described. Tissue samples from control mice (PBS administration) were similarly processed to quantify the

NGF expression of individual organs. Measured values were normalized by total protein levels in the samples, which were determined by BCA protein assay.

For study of transfection efficiency of liposomal formulations containing plasmid ApoE2, six C57BL/6 mice were injected with single dose of either PBS, or pApoE2 (1 mg pApoE2/kg body weight), or Plain-lip or PenTf-liposomes (~15.2 μmoles phospholipids/kg body weight) encapsulating 1 mg pApoE2/kg body weight. After 5 days of administration, different organs (brain, liver, kidneys, heart, lungs, spleen and blood) were removed, weighed, homogenized in RIPA buffer containing proteinase and phosphatase inhibitor cocktail and centrifuged at 4,000 rpm, 4 °C for 15 min. ApoE2 levels in the samples were quantified using ApoE ELISA kit, as previously described. Tissue samples from control mice (PBS administration) were similarly processed to quantify the ApoE expression of individual organs. Measured values were normalized by total protein levels in the samples, which were determined by BCA protein assay.

For immunohistochemical imaging, two C57BL/6 mice were injected with single dose of liposomal formulations (~15.2 μmoles phospholipids/kg body weight) encapsulating pGFP (1 mg/kg body weight). A control group of two mice did not receive the treatment. After 7 days, the brains were embedded in OCT compound and snap frozen in liquid nitrogen. Tissue sections (30 μm thick) were cut using cryostat, fixed in acetone and methanol and incubated with primary antibody (rabbit anti-GFP antibody 1:100, Invitrogen, Carlsbad, CA) at 4°C overnight. Thereafter, sections were incubated with secondary antibody (rabbit Alexa Fluor 488, 1:200, Invitrogen) or mouse anti-NeuN antibody (1:200, Millipore, Burlington, MA) and imaged using confocal microscope.

Tissues were sectioned into 30 µm slides and stained with hematoxylin-eosin (H&E) for evaluation of biocompatibility by observing morphological alterations, signs of inflammation, necrosis or cellular damage.

2.19. Neuroprotective effects of PenTf-liposomes containing chitosan-pNGF on APP/PS1 double transgenic mice

2.19.1. Liposome administration and experimental design

Three-months old APP/PS1 double transgenic mice were divided into three groups (n=14 for each group): the AD control group, the plasmid NGF group (40 µg pNGF/100 g of body weight) and PenTf-liposomes chitosan-pNGF group (40 µg pNGF/100 g of body weight). Wild type (C57BL/6) mice were used as controls. Four administrations of the treatments were performed, once per week, and the animals were analyzed on 28^{th} day of first administration.

2.19.2. Protein quantification

For determination of NGF, synaptophysin and PSD-95 levels, brain samples of APP/PS1 and C57BL/6 mice were homogenized in RIPA buffer containing protease and phosphatase inhibitor cocktail [171]. The levels of NGF, synaptophysin and PSD-95 were determined using NGF, Synaptophysin and PSD-95 ELISA kits, respectively. For measurements of Aβ in mouse brain, samples were sequentially homogenized in Tris-buffered saline (TBS), TBS buffer containing 1% Triton X-100 (TBS-TX), and then 5 M guanidine in 50mM Tris-HCl (GDN), pH 8.0. The levels of human $A\beta_{1-40}$ and human $A\beta_{1-42}$ were determined using AnaSpec ELISA kit. Synaptophysin and PSD-95 levels were quantified in TBS, TBS-TX and GDN fractions using

Synaptophysin and PSD-95 ELISA kits, respectively. Measured values were normalized by total protein levels in the samples, which were determined by BCA protein assay.

2.19.3. Immunohistochemical imaging

Brain samples were fixed in 10% neutralized buffer formalin, paraffin-embedded, and sectioned (4 μm thick). The brain tissue sections were incubated for 1 h with either anti-Ki-67 antibody (1:500) (Abcam, Cambridge, MA) for cell proliferation or with anti-beta amyloid antibody [MOAB-2] (5 μg/ml) (Abcam, Cambridge, MA) for detection of unaggregated, oligomeric and fibrillar forms of $A\beta_{1-42}$, and unaggregated $A\beta_{1-40}$. Thereafter, the tissue sections were incubated with goat anti-rabbit CF®633 (1:200) (Biotum, Inc., Fremont, CA). The slides were observed under Leica DMi8 fluorescence microscope.

2.20. Statistical analysis

All data are expressed as the mean ± standard deviation (S.D.; n=4 for *in vitro* and n=6 for *in vivo* studies). The statistical analysis were performed using one-way analysis of variance (ANOVA) with Tukey multiple comparison post-hoc test (GraphPad Prism 5.0- San Diego, CA, USA). Statistical significance was considered when $p< 0.05$.

3. RESULTS AND DISCUSSION

3.1. Characterization of liposomes

CPP-liposomes were prepared via two-step process while the dual-modified CPP-Tf-liposomes were prepared via three-step process: (1) preparation of a lipid film by drying chloroform:methanol solution of DOPE/DOTAP/Cholesterol/CPP-DSPE-PEG; (2) formation of CPP-liposomes by hydrating the lipid film with HEPES buffer followed by ultrasound treatment; (3) formation of CPP-Tf-liposomes after overnight stirring of Tf-micelles with CPP-liposomes, respectively. Details of hydrodynamic size distribution and zeta potential characterization by dynamic light scattering are present at Table 2. Particle size range was from 130.6±3.08 nm to 168.7±2.1 nm. Furthermore the formulations had small size distribution (PDI < 0.3), demonstrating tendency for monodispersity and lack of aggregation, suggesting stability. The preparation of nanocarriers with homogeneous particle size and low size distribution is essential for development of efficient and stable delivery systems [172]. The transmission electron microscopy (TEM) images showed that liposomal formulations had spherical morphology (Figure 1 a and b). Zeta potential range was from 10.6±1.20 mV to 34.2±1.06 mV. Despite being positively charged, the liposomal formulations exhibited differences in zeta potential which indicate that surface modification influence the charge of nanoparticles. In these formulations, the cationic lipid DOTAP may have contributed to overall positive zeta potential of formulations. Conversely, the lower zeta potential of Tf-coupled liposomes and CPP-Tf-coupled liposomes as compared to Plain-liposome and CPP-liposome, respectively, could be attributed to the presence of negatively charged Tf protein on the surface of liposomes.

The encapsulation of pDNA into liposomal formulations was not negatively affected by different plasmid DNA. High encapsulation efficiencies of plasmid DNAs were obtained for all liposomal formulations, which were above 80%, as shown in Table 2.

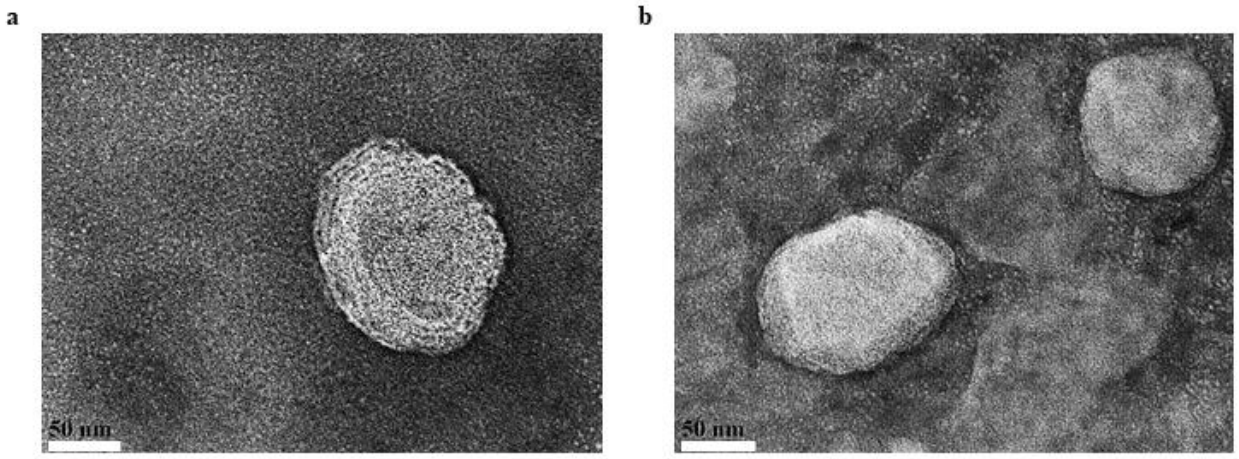

Figure 1. Transmission electron microscopy (TEM) images of Plain-liposomes (a) and PenTf-liposomes (b) which was negatively stained with 0.1% phosphotungstic acid aqueous solution (Scale 50 nm).

Table 2. Characterization of Liposome-pDNA: particle size, PDI, zeta potential and encapsulation efficiency

Liposomes	Particle size (nm)	PDI[a]	Zeta potential (mV)	EE[b]
Plain-liposome	147.9±1.12	0.17±0.04	21.9±0.48	87.9±3.23%
Tf-liposome	156.2±1.91	0.11±0.04	10.6±1.20	84.2±8.03%
Pen-liposome	167.3±2.21	0.19±0.03	28.3±1.73	87.2±1.89%
PenTf-liposome	156.2±1.84	0.08±0.06	19.5±1.22	90.7±6.82%
Mel-liposome	150.9±3.39	0.29±0.02	27.6±1.79	87.4±3.85%
MelTf-liposome	165.5±3.52	0.17±0.05	19.9±1.63	84.6±4.89%
pVec-liposome	136.1±1.78	0.02±0.02	34.2±1.06	87.4±3.85%
pVecTf-liposome	163.3±2.99	0.19±0.08	28.1±2.07	82.3±4.44%
QL-liposome	134.7±1.97	0.25±0.02	23.6±0.72	84.5±1.97%
QLTf-liposome	151.5±2.23	0.21±0.04	17.4±3.89	90.2±6.62%
PF-liposome	155.9±1.21	0.11±0.02	31.4±0.52	89.5±3.26%
PFTf-liposome	159.7±3.33	0.12±0.01	27.3±2.19	88.8±4.46%
kFGF-liposome	145.9±4.18	0.24±0.04	28.3±1.36	84.5±1.97%
kFGFTf-liposome	151.5±3.47	0.19±0.03	20.1±1.21	90.7±1.96%
TAT-liposome	144.1±4.29	0.22±0.03	27.5±1.67	88.2±7.40%
TATTf-liposome	138.3±1.84	0.22±0.01	19.5±2.69	90.2±7.30%
PasR8-liposome	153.4±3.39	0.23±0.03	28.7±1.13	92.4±3.73%
PasR8Tf-liposome	177.8±1.77	0.17±0.08	16.3±1.35	90.2±7.30%
R9F2-liposome	164.2±2.31	0.16±0.05	30.4±0.93	86.1±2.97%
R9F2Tf-liposome	168.7±2.15	0.17±0.05	25.0±1.24	92.7±3.27%
RVG-liposome	159.7±3.07	0.14±0.04	33.2±1.77	87.4±3.85%
RVGTf-liposome	130.6±3.08	0.15±0.01	22.5±1.60	84.6±4.89%

Data are presented as mean ± SD from four different preparations.

[a]PDI: polydispersity index

[b]EE: encapsulation efficiency

3.2. Chitosan-pDNA binding affinity

The formation of chitosan-pDNA complexes was evaluated using EtBr exclusion assay and confirmed by agarose gel retardation assay. Naked pDNA was used as positive control. EtBr intercalates with plasmid base pairs resulting in significant increase in fluorescence intensity. When the plasmid complexes with chitosan, the EtBr-plasmid intercalation is prevented, reducing

the fluorescence intensity [173]. Therefore, a decrease in fluorescence intensity indicates chitosan plasmid interaction. The polyplexes were prepared at different N/P ratios to investigate the optimal concentration of chitosan required to complex completely with pDNA while still being able to dissociate from the chitosan inside the cells. High ratios of chitosan-plasmid can result in very stable complexes, which will not dissociate easily inside the cells, compromising transfection efficiency. As shown in the Figure 2 a, EtBr fluorescence decreased as chitosan-plasmid N/P ratio increased and a significant reduction of up to 20% fluorescence was observed at N/P=5. Complex formation was confirmed using agarose gel electrophoresis, where light bands of pDNA (Figure 2 b, lane b) were observed at N/P= 1, but no bands were observed at higher N/P ratios. Based on this data, a N/P=5 was chosen for preparation of chitosan-pDNA complexes.

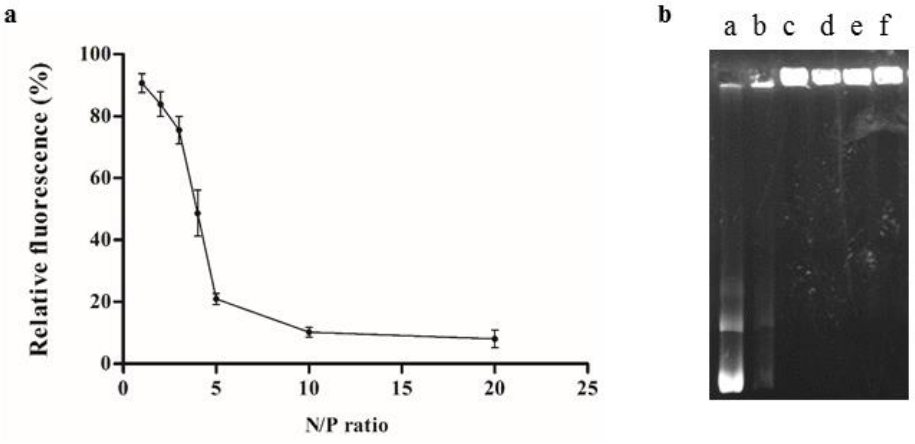

Figure 2. Binding affinity of plasmid DNA to chitosan. **a)** Relative fluorescence of chitosan-pDNA complexes in different N/P ratios (1, 2, 3, 4, 5, 10 and 20). Data expressed as mean ± SD (n=4). **b)** Agarose gel electrophoresis of chitosan-pDNA complexes in different N/P ratios (1-lane b, 5-lane c, 10-lane d, 15-lane e and 20-lane f). Naked pDNA was used as control.

3.3. DNase protection assay

A suitable gene delivery system should not only transport the therapeutic genes to the target cells, but also protect them against enzymatic degradation. Free DNA is vulnerable to DNase degradation and nanocarriers can potentially protect the encapsulated therapeutic molecules [74].

The ability of liposomal formulations containing chitosan-pDNA complexes to protect pDNA against enzymatic degradation was compared to free pDNA (Figure 3, lane a). Naked pDNA (Figure 3a, lane b) was fully degraded upon incubation with DNase I, while pDNA encapsulated in liposomal formulations remained intact as shown by presence of bright bands (Figure 3, lane c-x), suggesting that all liposomal formulations could effectively protect the pDNA from enzymatic degradation.

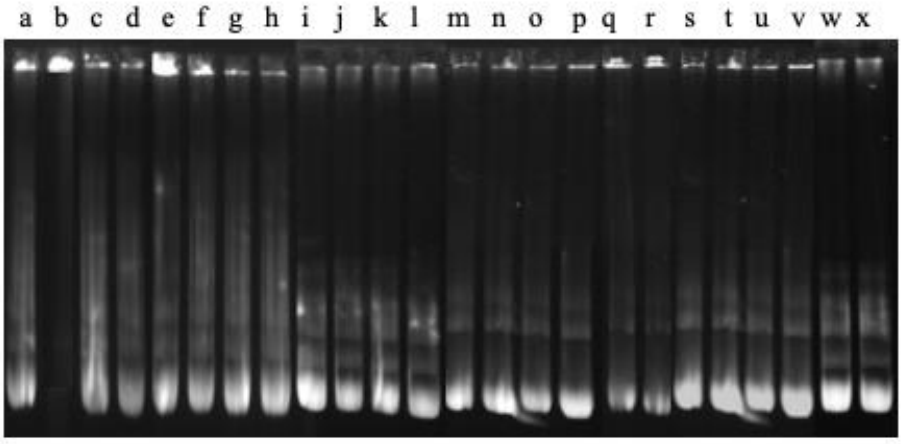

Figure 3. Protective effect of liposomal formulation encapsulating chitosan-pDNA (N/P 5) against nuclease degradation. Lane a, naked pDNA; lane b, naked pDNA+DNase I; lanes c-x, Plain-lip, Tf-lip, Pen-lip, PenTf- lip, Mel-lip, MelTf-lip, pVec-lip, pVecTf-lip, QL-lip, QLTf-lip, PF-lip, PFTf-lip, kFGF-lip, kFGFTf-lip, TAT-lip, TATTf-lip, PasR8-lip, PasR8Tf-lip, R9F2-lip, R9F2Tf-lip, RVG-lip and RVGTf-lip containing chitosan-DNA complexes, respectively + DNase I.

3.4. *In vitro* release

The cumulative release profile of pDNA (Figure 4) from the liposomal formulations were monitored at 37 °C for 24 h in phosphate buffer containing 5% FBS. Plasmid DNA was continually released in the first 8 h from all formulations that amounted to 22% cumulative release from Plain-lip, Pen-lip and PenTf-liposomes and 29% from Tf-liposomes. After 8 h, the liposomal formulations exhibited a relatively slow release profile. The release rates of pDNA from Plain-,

Tf-, Pen- and PenTf-liposomes were 37.3±0.4%, 42.2±0.8%, 29.9±2.7%, 29.4±2.3%, respectively after 24 h.

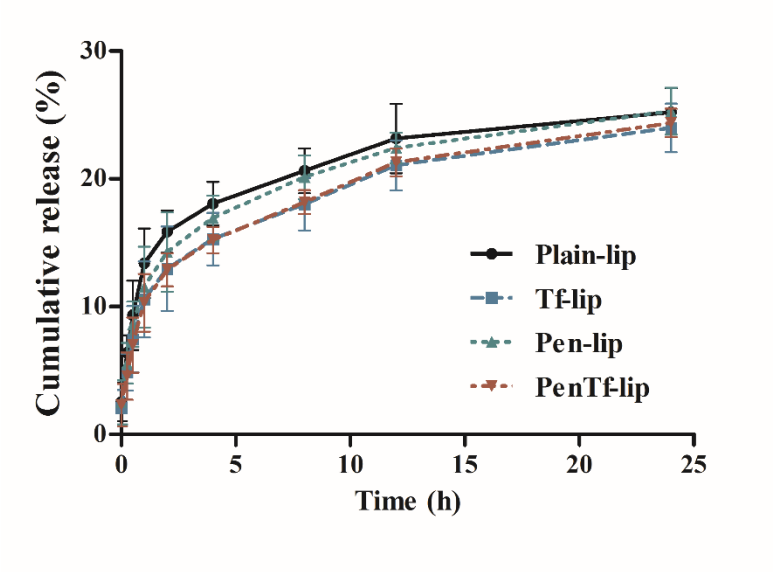

Figure 4. Cumulative release of chitosan-pDNA at N/P ratio 5 from liposomal formulations for up to 24 h. Data expressed as mean ± SD (n=4).

3.5. *In vitro* cytotoxicity assay

Cellular viability after treatment for 4 h with different liposomal phospholipid concentrations (100, 200, 400 and 600 nM) was studied in bEnd.3 (Figure 5), primary astrocytes (Figure 6) and primary neuronal cells (Figure 7). The cytotoxicity was concentration-dependent in all cell lines studied. Cell viability did not significantly decrease at 100 nM phospholipid concentration and more than 90% cells survived till the end of study at 4 h. Cell survival significantly ($p<0.05$) decreased to approximately ~67% at 600 nM phospholipid concentration of liposomal formulations. At 600 nM phospholipid, Mel-lip and MelTf-lip demonstrated 57.8% of cell viabilities, which is significantly ($p<0.05$) lesser as compared to other liposomal formulations at the same phospholipid concentration. This can be due to the cell lytic capabilities of Mel peptide. Corroborating to our findings, Mel has shown concentration and time-dependent cytotoxicity in

studies with lymphocytes and such properties were associated to direct membrane toxicity as well as DNA damage [174,175]. These results demonstrate the low cytotoxic potential of liposomal formulations at 100 nM phospholipid concentration. Therefore, this phospholipid concentration was chosen for the following experiments.

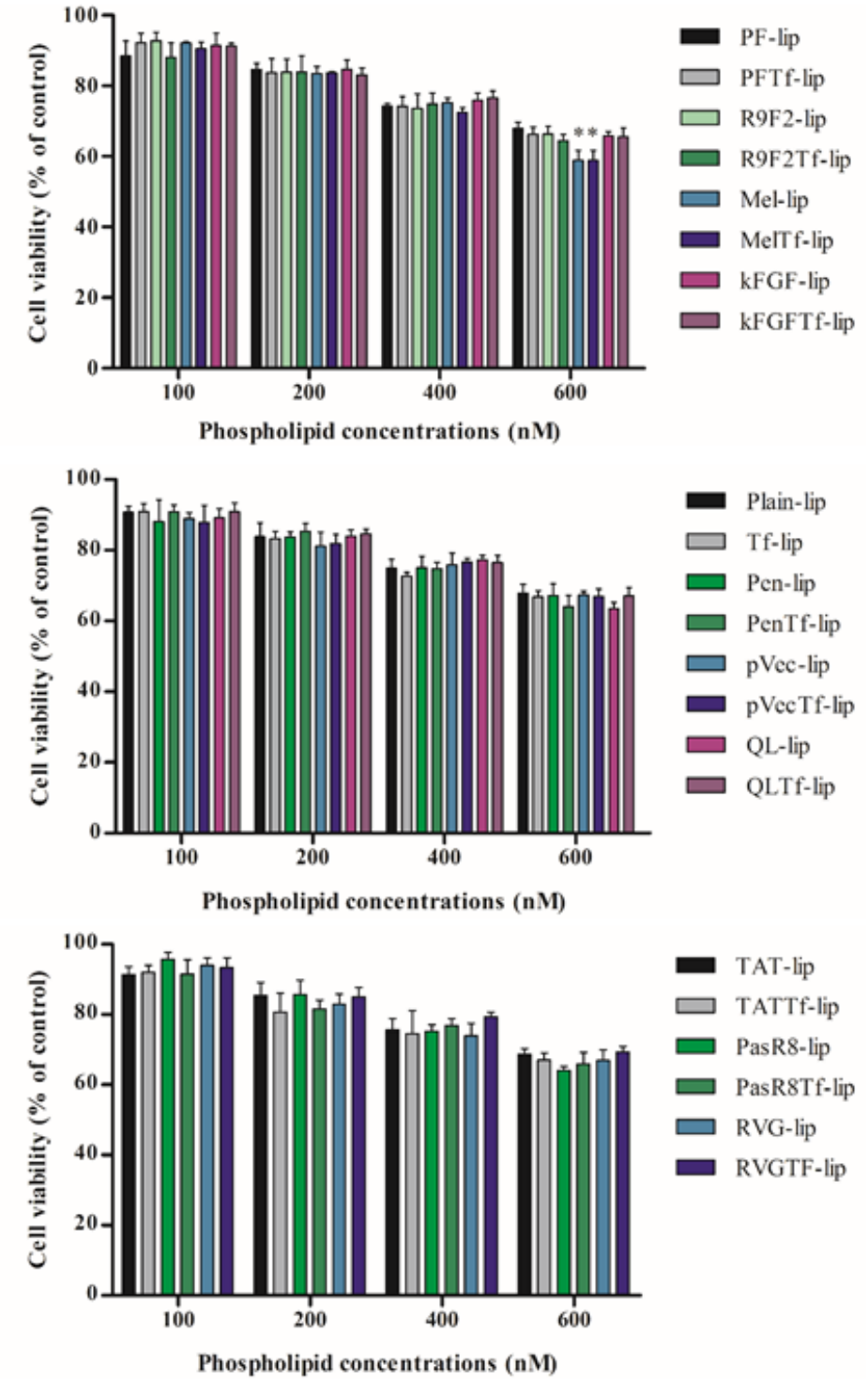

Figure 5. Viability of bEnd.3 cells after incubation with liposomes at different phospholipid concentrations (100, 200, 400 and 600 nM) for 4 h at 37 °C. Cells were incubated for a total of 48 h, after which an MTT assay was performed. Viability of untreated cells were used as control and considered 100%. Data are represented as mean ± SD (n=4). Statistically significant difference ($p<0.05$) are shown as (*).

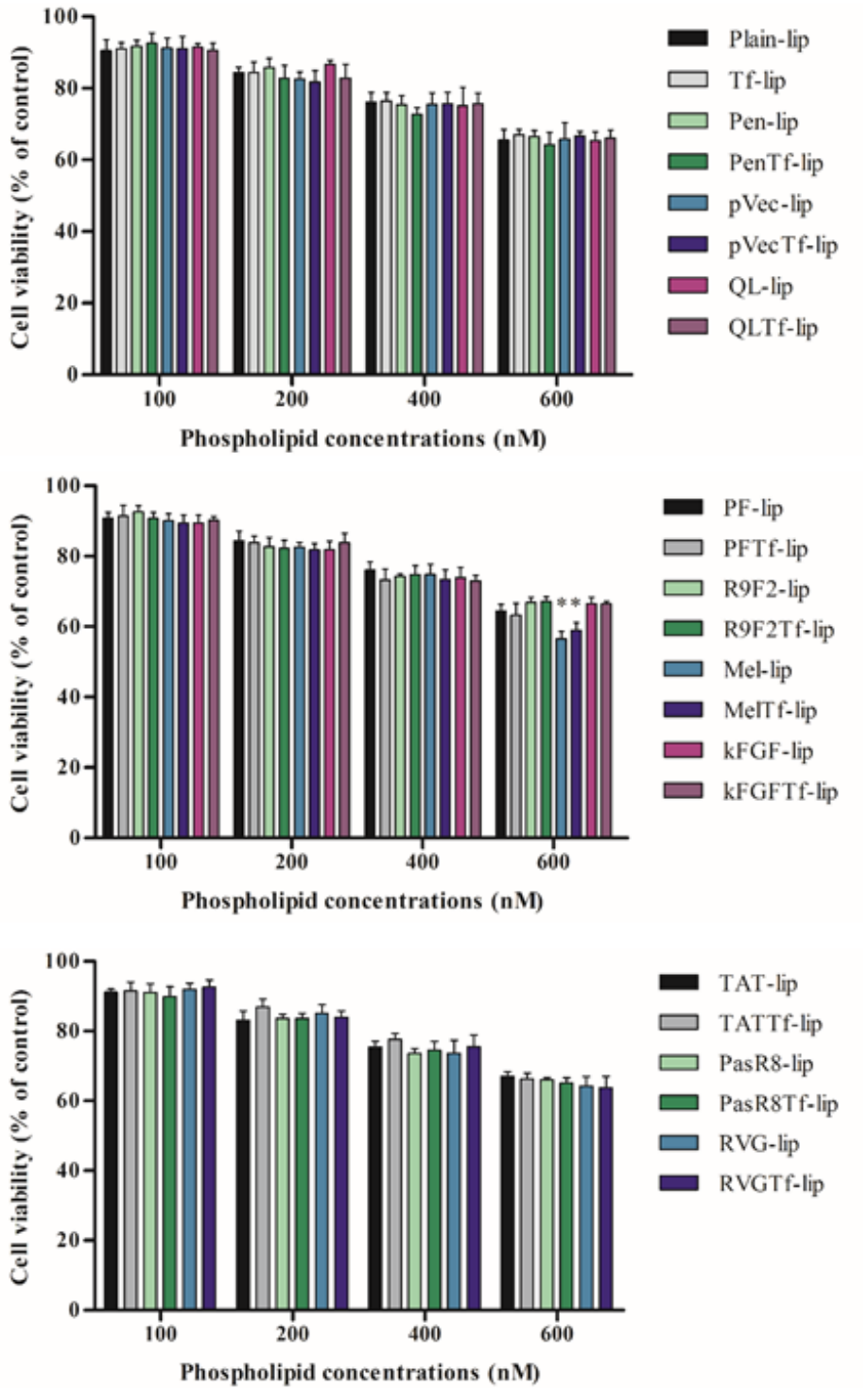

Figure 6. Viability of primary astrocytes cells after incubation with liposomes at different phospholipid concentrations (100, 200, 400 and 600 nM) for 4 h at 37 °C. Cells were incubated for a total of 48 h, after which an MTT assay was performed. Viability of untreated cells were used as control and considered 100%. Data are represented as mean ± SD (n=4). Statistically significant difference ($p<0.05$) are shown as (*).

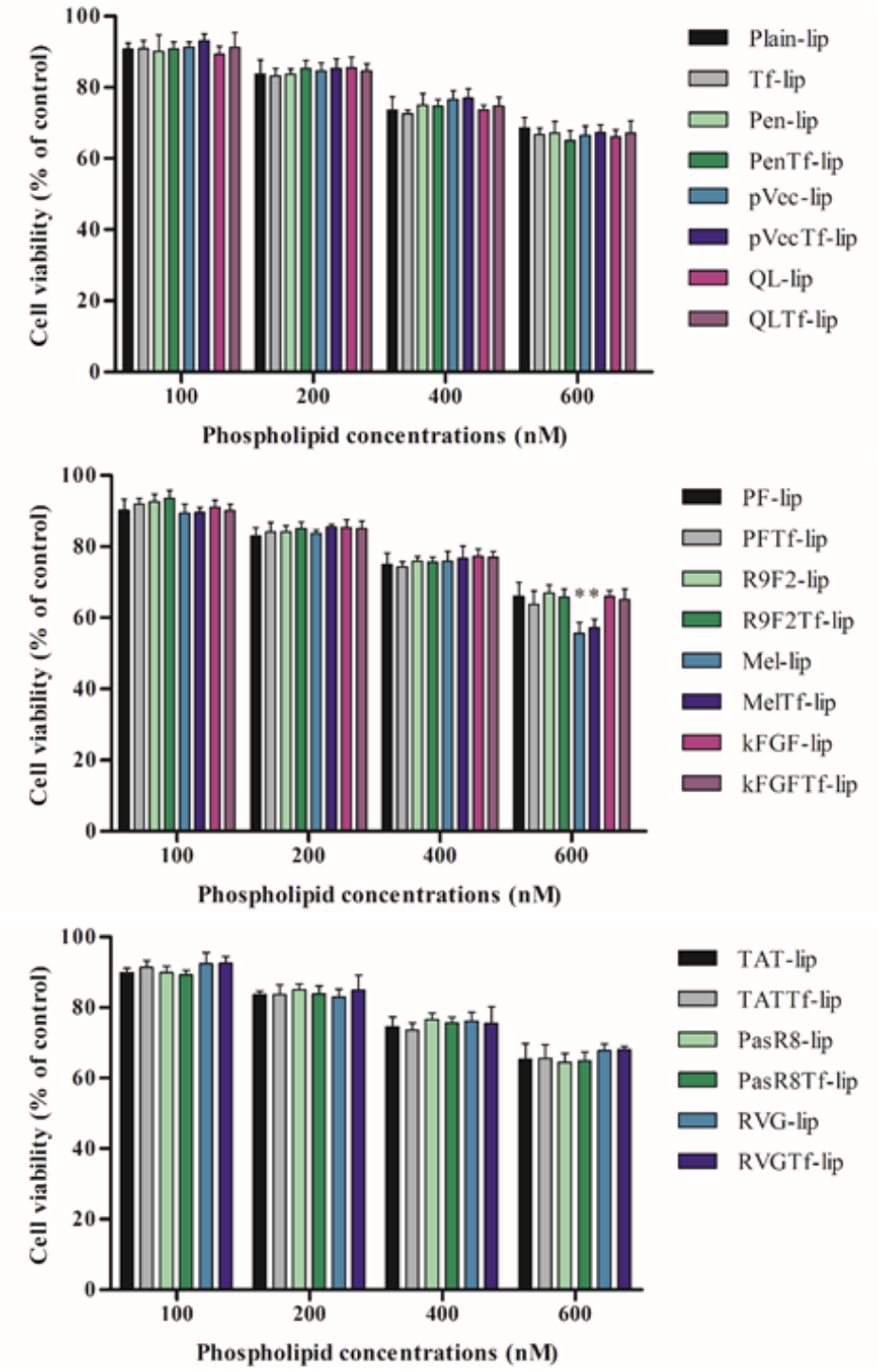

Figure 7. Viability of primary neuronal cells after incubation with liposomes at different phospholipid concentrations (100, 200, 400 and 600 nM) for 4 h at 37 °C. Cells were incubated for a total of 48 h, after which an MTT assay was performed. Viability of untreated cells were used as control and considered 100%. Data are represented as mean ± SD (n=4). Statistically significant difference ($p<0.05$) are shown as (*).

3.6. Cellular uptake

Cellular uptake of liposomes was investigated in bEnd.3, primary astrocytes and primary neuronal cells at different time intervals. Maximum liposome uptake was observed in bEnd.3 cells in 4 h (Figure 8 a) and an increase in incubation time to 6 h led to no significant difference in the uptake. For this cell line, the average uptake of Plain-lip, Tf-lip, Pen-lip and PenTf-liposomes after 4 h was ~78%, while that after 6 h was not significantly different at 81%. Based on this information, the uptake of liposomal formulations in other cells lines was subsequently investigated for up to 4 h. As shown in the Figure 8 a, b and c (bEnd.3), Figure 10 a, b and c (primary astrocytes) and Figure 12 a, b and c (primary neuronal cells), uptake amounts gradually increased from 0.1 h and reached optimal levels at 4 h, which was significantly higher for all formulations compared to other time points ($p<0.05$) in all the three cell lines tested. The uptake of liposomal formulations in bEnd.3 cells was in average 73.6% after 4 h, while the liposomal uptake in primary astrocytes and primary neuronal cells were in average 66.2% and 65.6%, respectively, after 4 h.

Mechanistic understanding of the biological processes that determine the uptake of CPP coupled liposomes as well as CPP and Tf coupled liposomes is important for further development of efficient gene delivery vectors with targeted properties, enhanced cellular internalization and efficient transfection. Liposome internalization into the cells begins with interaction of the liposome moieties to plasma membrane and subsequent activation of transport pathways [176,177], which may occur either *via* endocytosis or direct translocation through plasma membrane. We expected that the selected liposome moieties should trigger the activation of endocytosis through sequence-specific interaction to cellular surface. Furthermore, we also expected differences in liposome uptake among the tested cells due to cell-to-cell variation in

plasma membrane composition including proteoglycans and receptors, which consequently may influence intracellular fate of nanoparticles [177]. Figures 9 a, b and c (bEnd.3), Figure 11 a, b and c (primary astrocytes), and Figure 13 a, b and c (primary neuronal cells) depict the relative liposomal uptake percentages after pre-treatment with endocytosis inhibitors (sodium azide, chlorpromazine, amiloride and colchicine). The depletion of intracellular ATP by pre-incubating cells with sodium azide led to a substantial reduction in cellular internalization of liposomal formulations, which suggested active endocytotic uptake mechanism as the major route for liposome internalization.

The uptake of Plain-lip and Pen-lip in bEnd.3, primary astrocytes and primary neuronal cells occurred through multiple pathways, without predominance of endocytosis routes investigated. While uptake of Tf-lip and PenTf-liposomes occurred preferentially through clathrin-mediated endocytosis, which reduced ~47% for both liposomes compared to control cells. These observations are in accordance with the known endocytosis pathway of Tf-TfR complex and with studies that investigated the uptake of Tf-conjugated liposomes in various cell lines [178–181], thereby emphasizing the role of Tf ligand in liposomal uptake. Penetratin conjugation also assisted liposomal-cell interaction and subsequent internalization, therefore contributing to the liposome uptake through multiple pathways [123,182].

The internalization of pVec-liposomes in bEnd.3 cells showed lower dependence of caveolae-mediated endocytosis pathway, which inhibited 28% the uptake, but greater impact of clathrin-mediated endocytosis and macropinocytosis, corresponding to approximately 70% and 60% uptake inhibition, respectively. In primary astrocytes and primary neuronal cells, similar contribution of the studied pathways was observed in pVec-liposome uptake. Whereas, clathrin- and caveolae-mediated endocytosis were important for pVecTf-liposome uptake in bEnd.3 cells

causing 80% uptake inhibition and macropinocytosis had lower impact, reducing 24% the uptake. Equivalent contribution of the investigated endocytosis pathways was observed on uptake of pVecTf-liposomes in primary astrocytes and primary neuronal cells. Differently, low influence of endocytosis pathways was observed in QL-liposomes uptake in bEnd.3 (less than 20% uptake inhibition for all pathways) and primary astrocyte cells (less than 25% uptake inhibition for all pathways), suggesting that the transport could occur also through passive transport. While clathrin-mediated endocytosis, caveolae-mediated endocytosis and macropinocytosis participated in the uptake of QL-liposomes with equivalent contribution in primary neuronal cells. QLTf-liposomes internalization into the cells showed participation of all three investigated endocytosis pathways. When the same cell lines were pre-incubated with chlorpromazine, the percent uptake of PFTf-lip and R9F2Tf-liposomes was reduced about 70%, which indicates the involvement of clathrin-mediated endocytosis on uptake of dual-functionalized liposomes. Inhibition of macropinocytosis by amiloride reduced significantly ($p<0.05$) the cellular uptake of liposomal formulations, especially of PFTf-lip and R9F2Tf-liposomes. Pretreating cells with colchicine resulted in significant ($p<0.05$) decrease in cellular internalization of PFTf-lip and R9F2Tf-liposomes. The observed difference on the mechanisms of internalization between CPP-liposomes and CPP-Tf-liposomes suggests that interaction of Tf to TfR has important role on the energy-dependent liposome internalization. Concomitant presence of Tf and CPPs on liposome surface propitiated liposome uptake through multisite binding and electrostatic attraction binding and, consequently, maintaining high rate of uptake even in case of TfR saturation.

Mel-liposomes internalization in bEnd.3 cells and primary astrocytes occurred through multiple endocytosis mechanisms, without predominance of either clathrin-mediated endocytosis, caveolae-mediated endocytosis or macropinocytosis. While, the internalization into primary

neuronal cells preferentially occurred *via* caveolae-mediated endocytosis and direct translocation was also observed. Uptake of MelTf-liposomes in bEnd.3, primary astrocytes and primary neuronal cells was driven by multiple endocytosis pathways without significant predominance of one pathway.

Clathrin-mediated endocytosis showed to be the main mechanism for kFGF-lip internalization into bEnd.3 cells, whereas macropinocytosis was that for primary astrocytes and primary neuronal cells. Penetration of kFGF-Tf-lip into primary neuronal cells occurred mainly through clathrin-mediated endocytosis, but there was no preferential route for kFGF-Tf-lip uptake for bEnd.3 cells and primary astrocytes. The translocation potential of kFGF-conjugated cargos has been suggested to be related to the overall hydrophobic composition of the peptide [148]. Our findings are in accordance with earlier reports showing that internalization of hydrophobic CPPs into cells happened mainly *via* endocytotic pathway [183]. Penetration of TAT-liposomes into bEnd.3 and primary neuronal cells showed an average of 79% uptake reduction for clathrin-mediated endocytosis, caveolae-mediated endocytosis and macropinocytosis. While on primary astrocytes cells, macropinocytosis was significantly inhibited (68%). All studied pathways were involved in TATTf-liposomes internalization into the bEnd.3, primary astrocytes and primary neuronal cells. The results suggested that uptake of PasR8-lip and PasR8Tf-lip by the aforementioned cells employs energy-dependent pathways with the involvement of clathrin-mediated endocytosis, caveolae-mediated endocytosis and macropinocytosis. Similarly, the promotion of PasR8 or peptide-modified nanoparticles translocation into cytoplasm was observed to be predominantly an energy-dependent mechanism in different studies [117,141,142]. It suggested the mechanism was based on destabilization of plasma membrane during early stages

of endocytosis. The hydrophobic segment Pas attached to R8 facilitated the peptide-proteoglycan interactions, thereby enhancing their internalization [141,142].

We observed that RVG-liposomes and RVGTf-liposomes were internalized into the cells *via* multiple endocytosis mechanisms. RVG-liposome was predominantly internalized into bEnd.3 cells through macropinocytosis and clathrin-mediated endocytosis, as suggested by the significant ($p<0.05$) inhibition of uptake by amiloride and chlorpromazine pretreatment as compared to control. Amiloride and colchicine pretreatment significantly ($p<0.05$) reduced the uptake of RVGTf-liposomes in primary astrocytes as compared to control indicating this process involved macropinocytosis and caveolae-mediated endocytosis. Hence the study of cellular uptake mechanisms using endocytosis inhibitors suggested that our liposomal formulations were internalized into cells *via* multiple endocytosis pathways including macropynocytosis, clathrin-mediated endocytosis, caveolae-mediated endocytosis and intracellular trafficking. These findings were similarly observed in studies that characterized the uptake mechanisms involved in internalization of RVG-modified nanoparticles into cells [157,162].

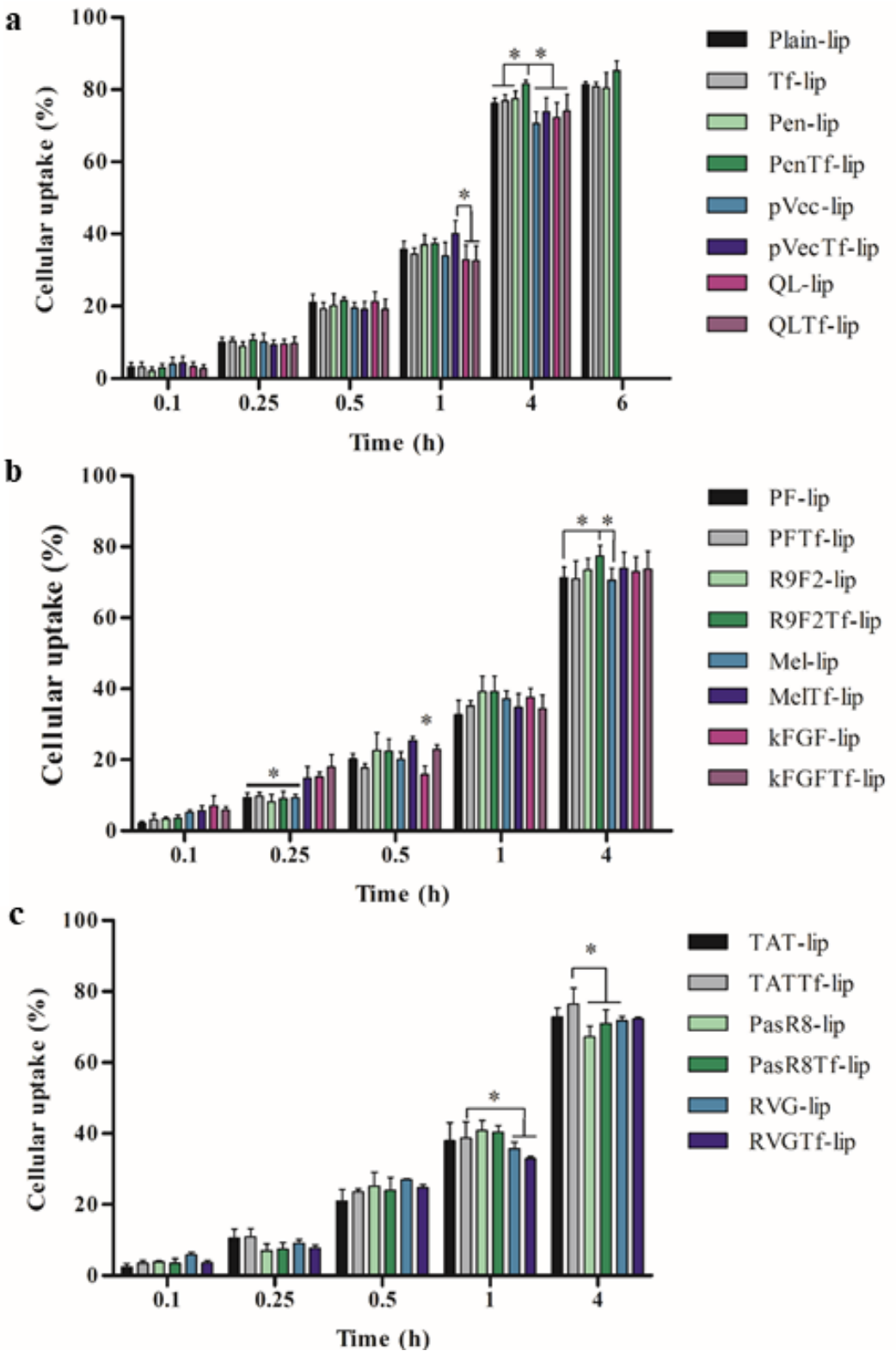

Figure 8. Cellular uptake in bEnd.3 treated with liposomal formulations for 0.1, 0.25, 1, 4 and 6 h (**a**, **b** and **c**). Data expressed as mean ± SD (n=4). Statistically significant difference ($p<0.05$) are shown as (*).

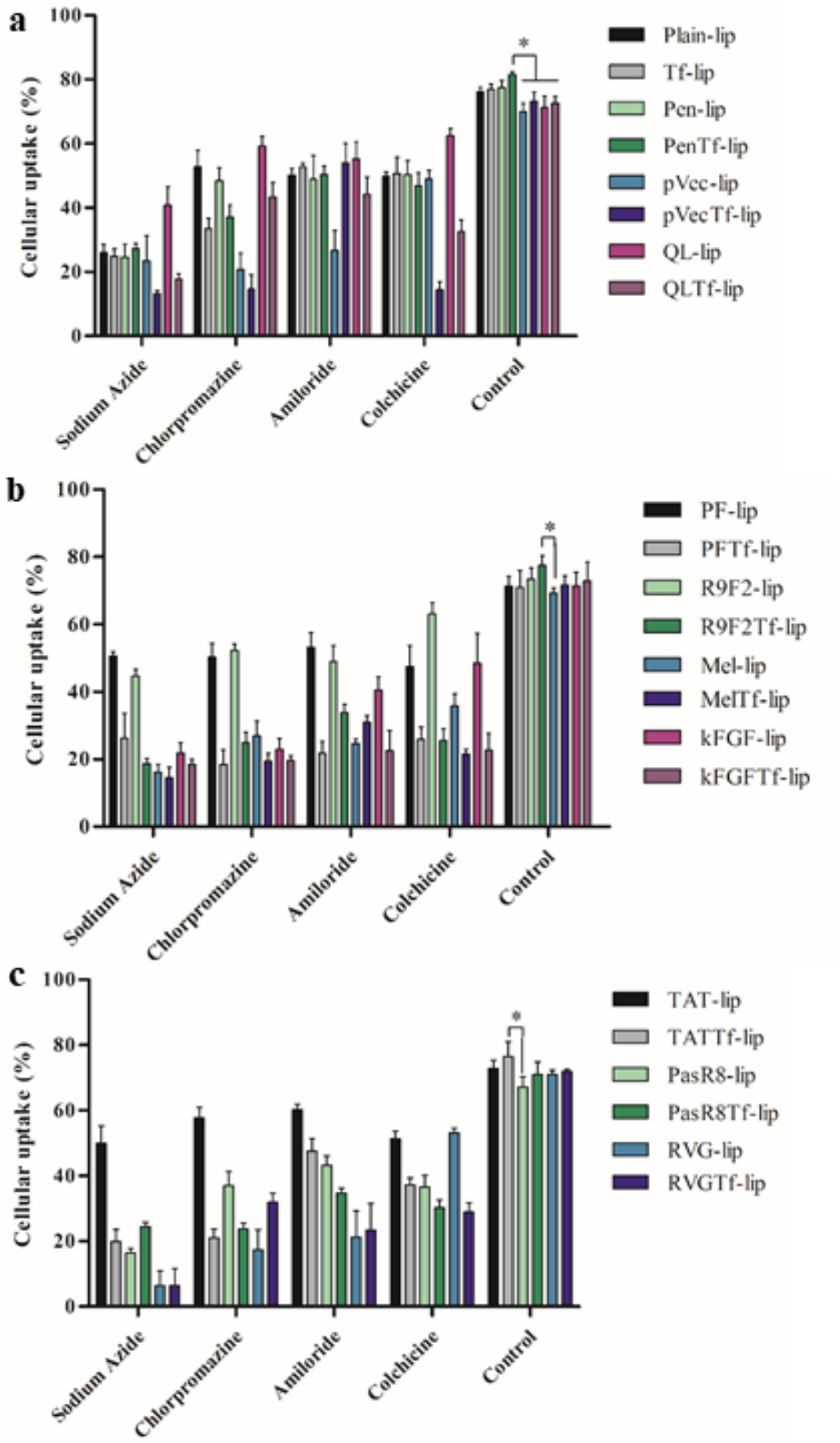

Figure 9. Effect of chemical inhibitors on uptake of liposomal formulations in bEnd.3 (**a**, **b** and **c**) after 4 h of incubation. Data expressed as mean ± SD (n=4). Statistically significant difference ($p<0.05$) are shown as (*).

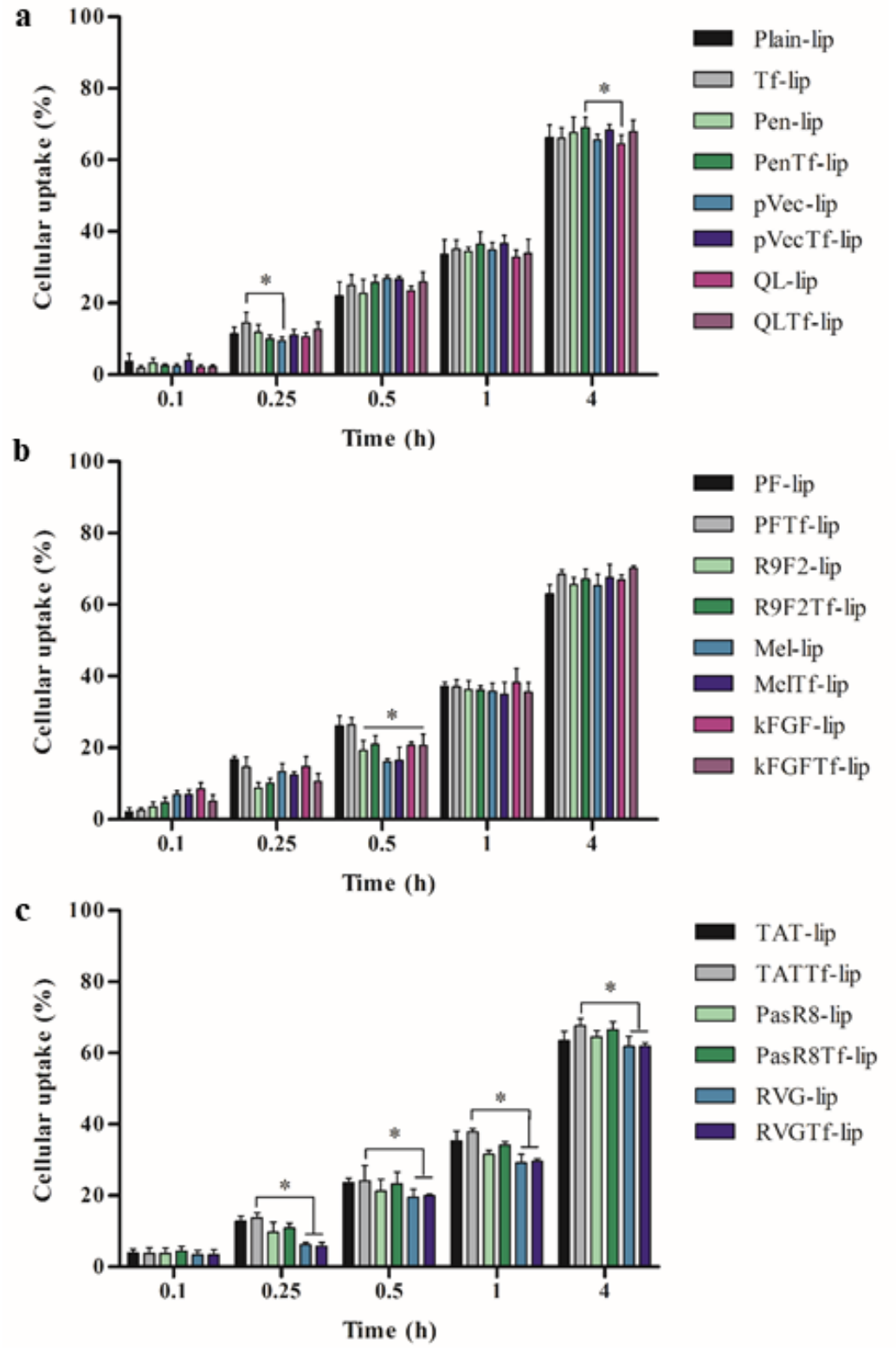

Figure 10. Cellular uptake in primary astrocytes treated with liposomal formulations for 0.1, 0.25, 1 and 4 h (**a**, **b** and **c**). Data expressed as mean ± SD (n=4). Statistically significant differences ($p<0.05$) are shown as (*).

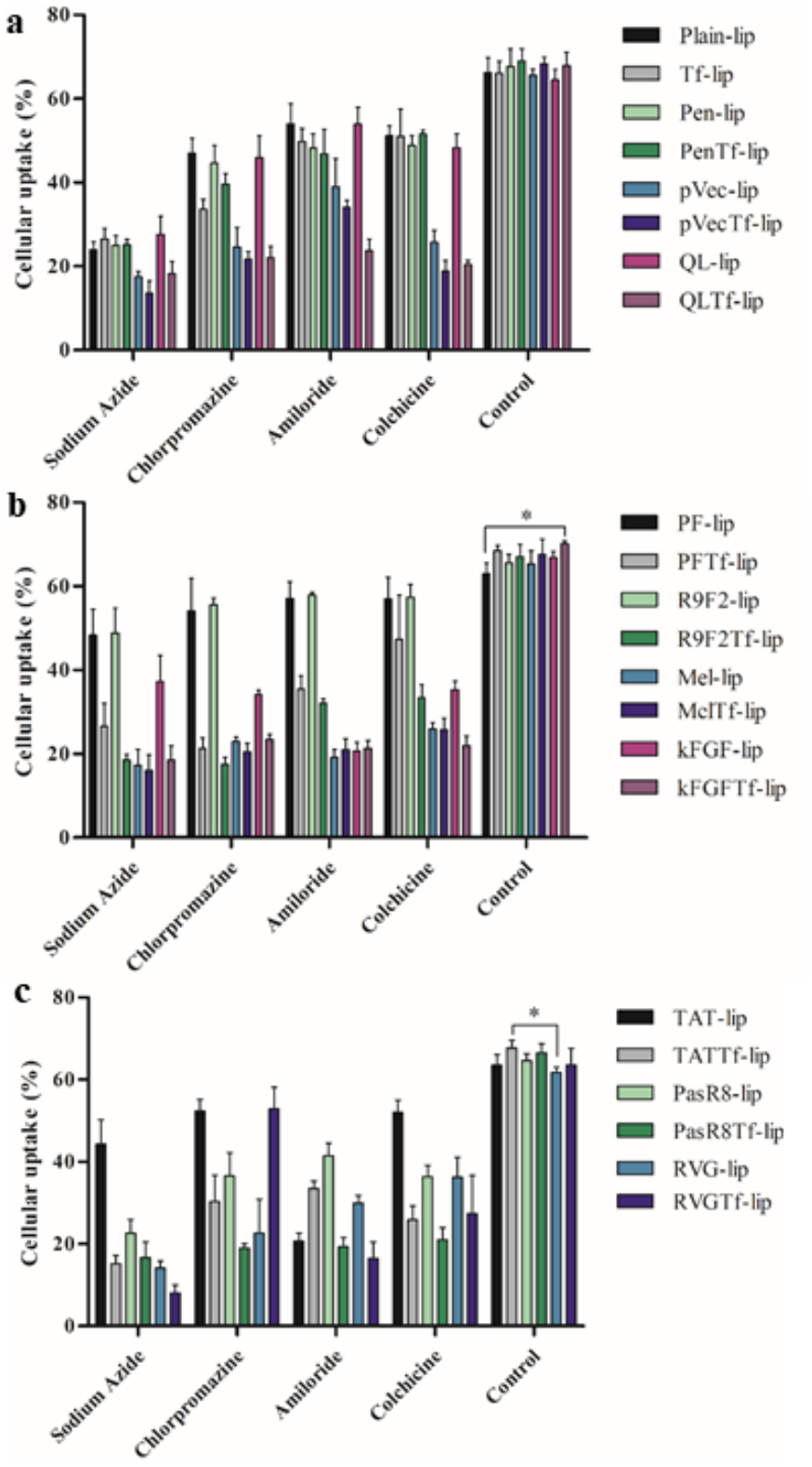

Figure 11. Effect of chemical inhibitors on uptake of liposomal formulations in primary astrocytes (**a**, **b** and **c**) after 4 h of incubation. Data expressed as mean ± SD (n=4). Statistically significant differences ($p<0.05$) are shown as (*).

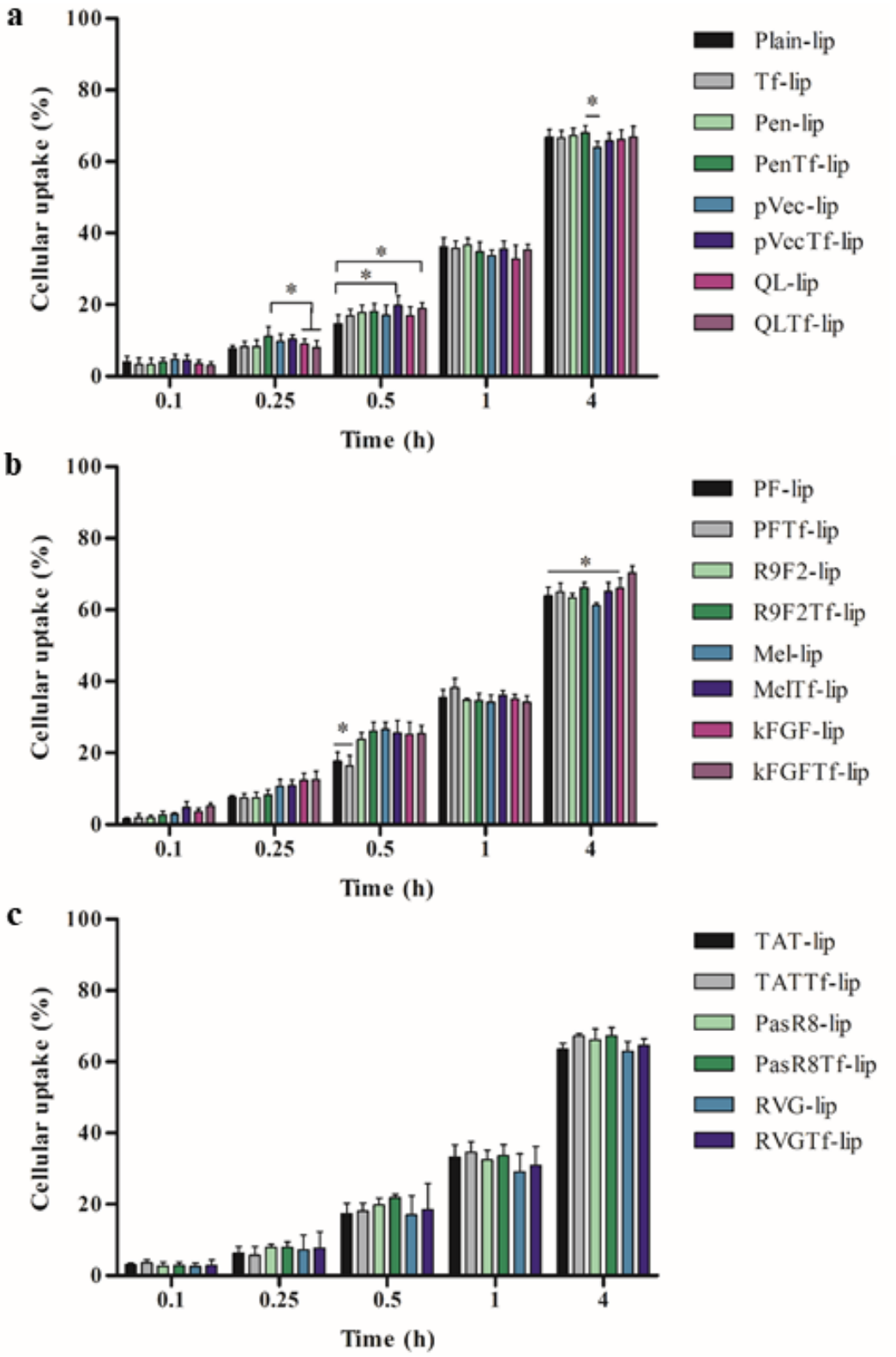

Figure 12. Cellular uptake in primary neuronal cells treated with liposomal formulations for 0.1, 0.25, 1 and 4 h (**a**, **b** and **c**). Data expressed as mean ± SD (n=4). Statistically significant difference ($p<0.05$) are shown as (*).

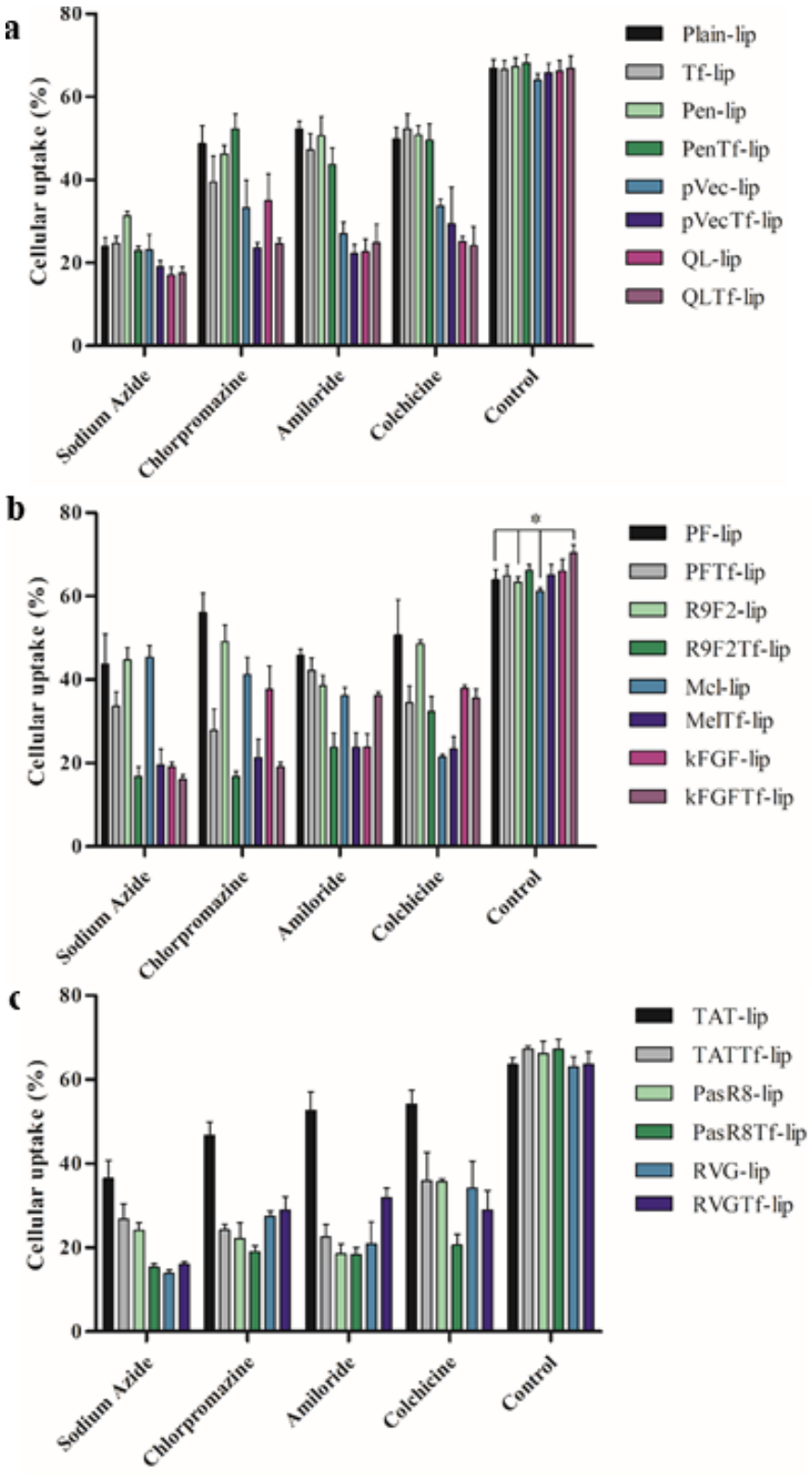

Figure 13. Effect of chemical inhibitors on uptake of liposomal formulations in primary neuronal cells (**a**, **b** and **c**) after 4 h of incubation. Data expressed as mean ± SD (n=4). Statistically significant difference ($p<0.05$) are shown as (*).

3.7. *In vitro* transfection efficiency

The efficiency of liposomal formulations as a gene carrier was evaluated in bEnd.3, primary astrocytes and primary neuronal cells using pβgal, pGFP, pNGF and pApoE2. The cell lines used in these experiments comprise the BBB and therefore they can be used as a model to evaluate the transfection in the targeted biological barrier. We observed that CPPTf-liposomes containing chitosan-pβgal complexes showed significantly ($p<0.05$) higher ability to induce protein expression in bEnd.3 (Figure 14 a) compared to the respective CPP-liposome. This trend was also observed in primary astrocytes (Figure 14 b) and primary neuronal cells (Figure 14 c). The protein expression was induced in differential extent in the tested cells. The highest levels of proteins were quantified in bEnd.3 cells, followed by primary astrocytes and primary neuronal cells.

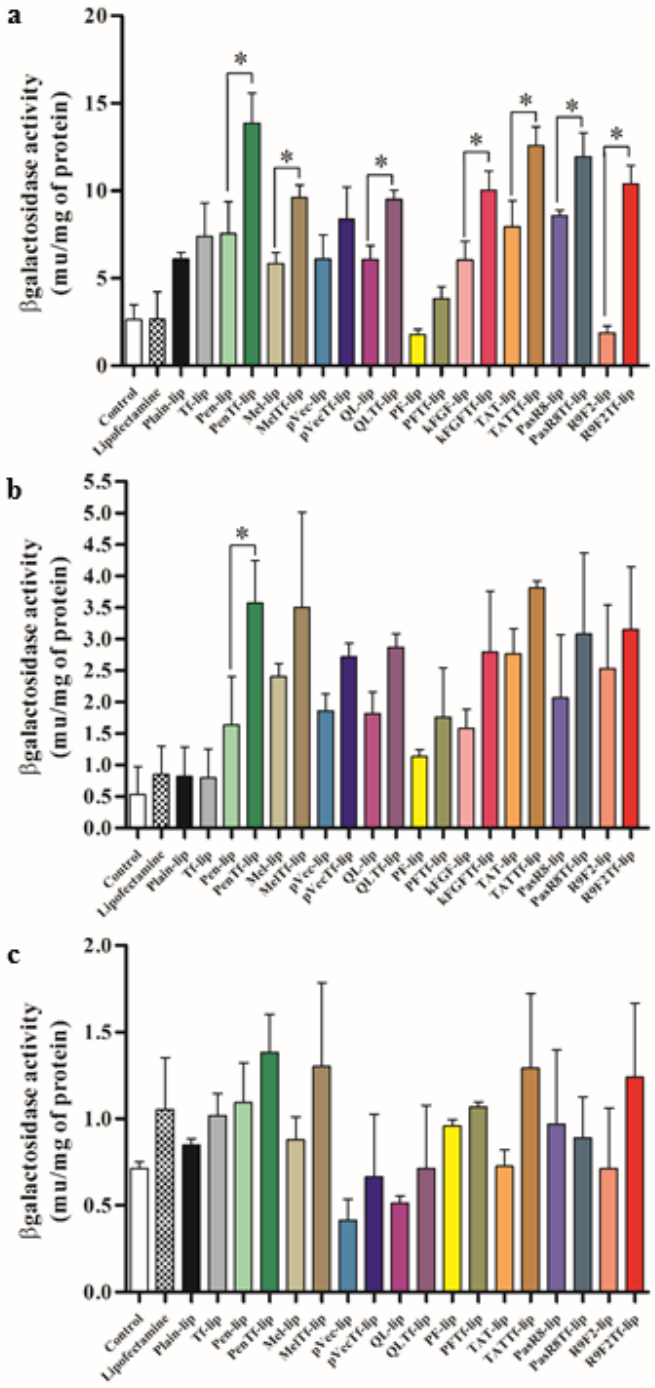

Figure 14. β-galactosidase expression levels 48 h after transfection in bEnd.3 cells (**a**), primary astrocytes (**b**) and primary neuronal cells (**c**) treated with liposomal formulations containing chitosan-pβgal complexes (1μg). Data expressed as mean ± SD (n=4). Statistically significant differences ($p<0.05$) are shown as (*).

Following the same trend observed on transfection studies with liposomes containing chitosan-pβgal complexes, liposomal formulations conjugated with both CPP and Tf could induce higher GFP gene levels in bEnd.3 (Figure 15 a), primary astrocytes (Figure 15 b) and primary neuronal cells (Figure 15 c) as compared to liposomes conjugated only with CPP. The expression of GFP in bEnd.3 (Figure 16), primary astrocytes (Figure 17) and primary neuronal cells (Figure 18) was also observed using a fluorescence microscope. Differential extent of GFP expression was observed in each cell line with bEnd.3 cells expressing the highest levels, followed by primary astrocytes and primary neuronal cells, subsequently.

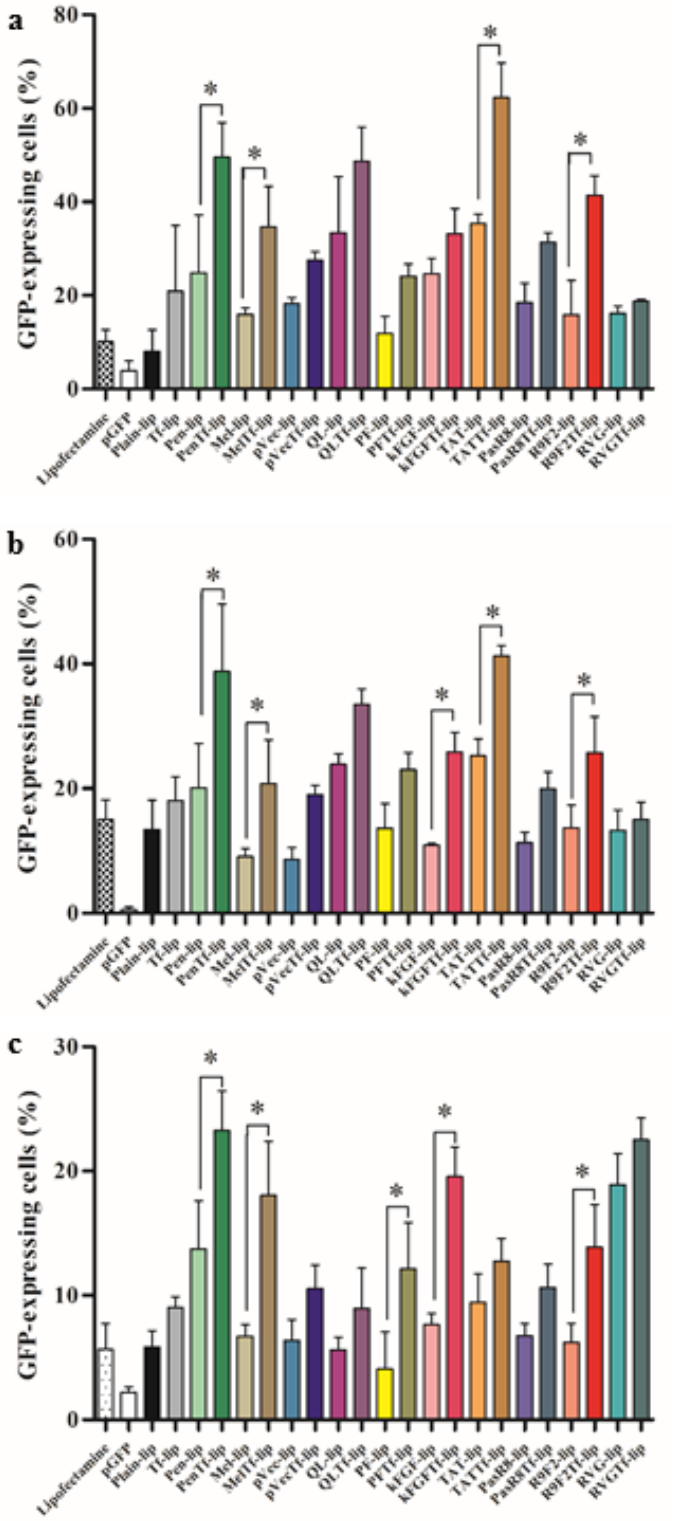

Figure 15. GFP expression levels 48 h after transfection in bEnd.3 cells (**a**), primary astrocytes (**b**) and primary neuronal cells (**c)** treated with liposomal formulations containing chitosan-pGFP complexes (1µg). Data expressed as mean ± SD (n=4). Statistically significant differences ($p<0.05$) are shown as (*).

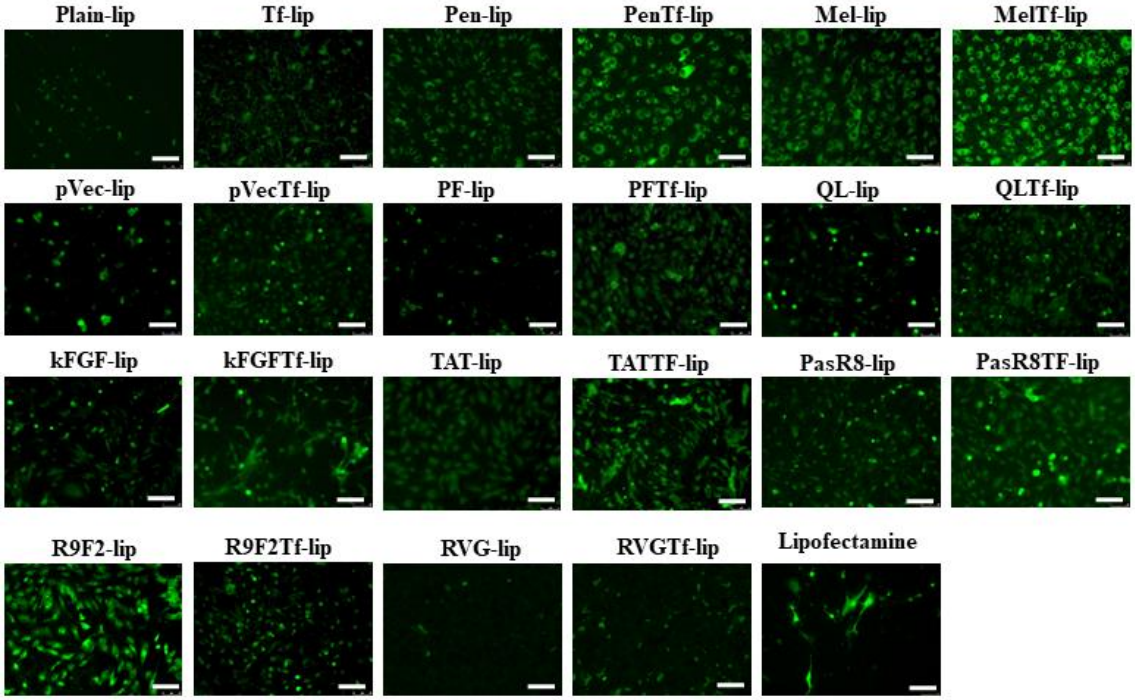

Figure 16. Fluorescence microscopy images of GFP expression in bEnd.3 treated with liposomal formulations encapsulating 1µg chitosan-pGFP complexes. Scale bar, 100 µm.

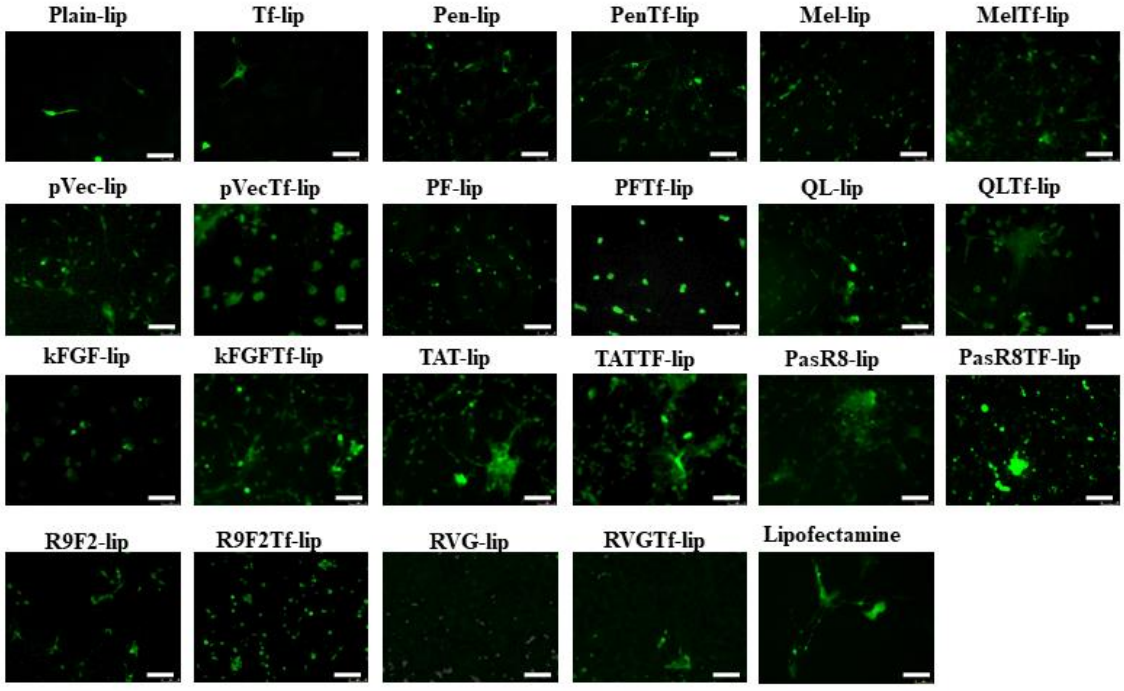

Figure 17. Fluorescence microscopy images of GFP expression in primary astrocytes treated with liposomal formulations encapsulating 1µg chitosan-pGFP complexes. Scale bar, 100 µm.

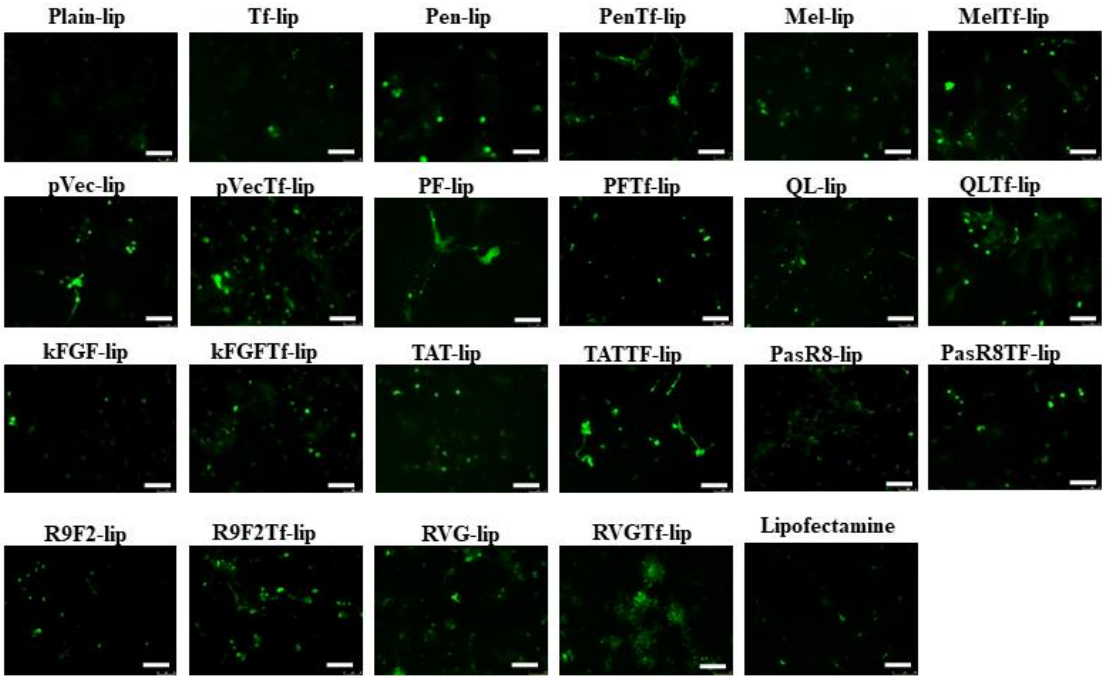

Figure 18. Fluorescence microscopy images of GFP expression primary neuronal cells treated with liposomal formulations encapsulating 1µg chitosan-pGFP complexes. Scale bar, 100 µm.

The induction of NGF expression by liposomal formulations containing chitosan-pNGF complexes investigated in bEnd.3 (Figure 19 a), primary astrocytes (Figure 19 b) and primary neuronal cells (Figure 19 c) showed significant ($p<0.05$) increase in NGF expression after treatment of the aforementioned cells with dual-functionalized liposomes as compared to cellular basal NGF levels and the positive control Lipofectamine 3000/pNGF treatment. Surface modifications on liposomes individually increased the gene expression and dual modification enlarged it.

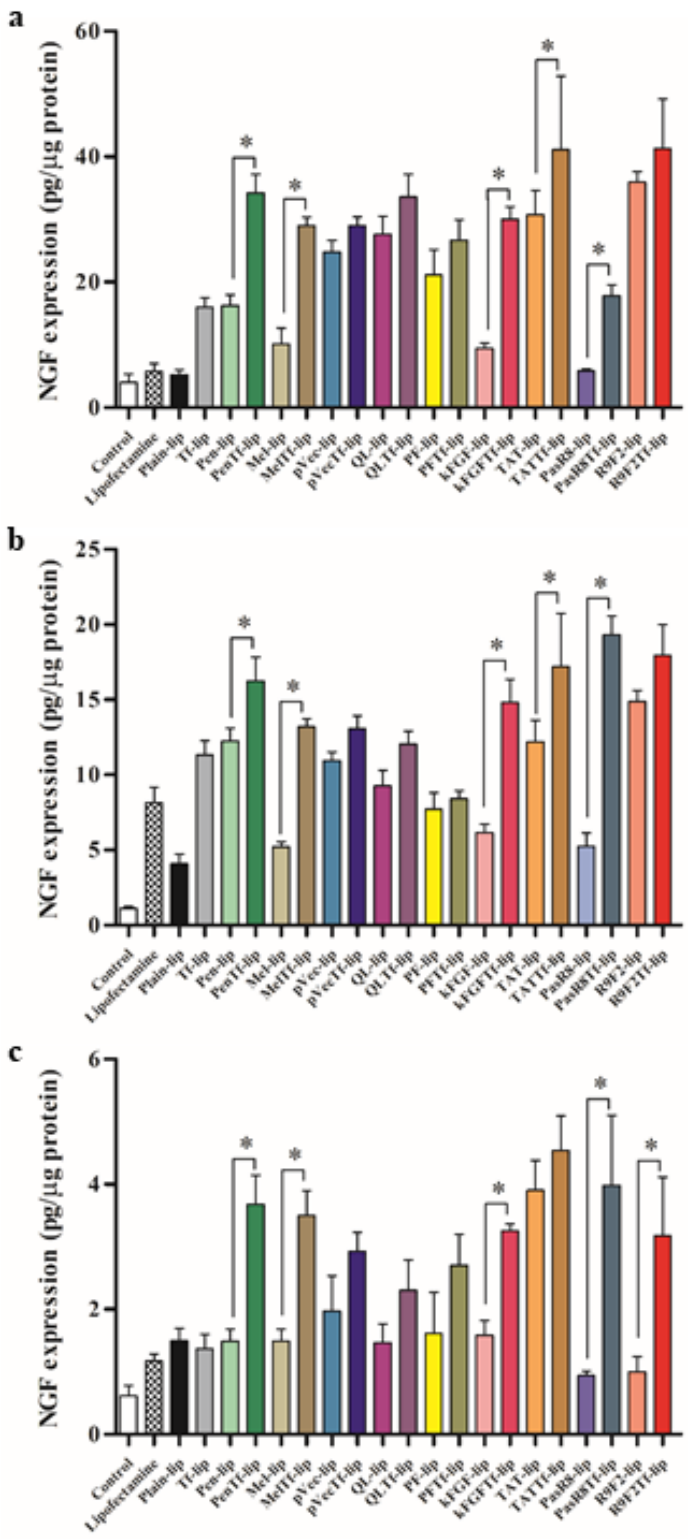

Figure 19. NGF expression levels 48 h after transfection in bEnd.3 cells (**a**), primary astrocytes (**b**) and primary neuronal cells(**c**) treated with liposomal formulations containing chitosan-pNGF complexes (1µg). Data expressed as mean ± SD (n=4). Statistically significant ($p<0.05$) differences are shown as (*).

Evaluation of ApoE levels in bEnd.3 (Figure 20 a), primary astrocytes (Figure 20 b) and primary neuronal cells (Figure 20 c) after treatment with liposomal formulations containing chitosan-pApoE2 complexes showed the enhanced ability of PenTf-liposomes to significantly ($p<0.05$) increase ApoE levels as compared to Plain-lip, Tf-lip, Pen-lip, endogenous ApoE levels, naked ApoE2 and Lipofectamine 3000/pApoE2 treatment in the aforementioned cells.

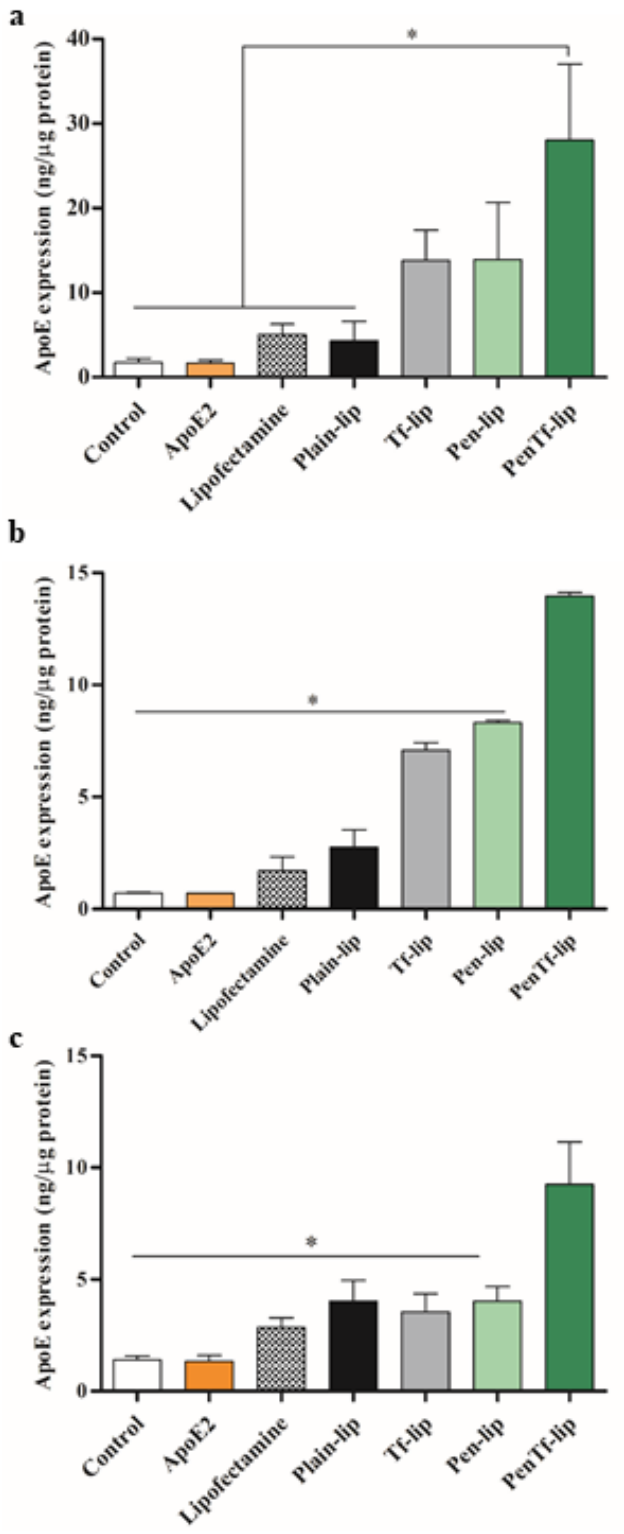

Figure 20. ApoE expression levels 48 h after transfection in bEnd.3 cells (**a**), primary astrocytes (**b**) and primary neuronal cells(**c**) treated with liposomal formulations containing chitosan-pApoE2 complexes (1µg). Data expressed as mean ± SD (n=4). Statistically significant ($p<0.05$) differences are shown as (*).

Our findings are in good accordance with studies that demonstrated the enhancement in transfection provided by liposome modified with specific ligands [74,184,185]. Additionally, combination to transferrin-receptor targeting has consolidated to be a consistent strategy for both targeting properties and enhanced transfection [78,186,187].

3.8. Endosomal escape

Endosomal escape of formulations in bEnd.3 cells was investigated by treating the cells with sucrose, a lysosomotropic agent that causes osmotic inflow of water into lysosomes, thereby reducing nuclease-mediated degradation [169]. Enhancement in transfection efficiency by sucrose was quantified using a GFP reporter gene. As shown in Figure 21 a, transfection efficiencies in bEnd.3 cells treated with sucrose and pGFP, Plain-lip, Tf-lip, Pen-lip or PenTf-liposomes were 1.3±0.1%, 16.0±1.6%, 16.6±0.8%, 27.2±7.8% and 48.6±12.8%, respectively. Significant ($p<0.05$) enhancement in transfection in bEnd.3 cells treated with Plain-liposomes + sucrose was observed compared to Plain-liposomes without sucrose, as evident by the increased fluorescent signal produced in the cells. In contrast, other treatment groups (pGFP, Tf-lip, Pen-lip and PenTf-liposomes + sucrose) did not enhance the transfection efficiency in bEnd.3 cells significantly ($p<0.05$) compared to the respective treatments without sucrose. As earlier observed, PenTf-liposomes showed higher capacity to transfect bEnd.3 cells irrespective of presence of sucrose compared to the other liposomal formulations. Fluorescence microscopy images of cells treated with liposomal formulation expressing GFP confirmed the quantitative analysis (Figure 21 b).

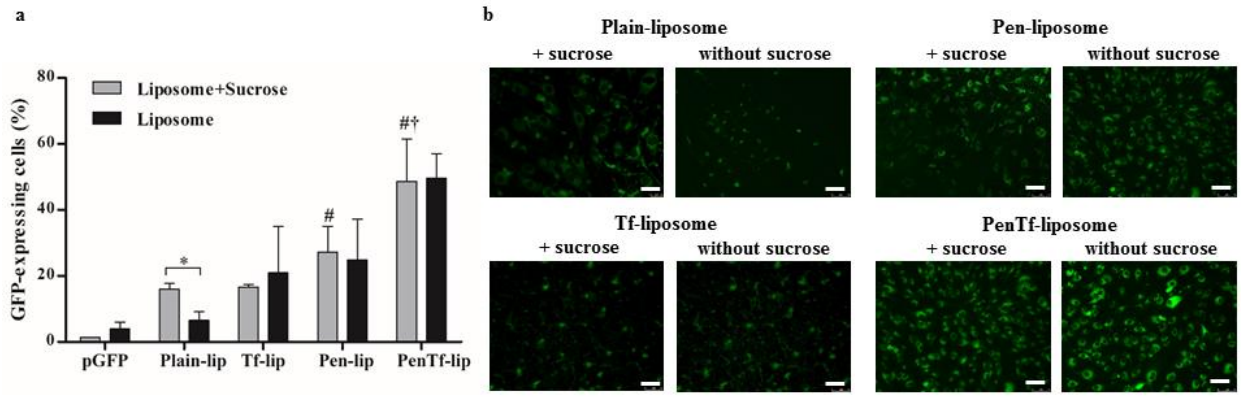

Figure 21. Assessment of ability of liposomes to escape endosome. (**a**) GFP expression levels 48 h after transfection in bEnd.3 cells treated with or without 50 mM sucrose and Plain-lip, Tf-lip, Pen-lip or PenTf-liposomes containing chitosan-pGFP complexes (1µg). Data expressed as mean ± SD (n=4). Statistically significant differences ($p<0.05$) are shown as (*) with Plain-liposome, (#) with pGFP+sucrose and (†) with Pen-lip+sucrose. (**b**) Fluorescence microscopy images of GFP expression in bEnd.3 cells treated with or without 50 mM sucrose and Plain-, Tf-, Pen- or PenTf-liposomes containing chitosan-pGFP complexes (1 µg). Scale bar, 100 µm.

3.9. Effect of PenTf-liposomes containing chitosan-pNGF on formation of new synaptic vesicles in primary neuronal cells

In AD, mounting evidence has demonstrated the role of Aβ deposition in synaptic dysfunction which leads to cognitive decline as well as reduction in synaptic markers [188]. Protection of synapses has been identified as a potential approach for treatment of AD by attenuating the cognitive deficits [189,190]. Knowing that NGF modulates the functional integrity of cholinergic neurons in the CNS, hence, NGF therapy may also potentially treat AD by promoting synapses protection. We investigated the effect of PenTf-liposomes containing chitosan-pNGF complexes treatment on formation of new synaptic vesicles in primary neuronal cells through quantification of synaptophysin levels. Synaptophysin is an abundant membrane protein of synaptic vesicles and it is considered a pre-synaptic marker. Studies with AD mouse models and AD patients have correlated the progressive loss of synaptophysin with cognitive decline and AD severity [188,191,192]. We performed qualitative (Figure 22 a) and quantitative

(Figure 22 b) evaluation of synaptophysin levels in different time points after the treatment of the cells. We observed that the levels of synaptophysin, i.e. number of synaptic vesicles, significantly ($p<0.05$) increased after 24 h of the treatment as compared to control levels and maximal relative fluorescence was observed after 48 h. After 14 days of the treatment, the number of synaptic vesicles was no different than that of control.

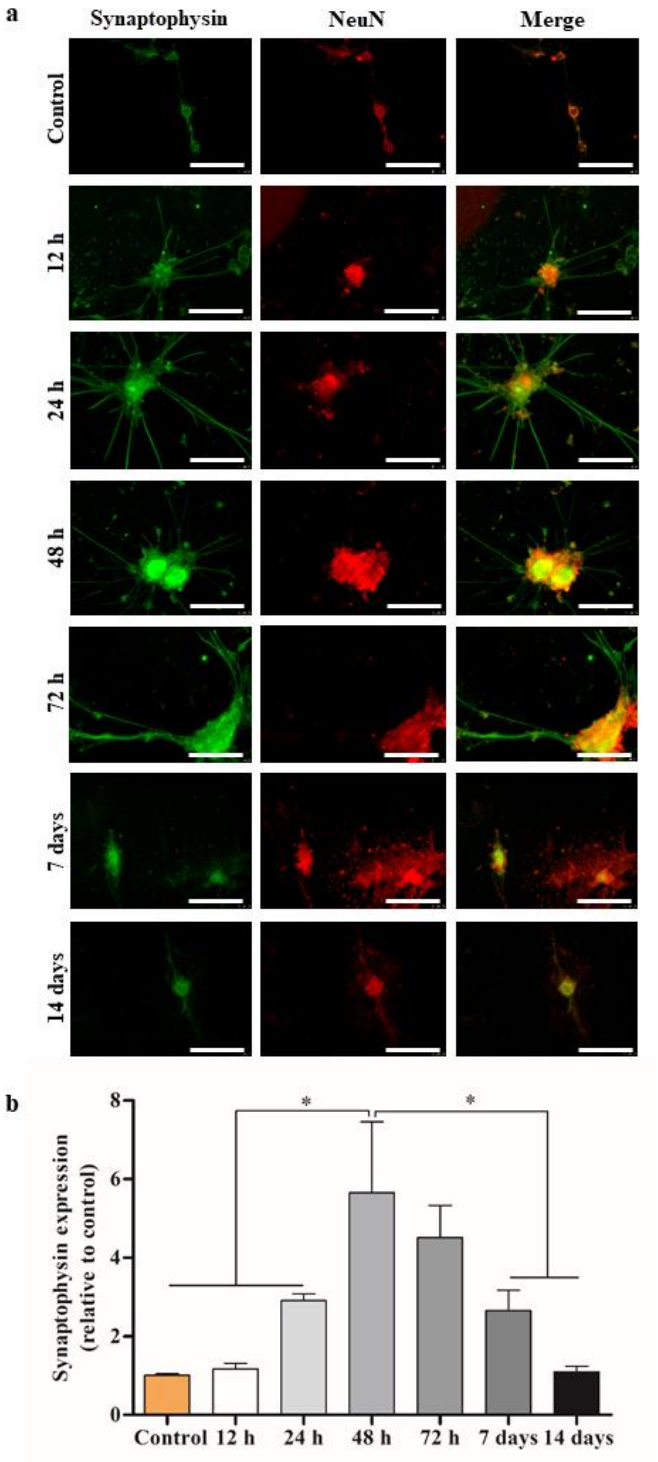

Figure 22. a) Effect of PenTf-liposomes containing chitosan-pNGF complexes (1 µg) treatment on formation of new synaptic vesicles in primary neuronal cells assessed in predetermined time points (12 h, 24 h, 48 h, 72 h, 7 days and 14 days after the treatment). Cells were stained with anti-synaptophysin antibody (green) and anti-NeuN antibody (red). Scale bar, 100 µm. **b**) Relative expression of Synaptophysin in primary neuronal cells after 12 h, 24 h, 48 h, 72 h, 7 days and 14 days of treatment with PenTf-liposomes containing chitosan-pNGF complexes (1 µg).

3.10. Transport across *in vitro* BBB

A significant number of potential formulations for the treatment of CNS diseases fail to bypass the BBB. Therefore, it is relevant to characterize BBB permeability of these candidates in a reliable *in vitro* BBB model. This system can provide a better understanding of mechanisms involved in crossing such tight barrier and can allow the screening as well as the optimization of candidate formulations [165,193]. The *in vitro* BBB model was developed co-culturing brain endothelial cells (bEnd.3 cells) on the upper surface of culture inserts, primary astrocytes seeded on the lower surface of the culture insert and primary neuronal cells on the bottom of the culture wells. This configuration provides close resemblance to the cell arrangement at the neurovasculature unit thereupon it has become a more widely accepted model [194]. In the developed *in vitro* BBB, TEER of cell culture inserts containing either bEnd.3 cells in the upper side of inserts or primary astrocytes on underside of inserts showed TEER of about 191.9±6.1 Ωcm^{-2} and 135.7±2.4 Ωcm^{-2}, respectively as shown in Figure 23 a. TEER of co-cultured insert was significantly ($p<0.05$) higher (401.5±7.3 Ωcm^{-2}) than the monolayer models, and there was no evident change in resistance after the co-culture was confluent (Figure 23 a). Astrocytes are postulated to increase the tightness of endothelial monolayers as reflected by the TEER values of the co-culture. The BBB model was characterized based on TEER values and permeability to sodium fluorescein (Na-Fl), a barrier integrity marker.

Using fluorescently labelled-liposomes, we showed that liposome transport across the *in vitro* co-culture BBB model occurred over time (Figure 23 b, c and d). Furthermore, the results were suggestive that transferrin receptor-targeting aided in the interaction of CPPTf-liposomes to Tf receptor on cell surface enhancing the transport across the *in vitro* barrier layer. Participation of Tf on liposome translocation also suggested the involvement of clathrin-mediated endocytosis

in this process. After 8h, approximately 10.1% of liposomal formulations crossed the *in vitro* BBB model and PenTf-liposomes showed the best ability to cross the barrier layer (15.2%). The permeability coefficients of the formulations were 2.1-fold to 5.2-fold higher as compared to that of Na-Fl (Figure 23 e). Despite the significantly ($p<0.05$) higher permeability of the liposomal formulations when compared to Na-Fl, the values of TEER (Figure 23 f) strongly indicate that liposomes did not cause membrane disruption or cellular damage after transport investigation. Therefore, the integrity of the cellular barrier was maintained throughout the experiment.

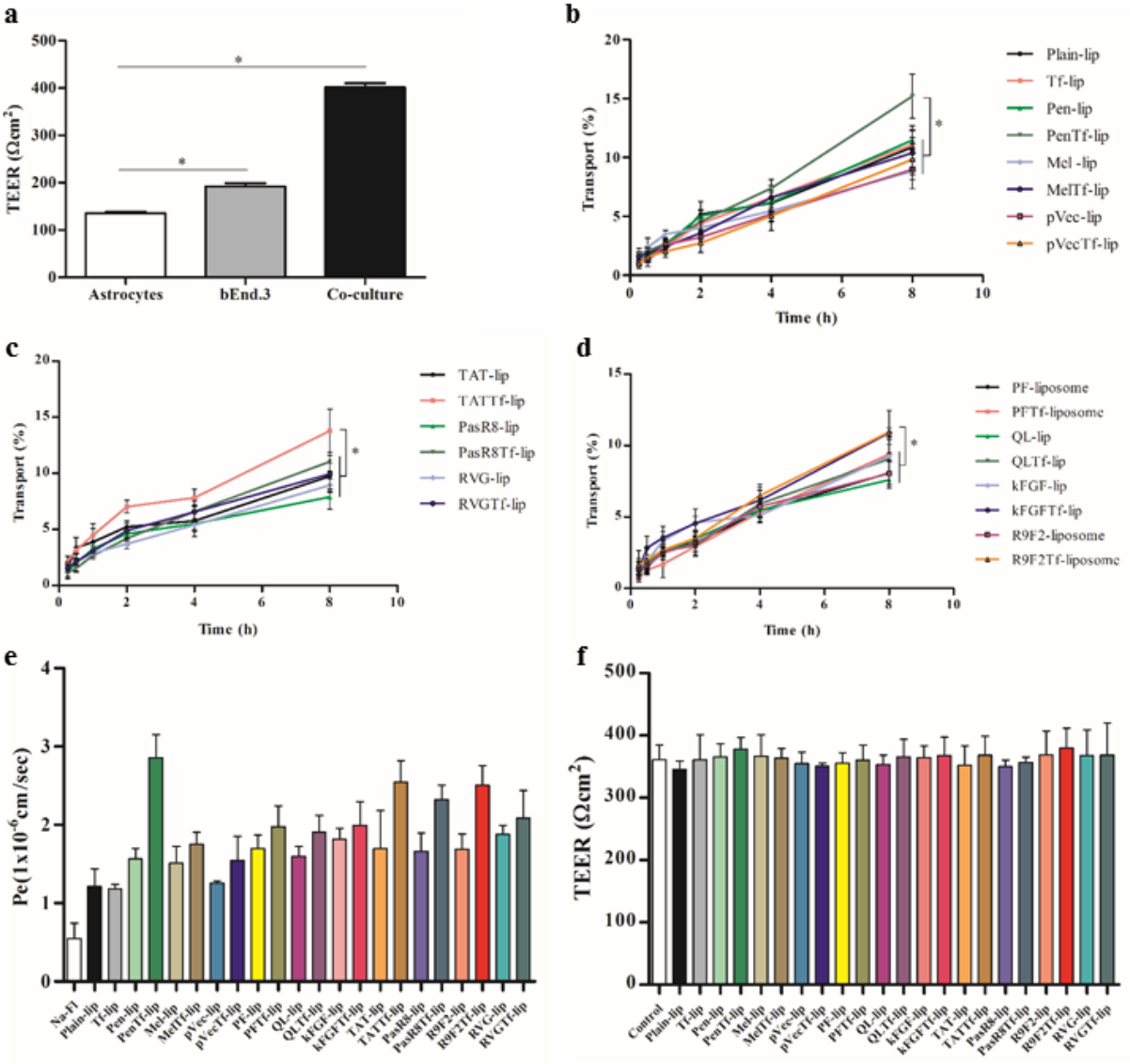

Figure 23. a) Transendothelial electrical resistance (TEER, expressed as Ωcm-2) of different BBB models constructed using astrocytes and bEnd.3 monolayers and co-culture of bEnd.3 and astrocytes. A significantly higher statistical difference in the TEER values between the groups was noted (*$p<0.05$). Liposomal transport through BBB model over a period of 8 h (**b**, **c** and **d**). Statistically significant differences are shown as (*). **e**) Endothelial cell permeability (Pe, expressed in $1x10^{-6}$ cm/s) coefficient for sodium fluorescein (Na-Fl) and liposomal formulations. **f**) TEER of co-cultured BBB model before and after 8 h of transport study upon incubation with liposomal formulations. All data are expressed as mean ± SD (n=4).

3.11. Transfection efficiency in primary neuronal cells after liposome transport across *in vitro* BBB model

The ability of dual modified liposomes to transfect primary neuronal cells after crossing the *in vitro* BBB model was assessed using plasmid GFP, plasmid NGF and plasmid ApoE2. We observed that the liposomes were able to transfect primary neuronal cells indicating that the nanoparticles were able to cross the *in vitro* BBB model and, thereafter, deliver the plasmid DNA into the nucleus of primary neuronal cells. PenTf-lip and TATTf-lip containing chitosan-pGFP complexes increased GFP expression in primary neuronal cells in average 7.1%. Plain-lip, Tf-lip, Pen-liposomes and QLTf-lip increased GFP expression in average 2.9%. While MelTf-lip, pVecTf-lip, PFTf-lip, kFGFTf-lip, PasR8Tf-lip, R9F2Tf-lip and RVGTf-lip increased GFP expression in average 5.4% (Figure 24 a). Fluorescence images of transfected cells confirmed the flow cytometry results (Figure 24 b). Similar transfection efficiency was observed with liposomes containing chitosan-pNGF complexes (Figure 25), which PenTf-lip and TATTf-liposomes showed superior ability to induce NGF production in primary neuronal cells.

Regarding liposomal formulation containing chitosan-pApoE2 complexes, PenTf-liposomes induced significantly ($p<0.05$) higher ApoE expression in primary neuronal cells after transport across the *in vitro* BBB model as compared to Plain-lip, Tf-lip and Pen-liposomes induced levels and cellular basal levels (Figure 26).

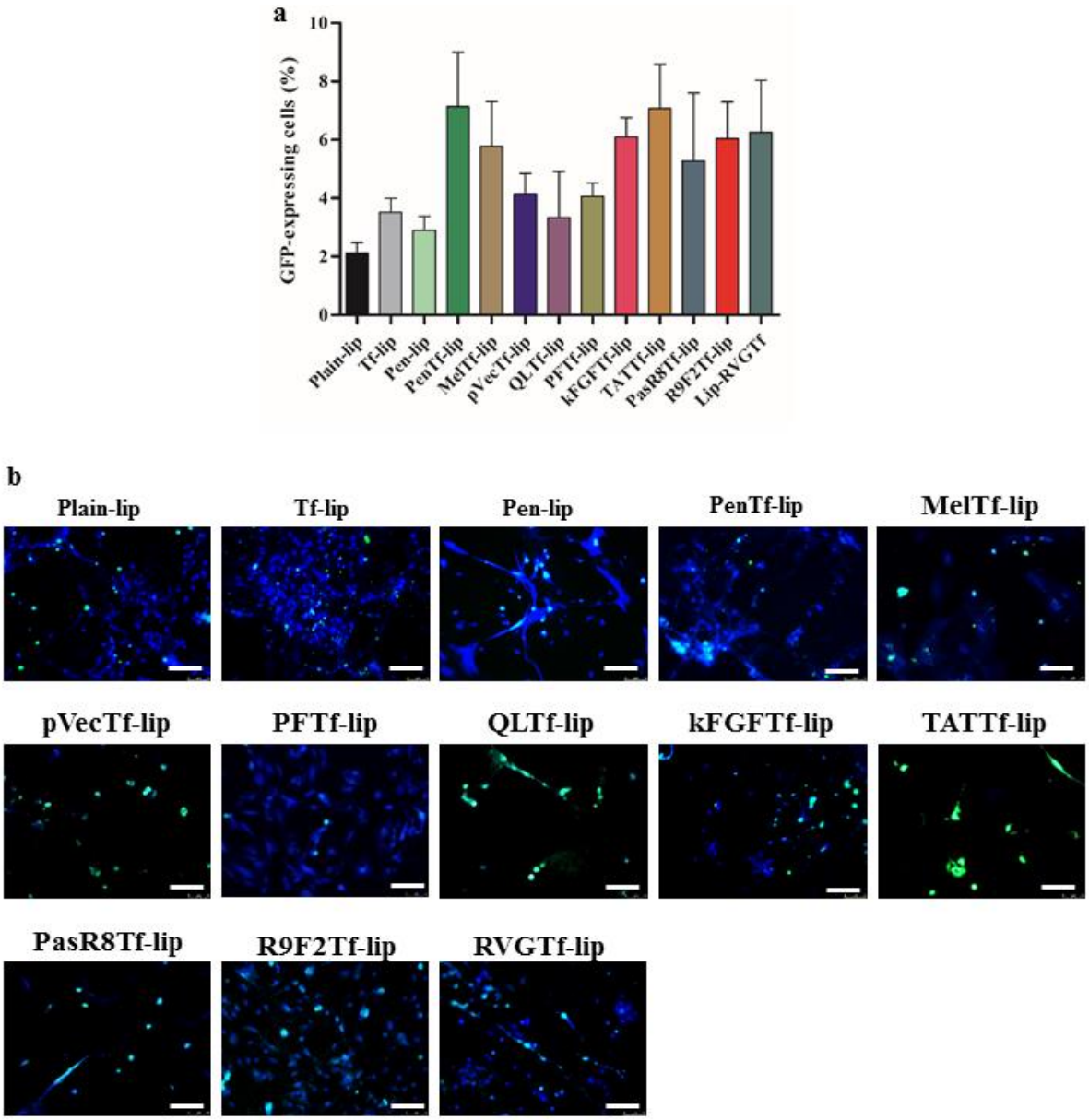

Figure 24. Transfection efficiency of liposomal formulations containing chitosan-pGFP complexes (**a**) in primary neuronal cells after transport across *in vitro* BBB barrier. **b**) Fluorescence images of primary neuronal cells transfected with liposomal formulations containing chitosan-pGFP complexes after transport study. Scale bar, 100 µm. Data are expressed as mean ± SD (n=4).

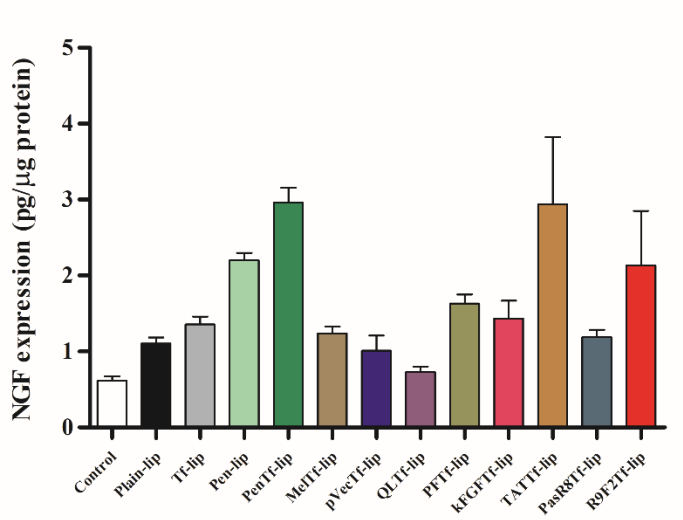

Figure 25. Transfection efficiency of liposomal formulations containing chitosan-pNGF complexes in primary neuronal cells after transport across *in vitro* BBB barrier. Data are expressed as mean ± SD (n=4).

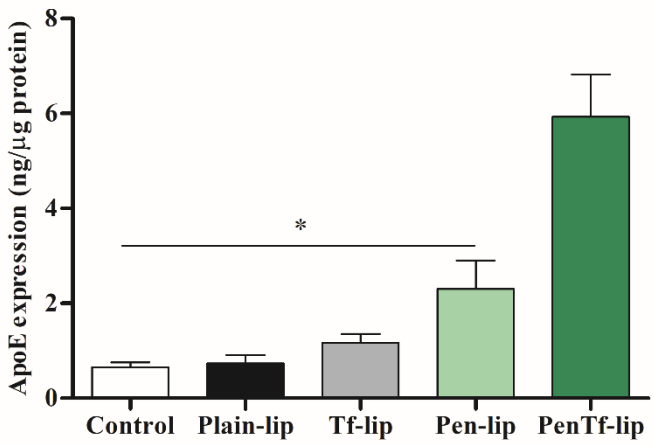

Figure 26. Transfection efficiency of liposomal formulations containing chitosan-pApoE2 complexes in primary neuronal cells after transport across *in vitro* BBB barrier. Data are expressed as mean ± SD (n=4). Statistically significant ($p<0.05$) differences are shown as (*).

3.12. Blood compatibility

Evaluation of interaction of liposomal formulations with blood cells can help examine possible undesirable effects after systemic administration *in vivo*. As shown in Figure 27, the hemoglobin release due to erythrocyte lysis was concentration dependent. At the lowest

phospholipid concentration (31.25 nM), 1.3% hemolysis in average was detected, which gradually increased to 11.5% hemolysis at 1000 nM phospholipid concentration. Whereas Mel-lip and MelTf-lip at 31.25 µM phospholipid concentration was 1.9% in average, these liposomal formulations significantly ($p<0.05$) increased hemolysis at 1000 nM phospholipid concentration to 15.6% in average. The higher levels of hemolysis induced by Mel-lip and MelTf-lip could be attributed to the strong interaction of Mel to cell membranes, which can cause disruption of lipid structure accounting for erythrocyte lysis. Membrane binding and lysis properties of Mel depend on not only the plasma membrane composition, but also depend on peptide concentration [128,130]. Furthermore, conjugation to DSPE-PEG has demonstrated to reduce the lytic activity of Mel [195]. Taken together, these could be an explanation for the lower levels of hemolysis induced by Mel-lip and MelTf-lip at low phospholipid concentration. The study of direct effects of Mel on erythrocytes exposed to Mel concentrations of 0.5 µM, 0.75 µM and 1µM demonstrated the lytic properties of this peptide, which produced variation on median cell volume followed by cell lysis [174]. Biomaterials with hemolytic index below 2% are classified as non-hemolytic, while the ones within the range 2%-5% are classified as slight hemolytic and the ones above 5% are classified as hemolytic, according to ISO Standard Practice for Assessment of Hemolytic Properties of Materials [196]. Therefore, liposomal formulations at low phospholipid concentration were considered non-hemolytic, which suggested to be appropriate for intravenous administration.

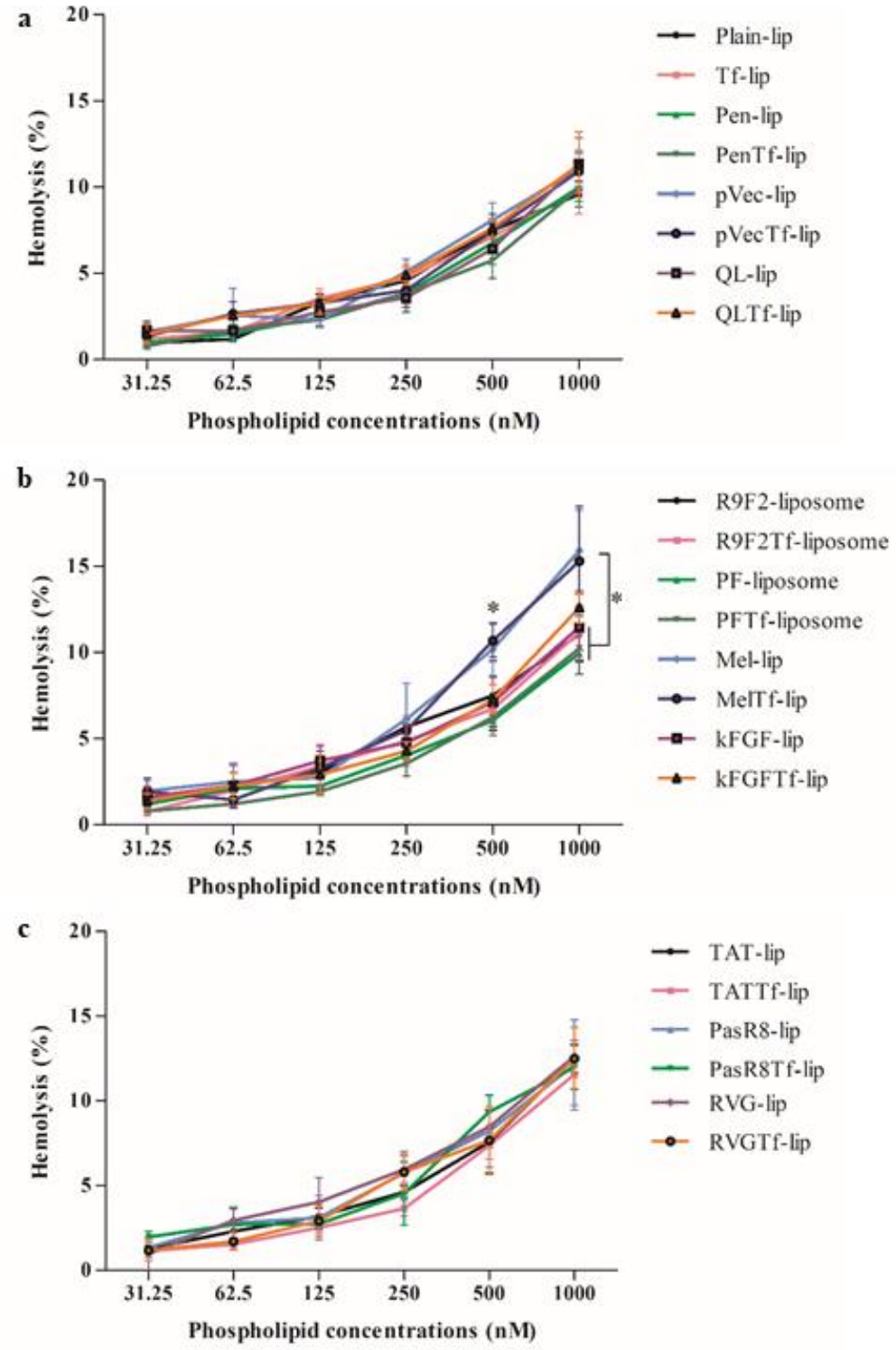

Figure 27. Hemolytic activity of liposomal formulations at different concentrations (31.25-1000 μM) in erythrocyte solution after 1 h of incubation at 37 °C. Hemolytic activity of 1% v/v Triton X-100 was considered as 100% hemolysis. Data are expressed as mean ± SD (n=4). Statistically significant ($p<0.05$) differences are shown as (*).

3.13. *In vivo* biodistribution in wild type mice

Quantitative estimation of liposome distribution showed accumulation mainly in the brain and to a lower extent in the liver and lungs. The fluorescence intensity found in brain treated with PenTf-liposomes was 11.9±1.3% ID/g, which was significantly ($p<0.05$) higher as compared to the fluorescence intensity detected for the other liposomal formulations (Figure 28). Additionally, we observed that liposomes conjugated with both CPP and Tf had superior ability to reach the brain of mice compared to liposomes conjugated only with CPP. No differences were found among liposomal formulations with respect to accumulation in the liver, kidneys, heart, lungs and blood. The biodistribution of DiR-liposomal formulations was tracked using NIR imaging, as shown in Figure 29.

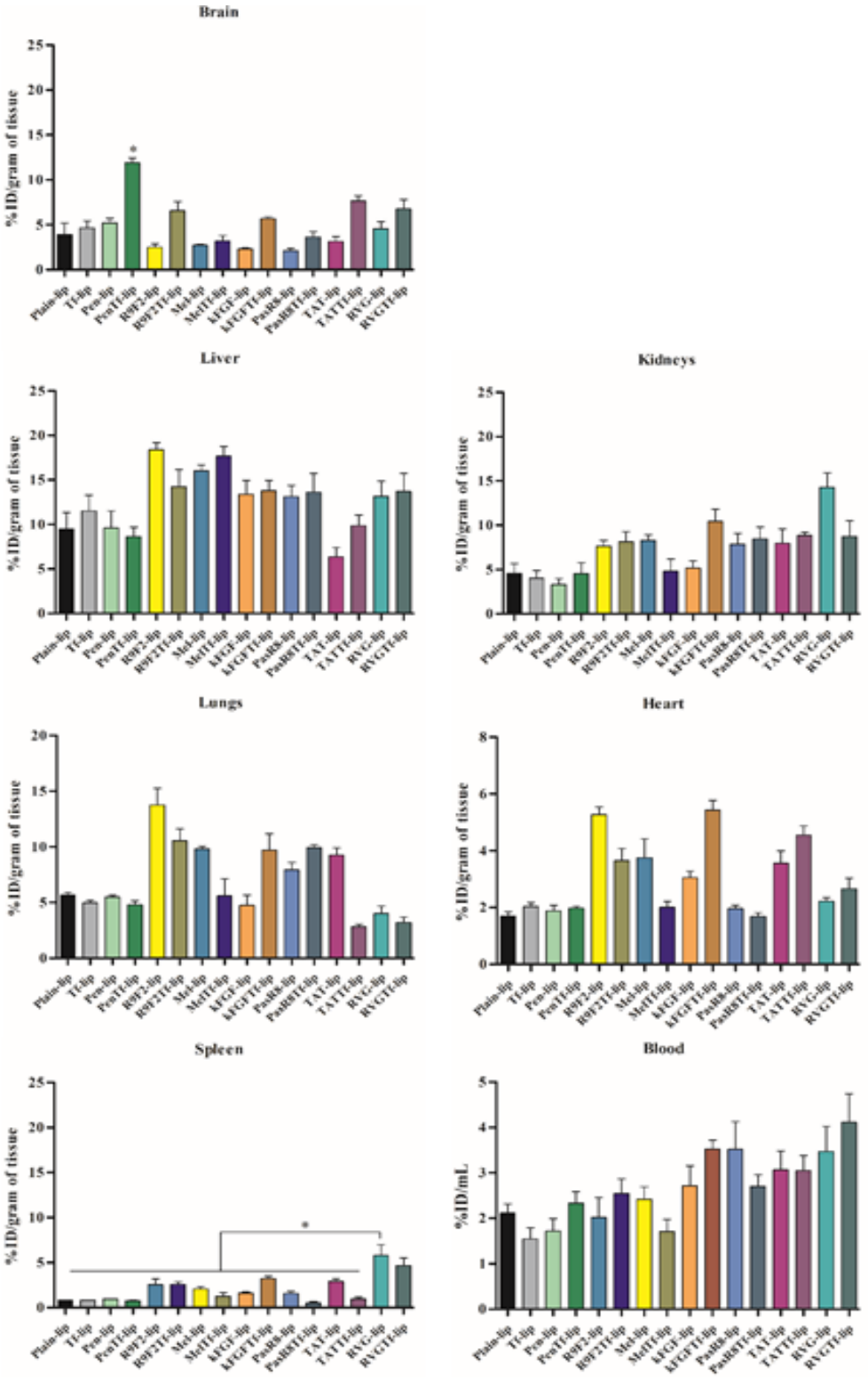

Figure 28. Biodistribution of fluorescent labeled-liposomes (15.2 µM of phospholipids/kg body weight) after 24 h of intravenous injection in C57BL/6 mice performed in brain, liver, kidneys, heart, lungs and spleen (n=6). Data are expressed as mean ± SD of injected dose percentage (%ID) per gram of tissue. Statistically significant differences ($p<0.05$) are shown as (*).

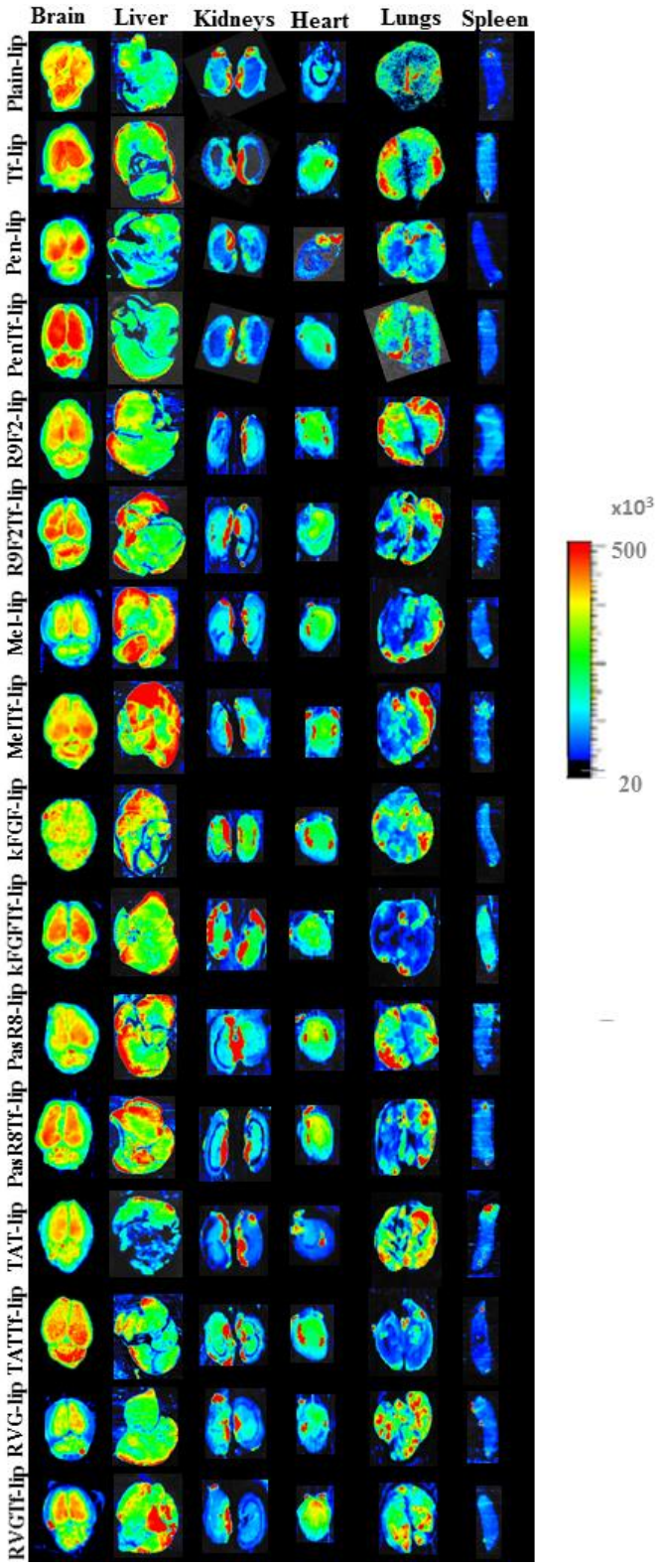

Figure 29. Biodistribution of DiR-liposomes in C57BL/6 mice. Liposomal formulations (15.2 µM of phospholipids/kg body weight) were intravenously administered to mice. NIR images were acquired 24 h after administration.

3.14. *In vivo* transfection efficiency in wild type mice

The capacity of liposomes to transfect cells of different organs after systemic administration was evaluated using liposomes containing plasmid βgal, plasmid GFP, plasmid NGF and plasmid ApoE2. The transfection of tissues was similar to the biodistribution of liposomal formulations. As shown in Figure 30, βgalactosidase activity was negligible in the heart, lungs, spleen and blood and no significant ($p<0.05$) difference was found between the endogenous levels of βgal and treatment with naked pDNA. Brain, liver and kidneys demonstrated significantly ($p<0.05$) higher βgalactosidase activity with Plain-lip, Tf-lip, Pen-lip and PenTf-liposomes compared to the endogenous levels. Furthermore, PenTf-liposomes demonstrated better transfection capacity in the brain (15.7 milliunits βgal activity/μg of total protein), that was significantly ($p<0.05$) higher than Plain-liposomes (11.7 milliunits/μg of total protein). For liver and kidneys, no significant difference ($p<0.05$) was found among the liposomal formulations.

Quantification of transfection efficiency of liposomal formulation containing the reporter gene βgal in different organs was a strategy used to determine pharmacological consequence of differential biodistribution of the liposomes. Additionally, quantification of βgal activity enable determination of gene delivery specifically to cell nucleus. Upon single administration, dual-functionalized liposomal formulations (PenTf-liposomes) were not only able to reach brain parenchyma in significant amount (~12%), but also transfect brain cells with βgal gene. Transfection efficiency of liposomal formulations followed the pattern observed in biodistribution study. The results indicate that the formulation accumulated at high levels mainly in the brain, liver, kidneys and to a lesser extent in the heart. The targeting properties along with protection from enzymatic degradation of PenTf-liposomes might have contributed to the higher protein expression observed in the brain.

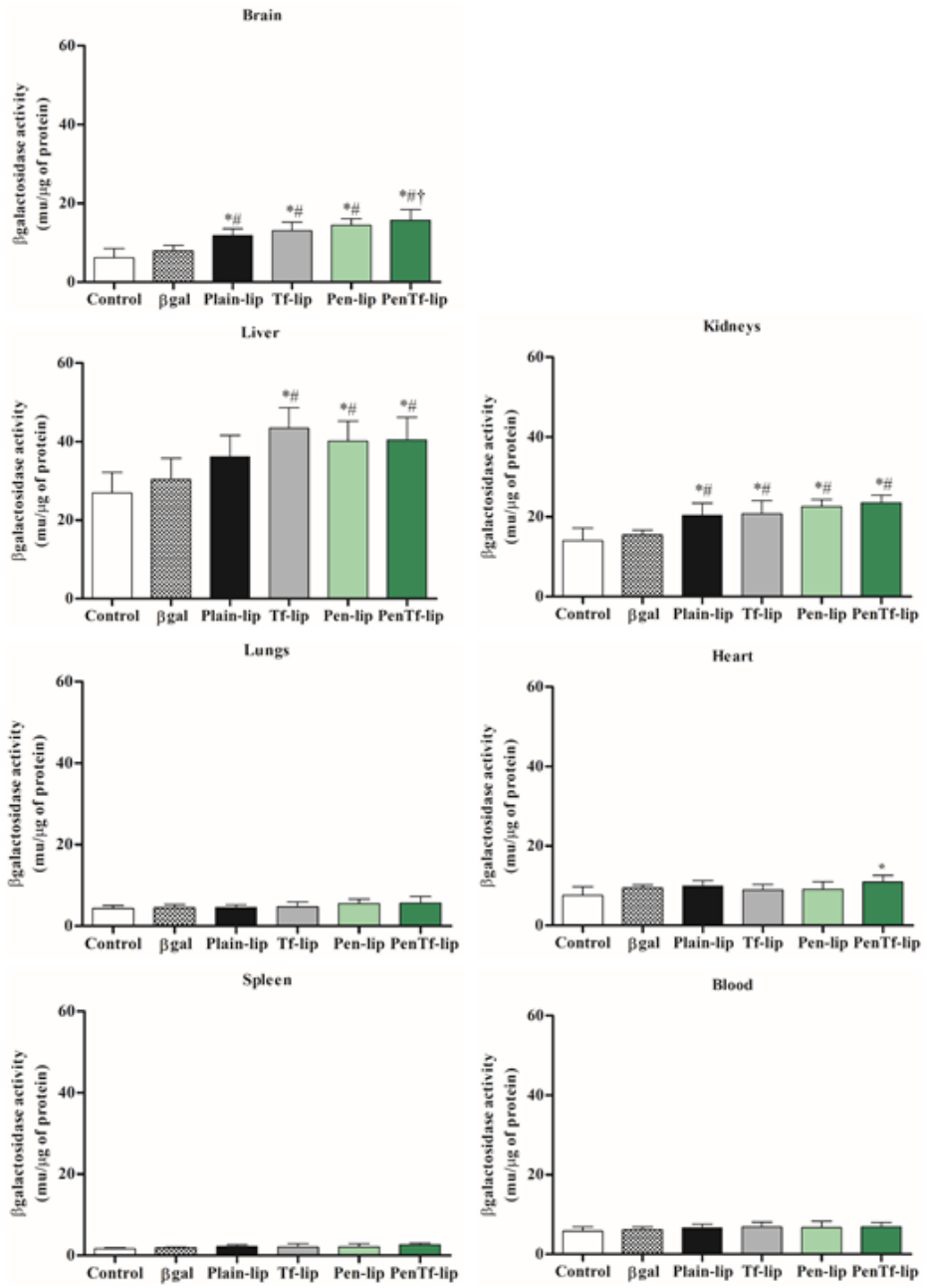

Figure 30. β-gal expression in C57BL/6 mice treated with liposomal formulations containing pβgal after 5 days of liposome administration. βgalactosidase activity was quantified in different organs (brain, liver, kidneys, heart, lungs, spleen and blood) harvested from mice treated with Plain-lip. Tf-lip, Pen-lip, PenTf-liposomes (15.2 μM of phospholipids/kg body weight) encapsulating pβgal (1 mg pDNA/kg body weight). Six mice were used per group. Data are expressed as mean ± SD. Statistically significant differences ($p<0.05$) are shown as (*) with control, (#) with βgal and (†) with Plain-lip.

We confirmed the ability of liposomes to cross BBB and induce the expression of GFP protein in hippocampus as well as in cortex of mice brain (Figure 31 a) after treating the animals with liposomes containing chitosan-pGFP complexes. Slightly increased fluorescence was observed in cortex and hippocampus of mouse treated with PenTf-liposomes compared to Plain-liposomes. These observations correlate well with the biodistribution and transfection efficiency profile of these liposomal formulations. Furthermore, the specificity of PenTf-liposomes to transfect neurons was demonstrated by GFP that was mainly expressed in neurons co-localized with the neuronal marker NeuN (Figure 31 b). Immunofluorescence images of GFP expression in the brain induced by liposomes confirmed the ability of these nanoparticles to reach brain parenchyma and specially, transfect neurons. The dual liposome surface modification with Tf ligand and Pen may have exerted an additive/synergistic effect on BBB targeting as well as neuronal transfection. Overall, these dual-functionalized liposomes have the potential to accurately and efficiently deliver pDNA into brain and should be considered for further development.

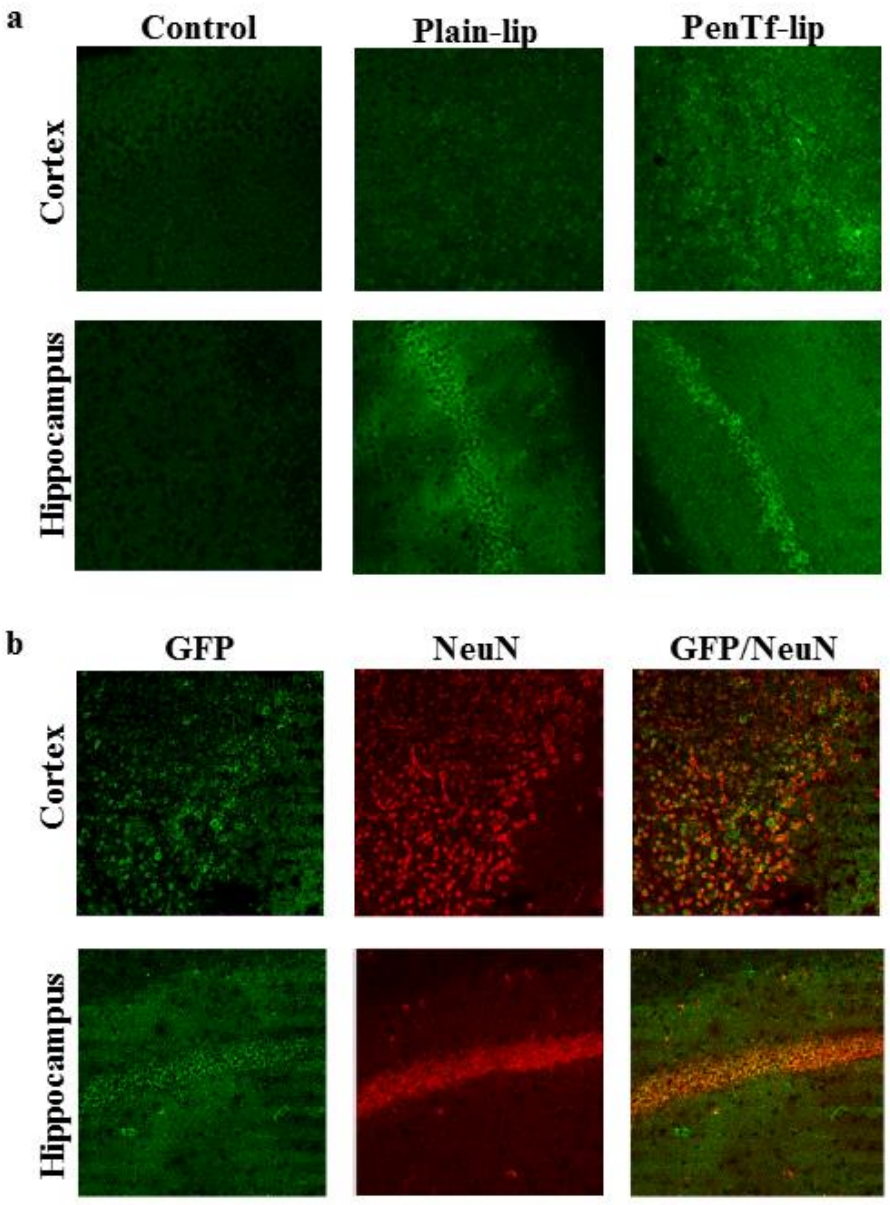

Figure 31. Immunofluorescence analysis of mouse brain sections. **a**) Cortex and hippocampus sections from non-treated mouse (control) and mouse treated with Plain- and Pentf-liposomes containing chitosan-pGFP complexes (1 mg pDNA/kg body weight) stained with anti-GFP antibody. **b**) Cortex and hippocampus sections of mouse treated with PenTf-liposomes containing chitosan-pGFP complexes (1 mg pDNA/kg body weight). Sections were stained with anti-GFP antibody (green) and anti-NeuN antibody (red) (40x magnification).

Hence, next we evaluated whether single intravenous administration of Plain-liposome or PenTf-liposomes containing chitosan-pApoE2 (1mg pApoE2/kg body weight) would significantly

increase the levels of ApoE in the brain of mice. We observed that PenTf-liposomes (20.8 ± 4.0 ng/μg of protein) significantly ($p<0.05$) increased ApoE expression in the brain as compared to Plain-liposomes chitosan-pApoE2 complexes (14.4 ± 3.4 ng/μg of protein), naked plasmid ApoE2 (3.4 ± 1.8 ng/μg of protein) and endogenous levels (2.5 ± 2.0 ng/μg of protein), as depicted in Figure 32. No differences were found in liver, kidneys, heart, lungs and spleen among ApoE endogenous levels and administration of naked ApoE2, Plain-lip and PenTf-liposomes containing chitosan-pApoE2 complexes. Additionally, we observed that PenTf-liposomes containing chitosan-pApoE2 significantly ($p<0.05$) increased the ApoE protein levels in the blood compared to endogenous protein levels (control group) and administration of plasmid ApoE2.

The engineered brain-targeted liposomes also showed *in vivo* brain targeting and gene delivery efficiencies. The *in vivo* results demonstrated that PenTf-liposomes encasing chitosan-pApoE2 was capable to significantly ($p<0.05$) increase ApoE levels in the brain of mice on single injection compared with unmodified liposomes encasing chitosan-pApoE2 complexes and equivalent dose of free plasmid ApoE2. Increasing ApoE2 levels in the brain of AD mouse model has demonstrated to decrease the endogenous Aβ as well as amyloid deposition [197–199]. It is particularly encouraging to note that the current study demonstrated the effectiveness of designed brain-targeted liposomes-mediated ApoE2 gene therapy as a potential disease-modifying therapy for AD. Additional studies are needed to investigate the therapeutic potential of liposome-mediated ApoE2 gene transfer for treatment of AD using AD mouse model.

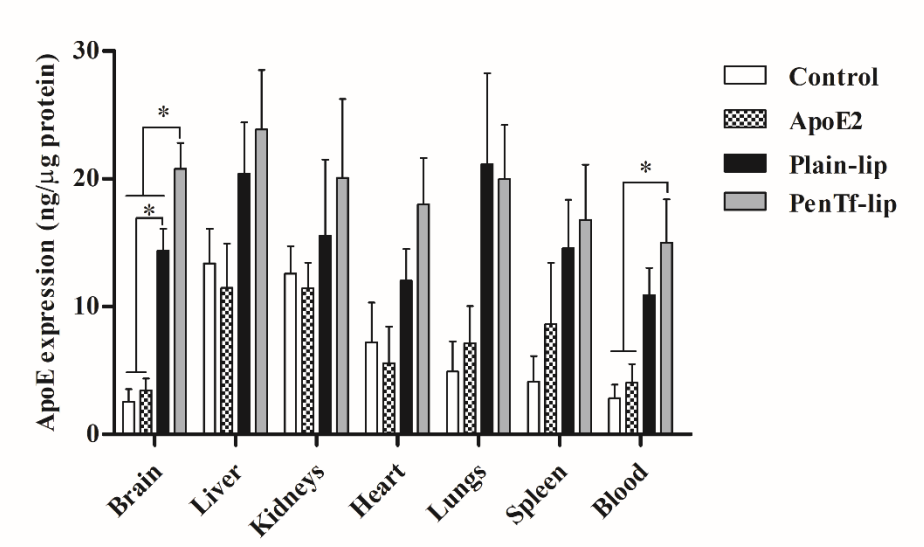

Figure 32. ApoE expression in C57BL/6 mice treated with liposomal formulations containing plasmid ApoE2 after 5 days of liposome administration. ApoE levels were quantified in different organs (brain, liver, kidneys, heart, lungs, spleen and blood) harvested from mice treated with plasmid ApoE2, Plain-liposome and PenTf-liposomes containing chitosan-pApoE2 complexes (1 mg pDNA/kg body weight). Twelve mice were used per group. Data are expressed as mean ± SD. Statistically significant differences ($p<0.05$) are shown as (*).

A dose response study of liposomal formulations containing plasmid NGF following single administration was performed into C57BL/6 mice to evaluate the effect of treatment on NGF expression. Three different doses of pNGF (4, 20 and 40 µg of pNGF/100 g of body weight) encapsulated in either Plain-liposomes or PenTf-liposomes were tested in C57BL/6 mice and protein expression was analyzed after 5 days. Additionally, the effect of treatment of the dual-functionalized liposome containing the highest dose (40 µg of pNGF/100 g of body weight) on protein expression was also evaluated after 15 days of administration (Figure 33). In our previous biodistribution study with the same type of liposomal formulations, we observed that liposomes were able to cross the BBB and transfect brain cells. Based on these findings, we hypothesized that our liposomal formulations containing plasmid NGF would be also capable to transfect brain cells. Moreover, a dose response study would suggest the adequate gene treatment. Comparing the

NGF expression induced by the liposomal formulations after 5 days of administration in the brain, we observed a dose dependent response. Additionally, PenTf-liposomes containing 40 µg of pNGF induced significantly higher NGF expression compared to NGF endogenous levels, free NGF administration and the treatment with Plain-liposomes. Covering from lowest to highest dose, we did not observe any significantly different NGF expression after 5 days of treatment with liposomal formulations compared to NGF endogenous levels in liver, kidneys, lungs, heart, spleen and blood. This observation shows that the NGF expression is transient. A decrease in NGF expression was observed in all organs after 15 days of administration of the highest dose of PenTf-liposomes containing NGF, and the expression was not significantly different compared to endogenous levels.

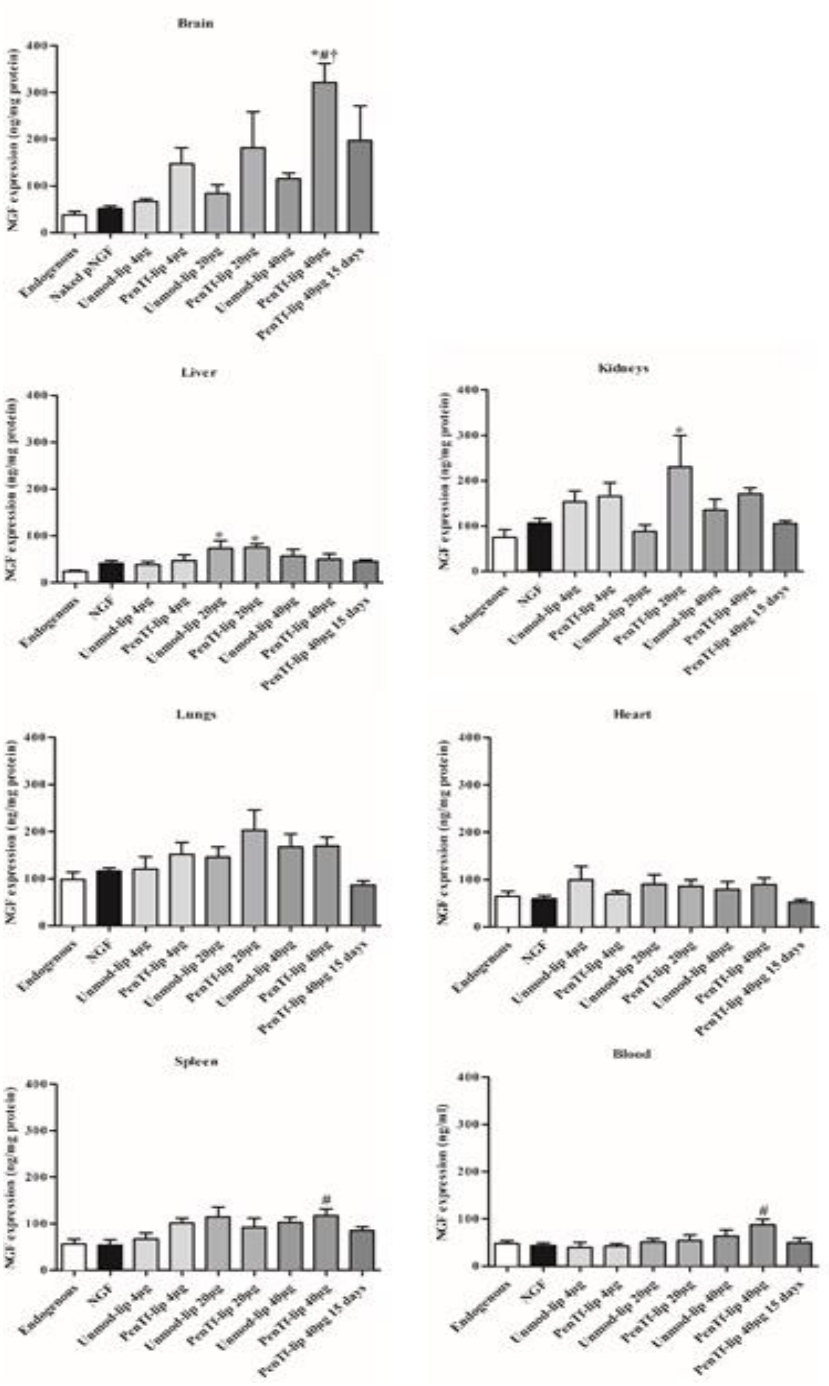

Figure 33. NGF expression in C57BL/6 mice treated with Plain-lip and PenTf-liposomes (15.2 µM of phospholipids/kg body weight) encapsulating either 4 µg, 20 µg or 40 µg pNGF/100g body weight after 5 days of liposomal administration and NGF expression in C57BL/6 mice treated with PenTf-liposomes encapsulating 40 µg pNGF/100g body weight after 15 days of liposomal administration. NGF expression was quantified in brain, liver, kidneys, heart, lungs, spleen and blood. Data are expressed as mean ± SD (n=6). Statistically significant ($p<0.05$) differences are shown as (*) with Endogenous levels, (#) free pNGF administration and (†) with Plain-liposomes 40µg.

3.15. Biocompatibility of liposomal formulations in wild type mice

Histological examination of organs was performed to investigate biocompatibility of the liposomal formulations containing chitosan-pβgal complexes (Figure 34 a), chitosan-pNGF complexes (Figure 34 b) and chitosan-pApOE2 complexes (Figure 34 c). The tissue samples from animals administered with PBS were used as control. H&E staining of the organs revealed no alterations in morphological appearance of the tissues. Additionally, no signs of necrosis, inflammation or cytotoxicity were observed, even in liver, lungs and brain, which demonstrated high accumulation of liposomes.

The *in vivo* biocompatibility of formulations administered systemically is fundamental to its safety. Low doses of cationic liposomes have shown good biocompatibility, biodegradability and low cytotoxicity [35,200]. Histological examination of brain, liver, kidneys, heart, lungs and spleen tissues demonstrated the non-cytotoxic profile of liposomal formulation, showing no cellular damage or morphological alterations. The H&E analysis of organs and hemocompatibility study confirmed the low toxicity and good biocompatibility of liposomal formulations. Additional detailed investigation is needed to evaluate *in vivo* liposomal toxicity including assessment of genotoxicity and inflammation markers, which are not obtained by histology and hematological analyses [200]. The use of organ specific biomarkers may be a more accurate way to investigate toxicity in drug development. For example, standard biomarkers of drug-induced liver injury including alanine aminotransferase and aspartate aminotransferase can be studied [201,202]. Also, evaluation of oxidative stress and quantification of blood biomarkers such as Tau and GFAP can potentially indicate brain injury [203,204]. Investigation of these different toxicity biomarkers will be included in our future studies. Based on H&E staining and blood compatibility studies, the dual-functionalized liposomes can be considered a suitable formulation for systemic administration.

Analysis of brain histological sections together with immunofluorescence images of cortex and hippocampus did not indicate any disruption of the BBB. Therefore, liposome accumulation in the brain suggests their ability to cross the BBB without damaging the barrier cells. During the experimental study, no sign of toxicity or change in animal behavior was observed.

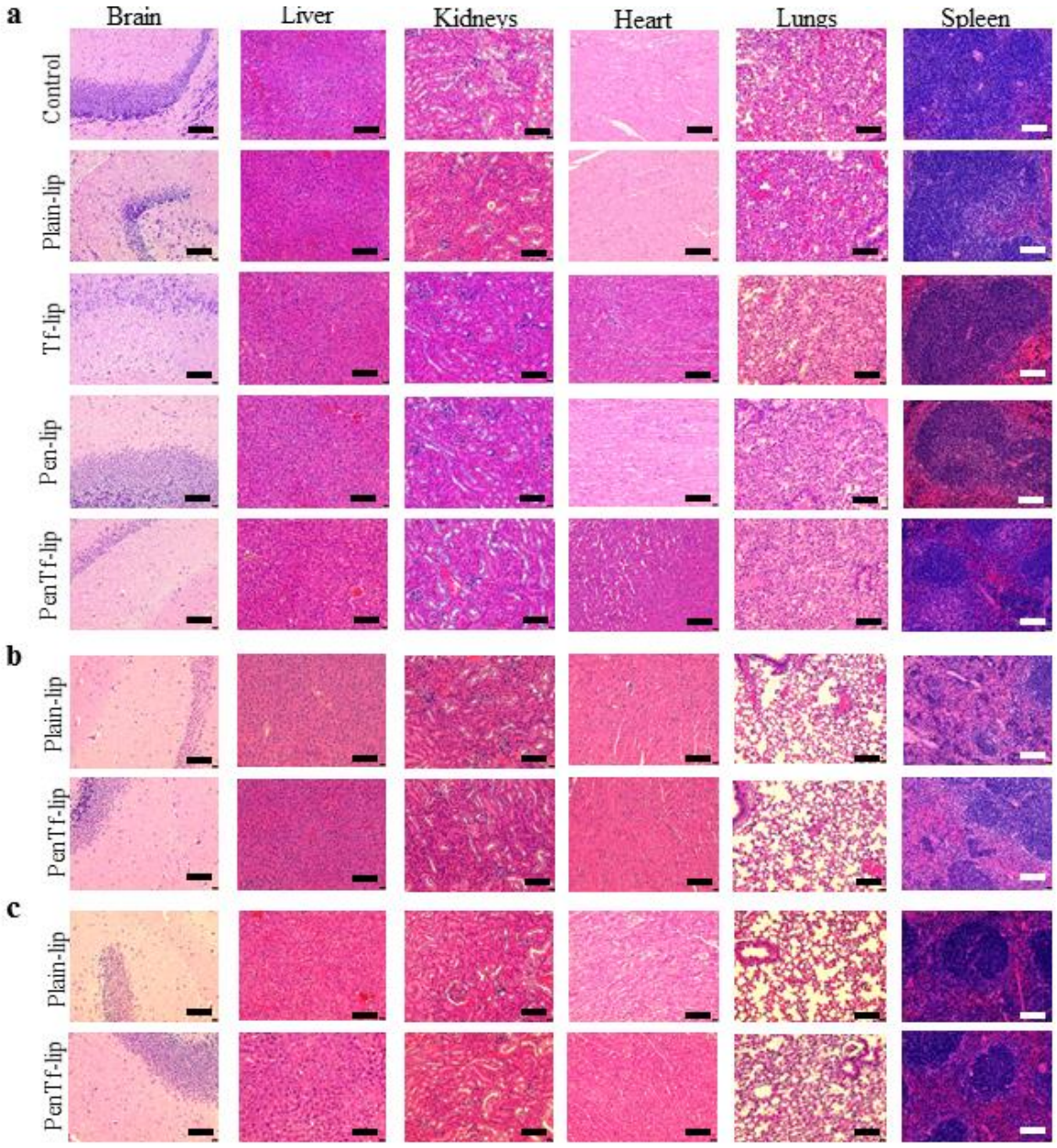

Figure 34. Histological analysis through H&E staining of organ sections (brain, liver, kidneys, heart, lungs and spleen) of C57BL/6 mice subjected to various liposomal formulations treatment. **a**) Representative organ sections of mice treated with Plain-lip, Tf-lip, Pen-lip and PenTf-liposomes containing chitosan-pβgal (1 mg/kg body weight). **b**) Representative organ sections of mice treated with Plain-lip and PenTf-liposomes containing chitosan-pApoE2 (1 mg/kg body weight). **c**) Representative organ sections of mice treated with Plain-lip and PenTf-liposomes containing chitosan-pNGF (40 µg/100 g body weight). The tissue sections from mice administered with PBS were used as controls. Scale bar, 100 µm.

3.16. Neuroprotective effects of PenTf-liposomes containing chitosan-pNGF on APP/PS1 double transgenic mice

APP/PS1 mice (3 months-old) were treated with four doses (one dose every seven days) of liposomal formulations containing chitosan-pNGF complexes (40 µg/100 g body weight). On the 28th day after the first dose, the NGF levels were quantified and compared with those of C57BL/6 mice, APP/PS1 mice and APP/PS1 mice treated with four doses of naked NGF. We observed that NGF levels in APP/PS1 mice treated with PenTf-liposomes were significantly ($p<0.05$) higher as compared to endogenous NGF levels of C57BL/6 mice and APP/PS1 mice (Figure 35).

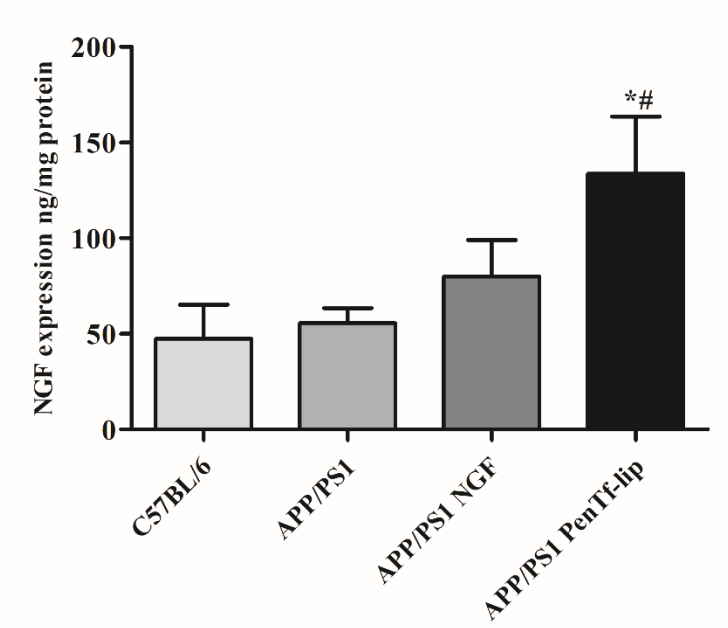

Figure 35. NGF levels in C57BL/6, APP/PS1, APP/PS1 treated with plasmid NGF and APP/PS1 mice treated with PenTf-liposomes (15.2 µM of phospholipids/kg body weight) encapsulating 40 µg pNGF/100g body weight after 30 days of liposomal administration. NGF expression was quantified in brain using NGF ELISA kit. Fourteen mice were used per group. Data are expressed as mean ± SD (n=14). Statistically significant ($p<0.05$) differences are shown as (*) with NGF endogenous levels in C57BL/6 and (#) NGF endogenous levels in APP/PS1 mice.

It is generally believed that production and aggregation of Aβ, which are generated from amyloidogenic cleavage of amyloid precursor protein (APP), are highly related to AD

pathogenesis [4,8]. Among the Aβ isoforms, $A\beta_{1-40}$ and $A\beta_{1-42}$ are the most important and elevated $A\beta_{1-42}/A\beta_{1-40}$ ratio is suggested to be related to neurotoxic effects. Accordingly, $A\beta_{1-42}$ peptide has demonstrated higher cellular toxicity and faster ability to aggregate as compared to $A\beta_{1-40}$ peptide, being $A\beta_{1-42}$ aggregates the major component of amyloid plaque in AD brain [9,205]. To this end, we investigated the levels of water soluble Aβ (Aβ in TBS fraction), soluble Aβ associated with lipid membranes (Aβ in TBS-TX fraction) and insoluble Aβ associated to plaque deposition (Aβ in GDN fraction) in APP/PS1 mice treated with PenTf-liposomes containing chitosan-pNGF complexes and compared to the levels of Aβ fractions in APP/PS1 and C57BL/6 mice. We observed in this study that APP/PS1 mice have higher levels of soluble and insoluble $A\beta_{1-40}$ and $A\beta_{1-42}$ as compared to those levels of normal mice, as depicted by the $A\beta_{1-40}$ and $A\beta_{1-42}$ levels in TBS, TBS-TX and GDN fractions in Figure 36 a, b and c, respectively. The treatment of APP/PS1 mice with PenTf-liposomes containing chitosan-pNGF complexes significantly ($p<0.05$) reduced the brain levels of $A\beta_{1-42}$ as compared to those levels quantified in APP/PS1 (without treatment), in all Aβ fractions. In addition, $A\beta_{1-42}$ levels of treated APP/PS1 mice reduced to levels similar to $A\beta_{1-42}$ levels of normal mice. We also observed that the treatment of AD mice with liposomal formulations reduced the brain $A\beta_{1-40}$ levels in TBS and TBS-TX fractions to similar levels found in normal mice. Analysis of $A\beta_{1-42}/A\beta_{1-40}$ ratio in TBS, TBS-TX and GDN fractions for APP/PS1 mice and APP/PS1 mice treated with liposomal formulation revealed that the treatment reduced the ratio 15-fold, 2-fold and 10-fold respectively. Our findings indicate that NGF gene transfer across BBB using brain targeted-liposomes could significantly ($p<0.05$) reduce the levels of $A\beta_{1-42}$ and $A\beta_{1-42}/A\beta_{1-40}$ ratio.

AD is characterized by a progressive cognitive impairment. Research studies have reported synapses as one of the earliest site of pathology with synapses dysfunction occurring before

neuronal death and correlating with cognitive impairment in AD [206,207]. Additionally, synaptic dysfunction would better correlate to soluble Aβ, rather than the plaque burden. Loss of synapses together with depletion in synaptic markers have been correlated with the extent of cognitive deficits and observed in early as well as late stages of AD [191,207,208]. In this study, we quantified the levels of synaptophysin (SYP), an abundant presynaptic vesicle membrane protein, and PSD-95, the major scaffold protein in the excitatory postsynaptic density responsible for the structural and functional integrity of excitatory synapses. SYP levels have been reported to be reduced in early AD and correlating to synapses dysfunction [208]. PSD-95 expression has demonstrated a tendency to decrease in increasing aging and pathology and transgenic AD mice model [209]. We observed that treatment of APP/PS1 mice with PenTf-liposomes containing chitosan-pNGF complexes increased the levels of SYP and PSD-95 (Figure 36 d and e, respectively), although the levels of these proteins were not significantly different than normal mice. The treatment of APP/PS1 mice also increased the levels of SYP and PSD-95 in TBS, TBS-TX and GDN fractions to levels similar to those of normal mice (Figure 36 f and g, respectively). Therefore, the data suggest that liposome-mediate NGF gene therapy facilitated the depletion of Aβ and stimulated synaptic activity by increasing the levels of pre (synaptophysin) and postsynaptic markers (PSD-95).

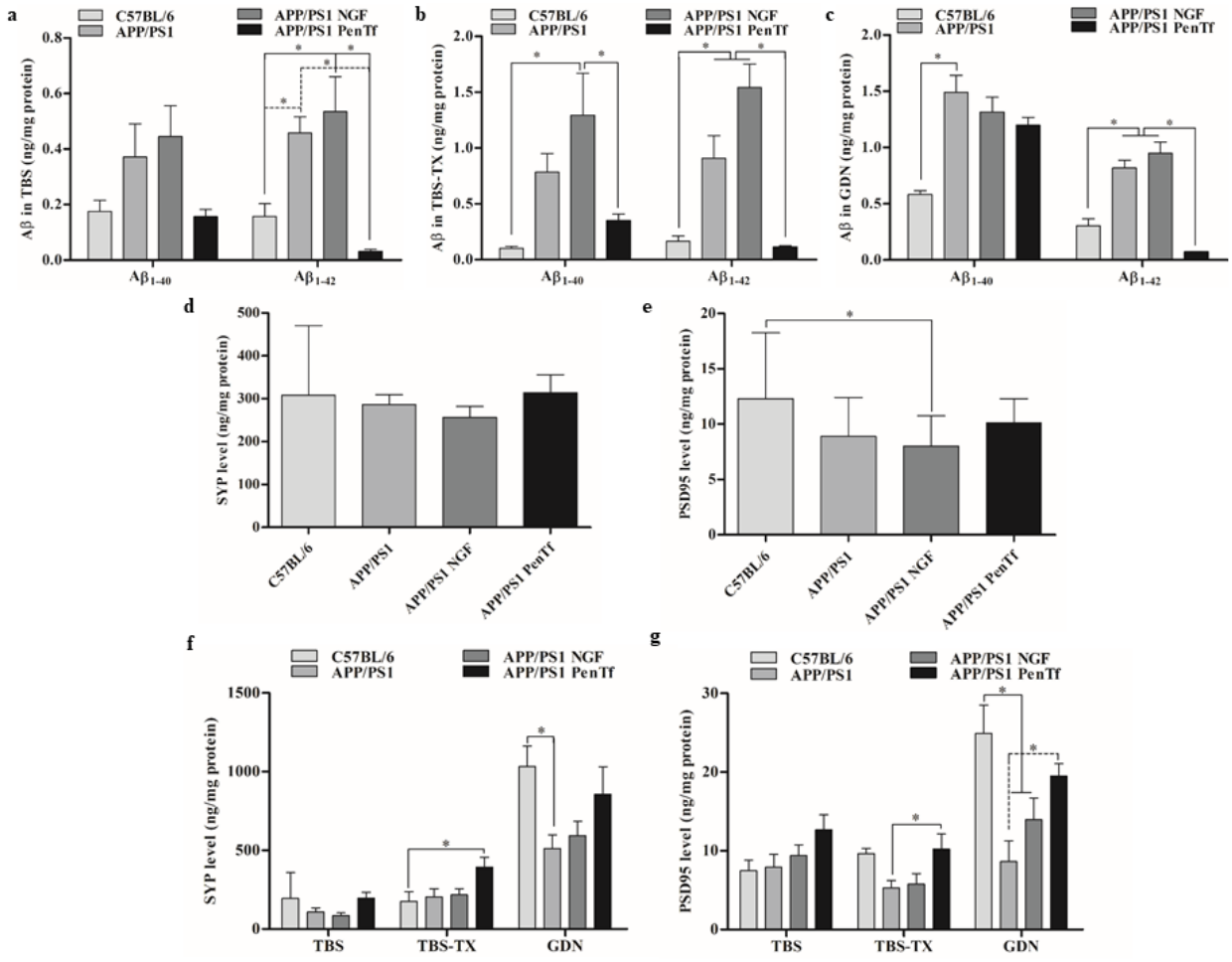

Figure 36. Distribution of $A\beta_{1-40}$ and $A\beta_{1-42}$ in TBS-soluble fraction (**a**), detergent-soluble (TBS-TX) fraction (**b**) and insoluble (guanidine-HCL, GDN) fraction (**c**). Levels of synaptophysin (SYP) (**d**) and PSD-95 (**e**) from one step protein extraction in brain tissue. Levels of SYP (**f**) and PSD-95 (**g**) in TBS, TBS-TX and GDN fractions. Brain tissue from C57BL/6 mice, APP/PS1 mice, APP/PS1 mice treated with plasmid NGF and APP/PS1 mice (3-4 months of age) treated with PenTf-liposomes containing chitosan-pNGF complexes. Data are mean ±SEM (n=14/group). Statistically significant differences ($p<0.05$) are shown as (*).

The mitosis marker Ki-67 was used to assess neurogenesis in APP/PS1 after treatment with PenTf-liposomes containing chitosan-pNGF complexes. The treatment of APP/PS1 mice with liposomal formulations significantly ($p<0.05$) increased the neurogenesis in these animals as compared to C57BL/6 mice, APP/PS1 mice and APP/PS1 mice treated with naked pNGF (Figure 37 a and c). Consistent with increased insoluble Aβ levels, Aβ deposition in the brain of APP/PS1 mice was significantly ($p<0.05$) higher than that of control C57BL/6 mice (Figure 37 b and d).

Although significant differences were not observed, treating APP/PS1 mice with PenTf-liposomes containing chitosan-pNGF complexes reduced Aβ deposition as compared to APP/PS1 mice and APP/PS1 mice treated with naked pNGF. NGF properties to restore CNS cholinergic deficits and prevent cholinergic neuronal degeneration is well documented [19,20,210–212]. However, the main limitations of NGF therapy include protein degradation, BBB impermeability and severe side effects from broad distribution. Therefore, our study demonstrates that NGF gene therapy by designed brain-targeted liposomes has potential to reduce the risk of Aβ accumulation, stimulate synaptic activity and promote cell proliferation.

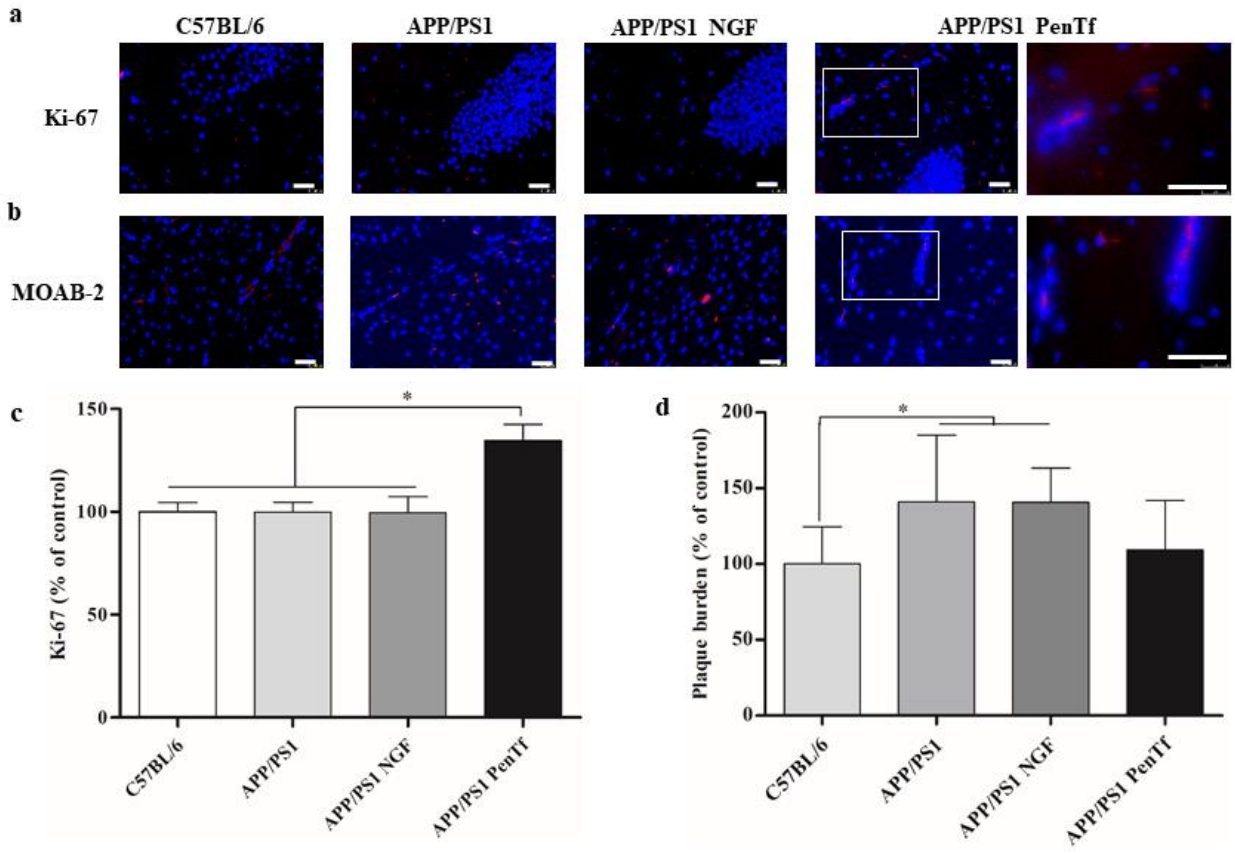

Figure 37. Brain from C57BL/6 mice, APP/PS1 mice, APP/PS1 mice treated with plasmid NGF and APP/PS1 mice (3-4 months of age) treated with PenTf-liposomes containing chitosan-pNGF complexes were stained with Ki-67 antibody (red) (**a**) and a pan-Aβ antibody (red) (**b**). Nucleus of the cells were stained with DAPI (blue). Scale bar, 50 μm. New cell formation (**c**) and amyloid plaque burdens (**d**) in the brain sections from C57BL/6 mice, APP/PS1 mice, APP/PS1 mice treated with plasmid NGF and APP/PS1 mice (3-4 months of age) treated with PenTf-liposomes containing chitosan-pNGF complexes were quantified after scanning Ki-67 and Aβ immunostaining, respectively. Statistically significant differences ($p<0.05$) are shown as (*).

4. SUMMARY AND CONCLUSION

We successfully prepared and characterized the dual functionalized liposomes by modifying their surface with Tf for receptor targeting and CPP for enhanced cell penetration for delivery of genes into the brain. Designed liposomes displayed uniform size distribution and positive zeta potential. These nanoparticles protected encapsulated plasmid DNA against enzymatic degradation and exhibited low hemolytic potential and low cytotoxicity. Cellular uptake occurred in a time-dependent manner through multiple energy-dependent pathways. Caveolae and clathrin-mediated endocytosis played important role as the main pathways involved on the ability of liposomes to overcome *in vitro* and *in vivo* BBB. Dual functionalization of liposomes enhanced the transfection efficiency of liposomes loaded pDNA in bEnd.3, astrocytes and primary neuronal cells as compared to single modified-liposomes. The ability of liposomal formulations to escape the endosome can play an important role in transfection efficiency.

The established *in vitro* co-culture BBB model proved to be a reliable model to estimate the ability of the delivery systems to penetrate into the CNS. Liposomes conjugated to Tf and CPP showed higher ability to overcome *in vitro* BBB model and transfect primary neuronal cells, without disrupting the integrity of *in vitro* barrier layer, showing greater advantages over single modified-liposomes.

Liposomal formulations showed ability to translocate across BBB and reach brain parenchyma of mice. Higher levels of dual-functionalized liposomes were detected in the brain of mice as compared to single modified-liposomes. Additionally, the fluorescence intensity found in brain treated with PenTf-liposomes was significantly ($p<0.05$) higher as compared to the fluorescence detected for the other liposomal formulations. PenTf-liposomes encapsulating chitosan-pβgal complexes released the pDNA in the cytoplasm of neurons, induced β-

galactosidase production *in vivo* and elicited a better effect than Plain-liposomes or naked pβgal. The superior ability of PenTf-liposomes encapsulating pDNA to accumulate in the brain and transfect neurons was confirmed by induction of GFP expression in brain cells, including neurons, after tail vein injection in mice with PenTf-liposomes encapsulating chitosan-pGFP complexes.

PenTf-liposomes containing pApoE2 efficiently delivered the therapeutic gene into the brain of mice and increased ApoE expression, showing a better effect than the preparations without targeted-modifications. ApoE2 gene transfer across BBB using dual-modified liposomes for brain targeting and gene delivery has a great potential for prevention and treatment of AD. The therapeutic efficacy of the system will be further studied in AD mouse model.

The therapeutic potential of PenTf-liposomes encasing chitosan-pNGF complexes-mediated gene therapy was evaluated in 3 months-old APP/PS1 mice. The treatment increased NGF levels in the brain, stimulated the formation of new cells, reduced the levels of toxic soluble and insoluble Aβ peptides as well as increased the levels of synaptic markers. Therefore, liposome-mediated NGF gene transfer could be a potential therapeutic approach for treating AD, presumably through depletion of Aβ and promotion of neurogenesis and synaptic activity.

In conclusion, we designed brain-targeted gene carrier for transferrin receptor targeting with enhanced cellular internalization by conjugating Tf ligand and CPP to liposome surface. We have demonstrated that liposome surface modification was a robust strategy in the design of gene delivery systems with brain-targeted properties. Dual-functionalized liposomes demonstrated to be more efficient systems for *in vitro* transfection, crossing *in vitro* and *in vivo* BBB as well as transfecting neurons in the brain of mice. Finally, PenTf-liposome-mediated NGF gene therapy has a great potential for prevention and treatment of AD.

4.1. Future Studies

This study illustrates that strategic design of liposomal formulations might serve as efficient approach to obtain gene delivery system with brain-targeted properties emphasizing the use of transferrin receptor-targeting and CPPs to improve carrier gene delivery properties. Improvement of liposome brain-targeted delivery properties could be achieved by modification of brain-targeted ligand. Conjugating ApoE ligand to liposomes would target the low-density lipoprotein receptor-related protein 1 (LRP1), which is abundantly expressed in neurons, glial and brain vascular cells, and up-regulated in AD brains. Therefore, optimization of liposome brain-targeted properties could lead to higher delivery efficiency.

Furthermore, liposomes dual modified with Pen and Tf encasing chitosan-pNGF complexes increased NGF levels in the brain of 3 months-old APP/PS1 mice, stimulated the formation of new cells as well as reduced the levels of toxic soluble and insoluble Aβ peptides. Considering the potential of liposome-mediated NGF gene therapy observed in 3 months-old APP/PS1 mice, the therapeutic effects of this formulation could be also evaluated in 12 months-old APP/PS1 mice. Although extracellular deposition of Aβ can be observed at 2.5 months in APP/PS1 mice, cerebral cortex similar to AD patients, neuronal loss and memory impairment are observed around 12 months. Consequently, memory and behavioral studies would evaluate the effects of liposome-mediated NGF gene therapy on memory improvement. Therefore, studies in 12 months-old APP/PS1 mice would provide better understanding of therapeutic potential of these liposome-mediated NGF gene therapy in late-stage disease.

REFERENCES

[1] M. Prince, A. Comas-Herrera, M. Knapp, M. Guerchet, M. Karagiannidou, World Alzheimer Report 2016 Improving healthcare for people living with dementia. Coverage, Quality and costs now and in the future, (2016) 1–140. https://www.alz.co.uk/research/world-report-2016.

[2] 2018 Alzheimer's disease facts and figures, Alzheimer's Dement. 14 (2018) 367–429. doi:10.1016/J.JALZ.2018.02.001.

[3] E. Nichols, C.E.I. Szoeke, S.E. Vollset, N. Abbasi, F. Abd-Allah, J. Abdela, M.T.E. Aichour, R.O. Akinyemi, F. Alahdab, S.W. Asgedom, A. Awasthi, S.L. Barker-Collo, B.T. Baune, Y. Béjot, A.B. Belachew, D.A. Bennett, B. Biadgo, A. Bijani, M.S. Bin Sayeed, C. Brayne, D.O. Carpenter, F. Carvalho, F. Catalá-López, E. Cerin, J.Y.J. Choi, A.K. Dang, M.G. Degefa, S. Djalalinia, M. Dubey, E.E. Duken, D. Edvardsson, M. Endres, S. Eskandarieh, A. Faro, F. Farzadfar, S.M. Fereshtehnejad, E. Fernandes, I. Filip, F. Fischer, A.K. Gebre, D. Geremew, M. Ghasemi-Kasman, E. V. Gnedovskaya, R. Gupta, V. Hachinski, T.B. Hagos, S. Hamidi, G.J. Hankey, J.M. Haro, S.I. Hay, S.S.N. Irvani, R.P. Jha, J.B. Jonas, R. Kalani, A. Karch, A. Kasaeian, Y.S. Khader, I.A. Khalil, E.A. Khan, T. Khanna, T.A.M. Khoja, J. Khubchandani, A. Kisa, K. Kissimova-Skarbek, M. Kivimäki, A. Koyanagi, K.J. Krohn, G. Logroscino, S. Lorkowski, M. Majdan, R. Malekzadeh, W. März, J. Massano, G. Mengistu, A. Meretoja, M. Mohammadi, M. Mohammadi-Khanaposhtani, A.H. Mokdad, S. Mondello, G. Moradi, G. Nagel, M. Naghavi, G. Naik, L.H. Nguyen, T.H. Nguyen, Y.L. Nirayo, M.R. Nixon, R. Ofori-Asenso, F.A. Ogbo, A.T. Olagunju, M.O. Owolabi, S. Panda-Jonas, V.M. d. A. Passos, D.M. Pereira, G.D. Pinilla-Monsalve, M.A. Piradov, C.D. Pond, H. Poustchi, M. Qorbani,

A. Radfar, R.C. Reiner, S.R. Robinson, G. Roshandel, A. Rostami, T.C. Russ, P.S. Sachdev, H. Safari, S. Safiri, R. Sahathevan, Y. Salimi, M. Satpathy, M. Sawhney, M. Saylan, S.G. Sepanlou, A. Shafieesabet, M.A. Shaikh, M.A. Sahraian, M. Shigematsu, R. Shiri, I. Shiue, J.P. Silva, M. Smith, S. Sobhani, D.J. Stein, R. Tabarés-Seisdedos, M.R. Tovani-Palone, B.X. Tran, T.T. Tran, A.T. Tsegay, I. Ullah, N. Venketasubramanian, V. Vlassov, Y.P. Wang, J. Weiss, R. Westerman, T. Wijeratne, G.M.A. Wyper, Y. Yano, E.M. Yimer, N. Yonemoto, M. Yousefifard, Z. Zaidi, Z. Zare, T. Vos, V.L. Feigin, C.J.L. Murray, Global, regional, and national burden of Alzheimer's disease and other dementias, 1990–2016: a systematic analysis for the Global Burden of Disease Study 2016, Lancet Neurol. 18 (2019) 88–106. doi:10.1016/S1474-4422(18)30403-4.

[4] A.M. Hurtado-Puerto, C. Russo, F. Fregni, Alzheimer's disease, Neuromethods. 138 (2018) 297–338. doi:10.1007/978-1-4939-7880-9_9.

[5] Y. Huang, L. Mucke, Alzheimer mechanisms and therapeutic strategies, Cell. 148 (2012) 1204–1222. doi:10.1016/j.cell.2012.02.040.

[6] A.G. Henriques, J.M. Oliveira, L.P. Carvalho, O.A.B. da Cruz e Silva, A?? Influences Cytoskeletal Signaling Cascades with Consequences to Alzheimer???s Disease, Mol. Neurobiol. 52 (2014) 1391–1407. doi:10.1007/s12035-014-8913-4.

[7] D. Holtzman, J. Herz, Apolipoprotein E and apolipoprotein receptors: normal biology and roles in Alzheimer's disease, Cold Spring Harb. Perspect. Med. 2 (2012) a006312. doi:10.1101/cshperspect.a006312.

[8] A. Kumar, A. Singh, Ekavali, A review on Alzheimer's disease pathophysiology and its management: An update, Pharmacol. Reports. 67 (2015) 195–203. doi:10.1016/j.pharep.2014.09.004.

[9] S. Sadigh-Eteghad, B. Sabermarouf, A. Majdi, M. Talebi, M. Farhoudi, J. Mahmoudi, Amyloid-beta: A crucial factor in Alzheimer's disease, Med. Princ. Pract. 24 (2015) 1–10. doi:10.1159/000369101.

[10] I.O. Korolev, Alzheimer 's Disease : A Clinical and Basic Science Review, Med. Student Res. J. 04 (2014) 24–33.

[11] C.C. Liu, N. Zhao, Y. Fu, N. Wang, C. Linares, C.W. Tsai, G. Bu, ApoE4 Accelerates Early Seeding of Amyloid Pathology, Neuron. 96 (2017) 1024-1032.e3. doi:10.1016/j.neuron.2017.11.013.

[12] X. Sun, C. Dong, B. Levin, E. Crocco, D. Loewenstein, H. Zetterberg, K. Blennow, C.B. Wright, APOE ε4 carriers may undergo synaptic damage conferring risk of Alzheimer's disease, Alzheimer's Dement. 12 (2016) 1159–1166. doi:10.1016/j.jalz.2016.05.003.

[13] Y.W.A. Huang, B. Zhou, M. Wernig, T.C. Südhof, ApoE2, ApoE3, and ApoE4 Differentially Stimulate APP Transcription and Aβ Secretion, Cell. 168 (2017) 427-441.e21. doi:10.1016/j.cell.2016.12.044.

[14] J. Cummings, G. Lee, A. Ritter, K. Zhong, Alzheimer's disease drug development pipeline: 2018, Alzheimer's Dement. Transl. Res. Clin. Interv. 4 (2018) 195–214. doi:10.1016/j.trci.2018.03.009.

[15] J. Cummings, A. Ritter, K. Zhong, Clinical Trials for Disease-Modifying Therapies in Alzheimer's Disease: A Primer, Lessons Learned, and a Blueprint for the Future, J. Alzheimer's Dis. 64 (2018) S3–S22. doi:10.3233/JAD-179901.

[16] J.L. Cummings, T. Morstorf, K. Zhong, Alzheimer's disease drug development pipeline few candidates frequent failures, Alzheimers. Res. Ther. (2014) 1–7.

[17] M.H. Tuszynski, H.S. U, D.G. Amaral, F.H. Gage, Nerve growth factor infusion in the primate brain reduces lesion-induced cholinergic neuronal degeneration., J. Neurosci. 10 (1990) 3604–14. doi:10.1523/JNEUROSCI.10-11-03604.1990.

[18] K. Chen, F. Gage, Somatic gene transfer of NGF to the aged brain: behavioral and morphological amelioration, J. Neurosci. 15 (1995) 2819–2825. doi:10.1523/JNEUROSCI.15-04-02819.1995.

[19] K.M. Frick, D.L. Price, V.E. Koliatsos, A.L. Markowska, The effects of nerve growth factor on spatial recent memory in aged rats persist after discontinuation of treatment., J. Neurosci. 17 (1997) 2543–50. doi:10.1523/JNEUROSCI.17-07-02543.1997.

[20] W. Fischer, A. Bjorklund, K. Chen, F. Gage, NGF improves spatial memory in aged rodents as a function of age, J. Neurosci. 11 (1991) 1889–1906. doi:10.1523/jneurosci.11-07-01889.1991.

[21] R. Levi-Montalcini, The nerve growth factor 35 years later, Science (80-.). 237 (1987) 1154 LP – 1162. doi:10.1126/science.3306916.

[22] L. Aloe, M.L. Rocco, P. Bianchi, L. Manni, Nerve growth factor: from the early discoveries to the potential clinical use, J Transl Med. 10 (2012) 239. doi:10.1186/1479-5876-10-239.

[23] J.M. Frade, Y. a Barde, Nerve growth factor: two receptors, multiple functions., BioEssays. 20 (1998) 137–45. doi:10.1002/(SICI)1521-1878(199802)20:2<137::AID-BIES6>3.0.CO;2-Q.

[24] P. Calissano, C. Matrone, G. Amadoro, Nerve growth factor as a paradigm of neurotrophins related to Alzheimer’s disease, Dev. Neurobiol. 70 (2010) 372–383. doi:10.1002/dneu.20759.

[25] J.F. Poduslo, G.L. Curran, C.T. Berg, Macromolecular permeability across the blood-nerve and blood-brain barriers., Proc. Natl. Acad. Sci. 91 (2006) 5705–5709. doi:10.1073/pnas.91.12.5705.

[26] J.F. Poduslo, G.L. Curran, Permeability at the blood-brain and blood-nerve barriers of the neurotrophic factors: NGF, CNTF, NT-3, BDNF, Mol. Brain Res. 36 (1996) 280–286. doi:10.1016/0169-328X(95)00250-V.

[27] M. Eriksdotter Jönhagen, A. Nordberg, K. Amberla, L. Bäckman, T. Ebendal, B. Meyerson, L. Olson, Å. Seiger, M. Shigeta, E. Theodorsson, M. Viitanen, B. Winblad, L.-O. Wahlund, Intracerebroventricular Infusion of Nerve Growth Factor in Three Patients with Alzheimer's Disease, Dement. Geriatr. Cogn. Disord. 9 (1998) 246–257. doi:10.1159/000017069.

[28] M.H. Tuszynski, J.H. Yang, D. Barba, H.-S. U, R. a. E. Bakay, M.M. Pay, E. Masliah, J.M. Conner, P. Kobalka, S. Roy, A.H. Nagahara, Nerve Growth Factor Gene Therapy, JAMA Neurol. 72 (2015) 1139–1147. doi:10.1001/jamaneurol.2015.1807.

[29] H.J. Federoff, Alzheimer's disease: reducing the burden with ApoE2., Gene Ther. 12 (2005) 1019–1029. doi:10.1038/sj.gt.3302522.

[30] A. Boehm-Cagan, D.M. Michaelson, Reversal of apoE4-Driven Brain Pathology and Behavioral Deficits by Bexarotene, J. Neurosci. 34 (2014) 7293–7301. doi:10.1523/JNEUROSCI.5198-13.2014.

[31] J. Pardo, G. Morel, M. Astiz, J. Schwerdt, M. Leon, S. Rodriguez, C. Herenu, R. Goya, Gene Therapy and Cell Reprogramming For the Aging Brain: Achievements and Promise, Curr. Gene Ther. 14 (2014) 24–34. doi:10.2174/1566523214666140120121733.

[32] L. Naldini, Gene therapy returns to centre stage, Nature. 526 (2015) 351–360. doi:10.1038/nature15818.

[33] H. Yin, R.L. Kanasty, A.A. Eltoukhy, A.J. Vegas, J.R. Dorkin, D.G. Anderson, Non-viral vectors for gene-based therapy, Nat Rev Genet. 15 (2014) 541–555. doi:10.1038/nrg3763.

[34] Y. Liu, S. An, J. Li, Y. Kuang, X. He, Y. Guo, H. Ma, Biomaterials Brain-targeted co-delivery of therapeutic gene and peptide by multifunctional nanoparticles in Alzheimer ' s disease mice, 80 (2016) 33–45. doi:10.1016/j.biomaterials.2015.11.060.

[35] X. Zheng, C. Zhang, Q. Guo, X. Wan, X. Shao, Q. Liu, Q. Zhang, Dual-functional nanoparticles for precise drug delivery to Alzheimer's disease lesions: Targeting mechanisms, pharmacodynamics and safety, Int. J. Pharm. 525 (2017) 237–248. doi:10.1016/j.ijpharm.2017.04.033.

[36] L. Ordóñez-Gutiérrez, A. Posado-Fernández, D. Ahmadvand, B. Lettiero, L. Wu, M. Antón, O. Flores, S.M. Moghimi, F. Wandosell, ImmunoPEGliposome-mediated reduction of blood and brain amyloid levels in a mouse model of Alzheimer's disease is restricted to aged animals, Biomaterials. 112 (2017). doi:http://dx.doi.org/10.1016/j.biomaterials.2016.07.027.

[37] M. Gregori, M. Taylor, E. Salvati, F. Re, S. Mancini, C. Balducci, G. Forloni, V. Zambelli, S. Sesana, M. Michael, C. Michail, C. Tinker-Mill, O. Kolosov, M. Scherer, S. Harris, N.J. Fullwood, M. Masserini, D. Allsop, Retro-inverso peptide inhibitor nanoparticles as potent inhibitors of aggregation of the Alzheimer's Aβ peptide, Nanomedicine Nanotechnology, Biol. Med. (2016) 1–10. doi:10.1016/j.nano.2016.10.006.

[38] E. Sánchez-López, M. Ettcheto, M.A. Egea, M. Espina, A.C. Calpena, J. Folch, A. Camins, M.L. García, New Potential Strategies for Alzheimer's Disease Prevention:

Pegylated Biodegradable Dexibuprofen Nanospheres Administration to APPswe/PS1dE9, Nanomedicine Nanotechnology, Biol. Med. (2016). doi:10.1016/j.nano.2016.12.003.

[39] C. Tapeinos, M. Battaglini, G. Ciofani, Advances in the design of solid lipid nanoparticles and nanostructured lipid carriers for targeting brain diseases, J. Control. Release. 264 (2017) 306–332. doi:10.1016/j.jconrel.2017.08.033.

[40] Y. Obata, S. Saito, N. Takeda, S. Takeoka, Plasmid DNA-encapsulating liposomes: Effect of a spacer between the cationic head group and hydrophobic moieties of the lipids on gene expression efficiency, Biochim. Biophys. Acta - Biomembr. 1788 (2009) 1148–1158. doi:10.1016/j.bbamem.2009.02.014.

[41] Y. Yang, Y. Yang, X. Xie, X. Cai, H. Zhang, W. Gong, Z. Wang, X. Mei, Biomaterials PEGylated liposomes with NGR ligand and heat-activable cell- penetrating peptide e doxorubicin conjugate for tumor-speci fi c therapy, Biomaterials. 35 (2014) 4368–4381. doi:10.1016/j.biomaterials.2014.01.076.

[42] D.B. Vieira, L.F. Gamarra, Getting into the brain: Liposome-based strategies for effective drug delivery across the blood–brain barrier, Int. J. Nanomedicine. 11 (2016) 5381–5414. doi:10.2147/IJN.S117210.

[43] J. Paterson, C.I. Webster, Exploiting transferrin receptor for delivering drugs across the blood-brain barrier, Drug Discov. Today Technol. 20 (2016) 49–52. doi:10.1016/j.ddtec.2016.07.009.

[44] M. Agrawal, Ajazuddin, D.K. Tripathi, S. Saraf, S. Saraf, S.G. Antimisiaris, S. Mourtas, M. Hammarlund-Udenaes, A. Alexander, Recent advancements in liposomes targeting strategies to cross blood-brain barrier (BBB) for the treatment of Alzheimer's disease, J. Control. Release. 260 (2017) 61–77. doi:10.1016/j.jconrel.2017.05.019.

[45] K.C. Gatter, G. Brown, I.S. Trowbridge, R.E. Woolston, D.Y. Mason, Transferrin receptors in human tissues: their distribution and possible clinical relevance., J. Clin. Pathol. 36 (1983) 539–545. doi:10.1136/jcp.36.5.539.

[46] W.A. Jefferies, M.R. Brandon, S. V. Hunt, A.F. Williams, K.C. Gatter, D.Y. Mason, Transferrin receptor on endothelium of brain capillaries, Nature. 312 (1984) 162–163. doi:10.1038/312162a0.

[47] M. Hersom, H.C. Helms, N. Pretzer, C. Goldeman, A.I. Jensen, G. Severin, M.S. Nielsen, R. Holm, B. Brodin, Transferrin receptor expression and role in transendothelial transport of transferrin in cultured brain endothelial monolayers, Mol. Cell. Neurosci. 76 (2016) 59–67. doi:10.1016/j.mcn.2016.08.009.

[48] K.B. Johnsen, T. Moos, Revisiting nanoparticle technology for blood-brain barrier transport: Unfolding at the endothelial gate improves the fate of transferrin receptor-targeted liposomes, J. Control. Release. 222 (2016) 32–46. doi:10.1016/j.jconrel.2015.11.032.

[49] G. Xiao, L.-S. Gan, Receptor-mediated endocytosis and brain delivery of therapeutic biologics., Int. J. Cell Biol. 2013 (2013) 703545. doi:10.1155/2013/703545.

[50] M. Srinivasarao, P.S. Low, Ligand-Targeted Drug Delivery, Chem. Rev. 117 (2017) 12133–12164. doi:10.1021/acs.chemrev.7b00013.

[51] D. Zhang, J. Wang, D. Xu, Cell-penetrating peptides as noninvasive transmembrane vectors for the development of novel multifunctional drug-delivery systems, J. Control. Release. 229 (2016) 130–139. doi:10.1016/j.jconrel.2016.03.020.

[52] S. Bashyal, G. Noh, T. Keum, Y.W. Choi, S. Lee, Cell penetrating peptides as an innovative approach for drug delivery; then, present and the future, J. Pharm. Investig. 46 (2016) 205–220. doi:10.1007/s40005-016-0253-0.

[53] Z. Yang, J. Li, Z. Wang, D. Dong, X. Qi, Biomaterials Tumor-targeting dual peptides-modi fi ed cationic liposomes for delivery of siRNA and docetaxel to gliomas, Biomaterials. 35 (2014) 5226–5239. doi:10.1016/j.biomaterials.2014.03.017.

[54] G. Sharma, A. Modgil, B. Layek, K. Arora, C. Sun, B. Law, J. Singh, Cell penetrating peptide tethered bi-ligand liposomes for delivery to brain in vivo: Biodistribution and transfection, J. Control. Release. 167 (2013) 1–10. doi:10.1016/j.jconrel.2013.01.016.

[55] N. Bien-Ly, Y.J. Yu, D. Bumbaca, J. Elstrott, C.A. Boswell, Y. Zhang, W. Luk, Y. Lu, M.S. Dennis, R.M. Weimer, I. Chung, R.J. Watts, Transferrin receptor (TfR) trafficking determines brain uptake of TfR antibody affinity variants., J. Exp. Med. 211 (2014) 233–44. doi:10.1084/jem.20131660.

[56] D. Furtado, M. Björnmalm, S. Ayton, A.I. Bush, K. Kempe, F. Caruso, Overcoming the Blood–Brain Barrier: The Role of Nanomaterials in Treating Neurological Diseases, Adv. Mater. 30 (2018). doi:10.1002/adma.201801362.

[57] S. Deaglio, A. Capobianco, A. Calı, F. Bellora, F. Alberti, L. Righi, A. Sapino, C. Camaschella, F. Malavasi, Structural , functional , and tissue distribution analysis of human transferrin receptor-2 by murine monoclonal antibodies and a polyclonal antiserum, 100 (2002) 3782–3789. doi:10.1182/blood-2002-01-0076.Supported.

[58] N. Düzgüneş, S. Nir, Mechanisms and kinetics of liposome-cell interactions, Adv. Drug Deliv. Rev. 40 (1999) 3–18. doi:10.1016/S0169-409X(99)00037-X.

[59] R.A. Petros, J.M. Desimone, Strategies in the design of nanoparticles for therapeutic applications, Nat. Rev. Drug Discov. 9 (2010) 615–627. doi:10.1038/nrd2591.

[60] S.Q. Jing, I.S. Trowbridge, Identification of the intermolecular disulfide bonds of the human transferrin receptor and its lipid-attachment site., EMBO J. 6 (1987) 327–31. doi:10.1002/j.1460-2075.1987.tb04758.x.

[61] P. Aisen, Transferrin receptor 1, Int. J. Biochem. Cell Biol. 36 (2004) 2137–2143. doi:10.1016/j.biocel.2004.02.007.

[62] S. Tortorella, T.C. Karagiannis, Transferrin receptor-mediated endocytosis: a useful target for cancer therapy., J. Membr. Biol. 247 (2014) 291–307. doi:10.1007/s00232-014-9637-0.

[63] T.R. Daniels, T. Delgado, J.A. Rodriguez, G. Helguera, M.L. Penichet, The transferrin receptor part I: Biology and targeting with cytotoxic antibodies for the treatment of cancer, (2006). doi:10.1016/j.clim.2006.06.010.

[64] S.T. Sawyer, S.B. Krantz, Transferrin receptor number, synthesis, and endocytosis during erythropoietin-induced maturation of Friend virus-infected erythroid cells., J. Biol. Chem. 261 (1986) 9187–95. http://www.ncbi.nlm.nih.gov/pubmed/3013876 (accessed August 1, 2019).

[65] P. Ponka, C.N. Lok, The transferrin receptor: role in health and disease, Int. J. Biochem. Cell Biol. 31 (1999) 1111–1137. doi:10.1016/S1357-2725(99)00070-9.

[66] M.J. Kroos, J.S. Starreveld, C.E.H. Verrijt, H.G. van Eijk, J.P. van Dijk, Regulation of transferrin receptor synthesis by human cytotrophoblast cells in culture, Eur. J. Obstet. Gynecol. Reprod. Biol. 65 (1996) 231–234. doi:10.1016/0301-2115(95)02368-2.

[67] D. Hare, S. Ayton, A. Bush, P. Lei, A delicate balance: Iron metabolism and diseases of the brain, Front. Aging Neurosci. 5 (2013) 1–19. doi:10.3389/fnagi.2013.00034.

[68] D.F. Leitner, J.R. Connor, Functional roles of transferrin in the brain., Biochim. Biophys. Acta. (2012). doi:10.1016/j.bbagen.2011.10.016.

[69] K.M. Mayle, A.M. Le, D.T. Kamei, The intracellular trafficking pathway of transferrin, Biochim. Biophys. Acta - Gen. Subj. 1820 (2012) 264–281. doi:10.1016/j.bbagen.2011.09.009.

[70] N. Bien-Ly, Y.J. Yu, D. Bumbaca, J. Elstrott, C.A. Boswell, Y. Zhang, W. Luk, Y. Lu, M.S. Dennis, R.M. Weimer, I. Chung, R.J. Watts, Transferrin receptor (TfR) trafficking determines brain uptake of TfR antibody affinity variants, J. Exp. Med. 211 (2014) 233–244. doi:10.1084/jem.20131660.

[71] J. Huwyler, D. Wu, W.M. Pardridge, Brain drug delivery of small molecules using immunoliposomes., Proc. Natl. Acad. Sci. U. S. A. 93 (1996) 14164–9. doi:10.1073/pnas.93.24.14164.

[72] H. Sade, C. Baumgartner, A. Hugenmatter, E. Moessner, P.O. Freskgård, J. Niewoehner, A human blood-brain barrier transcytosis assay reveals antibody transcytosis influenced by pH-dependent receptor binding, PLoS One. 9 (2014). doi:10.1371/journal.pone.0096340.

[73] I. Van Rooy, E. Mastrobattista, G. Storm, W.E. Hennink, R.M. Schiffelers, Comparison of five different targeting ligands to enhance accumulation of liposomes into the brain, J. Control. Release. 150 (2011) 30–36. doi:10.1016/j.jconrel.2010.11.014.

[74] C. Zylberberg, K. Gaskill, S. Pasley, S. Matosevic, Engineering liposomal nanoparticles for targeted gene therapy, Gene Ther. 24 (2017) 441–452. doi:10.1038/gt.2017.41.

[75] Sonali, R.P. Singh, N. Singh, G. Sharma, M.R. Vijayakumar, B. Koch, S. Singh, U. Singh, D. Dash, B.L. Pandey, M.S. Muthu, Transferrin liposomes of docetaxel for brain-targeted cancer applications: formulation and brain theranostics, Drug Deliv. 23 (2016) 1261–1271. doi:10.3109/10717544.2016.1162878.

[76] B. dos Santos Rodrigues, H. Oue, A. Banerjee, T. Kanekiyo, J. Singh, Dual functionalized liposome-mediated gene delivery across triple co-culture blood brain barrier model and specific in vivo neuronal transfection, J. Control. Release. 286 (2018) 264–278. doi:10.1016/j.jconrel.2018.07.043.

[77] Z.L. Chen, M. Huang, X.R. Wang, J. Fu, M. Han, Y.Q. Shen, Z. Xia, J.Q. Gao, Transferrin-modified liposome promotes ??-mangostin to penetrate the blood-brain barrier, Nanomedicine Nanotechnology, Biol. Med. 12 (2016) 421–430. doi:10.1016/j.nano.2015.10.021.

[78] M.T. Girão da Cruz, A.L.C. Cardoso, L.P. de Almeida, S. Simões, M.C. Pedroso de Lima, Tf-lipoplex-mediated NGF gene transfer to the CNS: Neuronal protection and recovery in an excitotoxic model of brain injury, Gene Ther. 12 (2005) 1242–1252. doi:10.1038/sj.gt.3302516.

[79] J.M. Castellano, R. Deane, A.J. Gottesdiener, P.B. Verghese, F.R. Stewart, T. West, A.C. Paoletti, T.R. Kasper, R.B. DeMattos, B. V. Zlokovic, D.M. Holtzman, Low-density lipoprotein receptor overexpression enhances the rate of brain-to-blood A clearance in a mouse model of -amyloidosis, Proc. Natl. Acad. Sci. 109 (2012) 15502–15507. doi:10.1073/pnas.1206446109.

[80] B. Dehouck, L. Fenart, M.P. Dehouck, A. Pierce, G. Torpier, R. Cecchelli, A new function for the LDL receptor: Transcytosis of LDL across the blood-brain barrier, J. Cell Biol. 138 (1997) 877–889. doi:10.1083/jcb.138.4.877.

[81] J.M. Basak, P.B. Verghese, H. Yoon, J. Kim, D.M. Holtzman, Low-density lipoprotein receptor represents an apolipoprotein E-independent pathway of Aβ uptake and degradation by astrocytes, J. Biol. Chem. 287 (2012) 13959–13971. doi:10.1074/jbc.M111.288746.

[82] J. Kreuter, P. Ramge, V. Petrov, S. Hamm, S.E. Gelperina, B. Engelhardt, R. Alyautdin, H. Von Briesen, D.J. Begley, Direct evidence that polysorbate-80-coated poly(butylcyanoacrylate) nanoparticles deliver drugs to the CNS via specific mechanisms requiring prior binding of drug to the nanoparticles, Pharm. Res. 20 (2003) 409–416. doi:10.1023/A:1022604120952.

[83] G. Almer, H. Mangge, A. Zimmer, R. Prassl, Lipoprotein-Related and Apolipoprotein-Mediated Delivery Systems for Drug Targeting and Imaging, Curr. Med. Chem. 22 (2015) 3631–3651. doi:10.2174/0929867322666150716114625.

[84] J.M. Lajoie, E. V. Shusta, Targeting Receptor-Mediated Transport for Delivery of Biologics Across the Blood-Brain Barrier, Annu. Rev. Pharmacol. Toxicol. 55 (2014) 613–631. doi:10.1146/annurev-pharmtox-010814-124852.

[85] A.R. Jones, E. V. Shusta, Blood-brain barrier transport of therapeutics via receptor-mediation, Pharm. Res. 24 (2007) 1759–1771. doi:10.1007/s11095-007-9379-0.

[86] E.M. Rhea, C. Rask-Madsen, W.A. Banks, Insulin transport across the blood–brain barrier can occur independently of the insulin receptor, J. Physiol. 596 (2018) 4753–4765. doi:10.1113/JP276149.

[87] R.J. Boado, Y. Zhang, Y. Zhang, W.M. Pardridge, Humanization of anti-human insulin receptor antibody for drug targeting across the human blood-brain barrier, Biotechnol. Bioeng. 96 (2007) 381–391. doi:10.1002/bit.21120.

[88] S. Ohtsuki, T. Terasaki, Contribution of carrier-mediated transport systems to the blood-brain barrier as a supporting and protecting interface for the brain; importance for CNS drug discovery and development, Pharm. Res. 24 (2007) 1745–1758. doi:10.1007/s11095-007-9374-5.

[89] S.G. Patching, Glucose Transporters at the Blood-Brain Barrier: Function, Regulation and Gateways for Drug Delivery, Mol. Neurobiol. 54 (2017) 1046–1077. doi:10.1007/s12035-015-9672-6.

[90] L. Kou, Y.D. Bhutia, Q. Yao, Z. He, J. Sun, V. Ganapathy, Transporter-guided delivery of nanoparticles to improve drug permeation across cellular barriers and drug exposure to selective cell types, Front. Pharmacol. 9 (2018) 1–16. doi:10.3389/fphar.2018.00027.

[91] F. Xie, N. Yao, Y. Qin, Q. Zhang, H. Chen, M. Yuan, J. Tang, X. Li, W. Fan, Q. Zhang, Y. Wu, L. Hai, Q. He, Investigation of glucose-modifed liposomes using polyethylene glycols with different chain lengths as the linkers for brain targeting, Int. J. Nanomedicine. 7 (2012) 163–175. doi:10.2147/IJN.S23771.

[92] M. Green, P.M. Loewenstein, Autonomous functional domains of chemically synthesized human immunodeficiency virus tat trans-activator protein, Cell. 55 (1988) 1179–1188. doi:10.1016/0092-8674(88)90262-0.

[93] A.D. Frankel, C.O. Pabo, Cellular uptake of the tat protein from human immunodeficiency virus, Cell. 55 (1988) 1189–1193. doi:10.1016/0092-8674(88)90263-2.

[94] A.T. Jones, E.J. Sayers, Cell entry of cell penetrating peptides: Tales of tails wagging dogs, J. Control. Release. 161 (2012) 582–591. doi:10.1016/j.jconrel.2012.04.003.

[95] G. Guidotti, L. Brambilla, D. Rossi, Cell-Penetrating Peptides: From Basic Research to Clinics, Trends Pharmacol. Sci. 38 (2017) 406–424. doi:10.1016/j.tips.2017.01.003.

[96] F. Milletti, Cell-penetrating peptides: Classes, origin, and current landscape, Drug Discov. Today. 17 (2012) 850–860. doi:10.1016/j.drudis.2012.03.002.

[97] M. Pooga, M. Hällbrink, M. Zorko, U. Langel, Cell penetration by transportan, FASEB J. 12 (1998) 67–77. doi:10.1096/fasebj.12.1.67.

[98] Y. Qin, H. Chen, Q. Zhang, X. Wang, W. Yuan, R. Kuai, J. Tang, L. Zhang, Z. Zhang, Q. Zhang, J. Liu, Q. He, Liposome formulated with TAT-modified cholesterol for improving brain delivery and therapeutic efficacy on brain glioma in animals, Int. J. Pharm. 420 (2011) 304–312. doi:10.1016/j.ijpharm.2011.09.008.

[99] D. Derossi, A.H. Joliot, G. Chassaing, A. Prochiantz, The third helix of the Antennapedia homeodomain translocates through biological membranes, J. Biol. Chem. 269 (1994) 10444–10450. doi:10444-50.

[100] A. Elmquist, M. Hansen, U. Langel, Structure-activity relationship study of the cell-penetrating peptide pVEC., Biochim. Biophys. Acta. 1758 (2006) 721–729. doi:10.1016/j.bbamem.2006.05.013.

[101] J.D. Ramsey, N.H. Flynn, Cell-penetrating peptides transport therapeutics into cells, Pharmacol. Ther. 154 (2015) 78–86. doi:10.1016/j.pharmthera.2015.07.003.

[102] M.L. Jobin, M. Blanchet, S. Henry, S. Chaignepain, C. Manigand, S. Castano, S. Lecomte, F. Burlina, S. Sagan, I.D. Alves, The role of tryptophans on the cellular uptake and

membrane interaction of arginine-rich cell penetrating peptides, Biochim. Biophys. Acta - Biomembr. 1848 (2015) 593–602. doi:10.1016/j.bbamem.2014.11.013.

[103] P.A. Wender Mitchell, D. J., Pattabiraman, K., Pelkey, E. T., Steinman, L., Rothbard, J. B., P. a Wender, D.J. Mitchell, K. Pattabiraman, E.T. Pelkey, L. Steinman, J.B. Rothbard, The design, synthesis, and evaluation of molecules that enable or enhance cellular uptake: Peptoid molecular transporters, Proc. Natl. Acad. Sci. U. S. A. 97 (2000) 13003–13008. doi:10.1073/pnas.97.24.13003.

[104] I.R. De Figueiredo, J.M. Freire, L. Flores, A.S. Veiga, M.A.R.B. Castanho, Cell-penetrating peptides: A tool for effective delivery in gene-targeted therapies, IUBMB Life. 66 (2014) 182–194. doi:10.1002/iub.1257.

[105] H. Derakhshankhah, S. Jafari, Cell penetrating peptides: A concise review with emphasis on biomedical applications, Biomed. Pharmacother. 108 (2018) 1090–1096. doi:10.1016/j.biopha.2018.09.097.

[106] F. Wang, Y. Wang, X. Zhang, W. Zhang, S. Guo, F. Jin, Recent progress of cell-penetrating peptides as new carriers for intracellular cargo delivery, J. Control. Release. 174 (2014) 126–136. doi:10.1016/j.jconrel.2013.11.020.

[107] M.C. Morris, S. Deshayes, F. Heitz, G. Divita, Cell-penetrating peptides: from molecular mechanisms to therapeutics, Biol. Cell. 100 (2008) 201–217. doi:10.1042/bc20070116.

[108] H.J. Johansson, S. El-Andaloussi, T. Holm, M. Mäe, J. Jänes, T. Maimets, Ü. Langel, Characterization of a novel cytotoxic cell-penetrating peptide derived from p14ARF protein, Mol. Ther. 16 (2008) 115–123. doi:10.1038/sj.mt.6300346.

[109] M. Magzoub, S. Sandgren, P. Lundberg, K. Oglecka, J. Lilja, A. Wittrup, L.E. Göran Eriksson, Ü. Langel, M. Belting, A. Gräslund, N-terminal peptides from unprocessed

prion proteins enter cells by macropinocytosis, Biochem. Biophys. Res. Commun. 348 (2006) 379–385. doi:10.1016/j.bbrc.2006.07.065.

[110] E. Klauschenz, A. Scheller, B. Wiesner, M. Bienert, E. Krause, J. Oehlke, M. Melzig, M. Beyermann, Cellular uptake of an α-helical amphipathic model peptide with the potential to deliver polar compounds into the cell interior non-endocytically, Biochim. Biophys. Acta - Biomembr. 1414 (1998) 127–139. doi:10.1016/s0005-2736(98)00161-8.

[111] J. Durzy ska, ucja Przysiecka, R. Nawrot, J. Barylski, G. Nowicki, A. Warowicka, O. Musidlak, A. Go dzicka-Jozefiak, Viral and Other Cell-Penetrating Peptides as Vectors of Therapeutic Agents in Medicine, J. Pharmacol. Exp. Ther. 354 (2015) 32–42. doi:10.1124/jpet.115.223305.

[112] D. Cai, W. Gao, B. He, W. Dai, H. Zhang, X. Wang, J. Wang, X. Zhang, Q. Zhang, Hydrophobic penetrating peptide PFVYLI-modified stealth liposomes for doxorubicin delivery in breast cancer therapy, Biomaterials. 35 (2014) 2283–2294. doi:10.1016/j.biomaterials.2013.11.088.

[113] J.A. Gomez, J. Chen, J. Ngo, D. Hajkova, I.J. Yeh, V. Gama, M. Miyagi, S. Matsuyama, Cell-penetrating penta-peptides (CPP5s): Measurement of cell entry and protein-transduction activity, Pharmaceuticals. 3 (2010) 3594–3613. doi:10.3390/ph3123594.

[114] H.M. Moulton, M.H. Nelson, S.A. Hatlevig, M.T. Reddy, P.L. Iversen, Cellular Uptake of Antisense Morpholino Oligomers Conjugated to Arginine-Rich Peptides, Bioconjug. Chem. 15 (2004) 290–299. doi:10.1021/bc034221g.

[115] H. Kyung, H. Kim, H. Lee, S.J. Lee, Enhanced intracellular delivery of macromolecules by melittin derivatives mediated cellular uptake, J. Ind. Eng. Chem. 58 (2018) 290–295. doi:10.1016/j.jiec.2017.09.039.

[116] I.O. Akdag, E. Ozkirimli, The uptake mechanism of the cell-penetrating pVEC peptide, J. Chem. 2013 (2013). doi:10.1155/2013/851915.

[117] B.R. Liu, S.Y. Lo, C.C. Liu, C.L. Chyan, Y.W. Huang, R.S. Aronstam, H.J. Lee, Endocytic Trafficking of Nanoparticles Delivered by Cell-penetrating Peptides Comprised of Nona-arginine and a Penetration Accelerating Sequence, PLoS One. 8 (2013) 1–12. doi:10.1371/journal.pone.0067100.

[118] A. Manceur, A. Wu, J. Audet, Flow cytometric screening of cell-penetrating peptides for their uptake into embryonic and adult stem cells, Anal. Biochem. 364 (2007) 51–59. doi:10.1016/j.ab.2007.02.015.

[119] M. Rhee, P. Davis, Mechanism of uptake of C105Y, a novel cell-penetrating peptide, J. Biol. Chem. 281 (2006) 1233–1240. doi:10.1074/jbc.M509813200.

[120] X. Wang, X. Chen, X. Yang, W. Gao, B. He, W. Dai, H. Zhang, X. Wang, J. Wang, X. Zhang, Z. Dai, Q. Zhang, A nanomedicine based combination therapy based on QLPVM peptide functionalized liposomal tamoxifen and doxorubicin against Luminal A breast cancer, Nanomedicine Nanotechnology, Biol. Med. 12 (2016) 387–397. doi:10.1016/j.nano.2015.12.360.

[121] G. Dom, C. Shaw-Jackson, C. Matis, O. Bouffioux, J.J. Picard, A. Prochiantz, M.P. Mingeot-Leclerq, R. Brasseur, R. Rezsohazy, Cellular uptake of Antennapedia Penetratin peptides is a two-step process in which phase transfer precedes a tryptophan-dependent translocation, Nucleic Acids Res. 31 (2003) 556–561. doi:10.1093/nar/gkg160.

[122] X. Wu, W. Gehring, Cellular uptake of the Antennapedia homeodomain polypeptide by macropinocytosis, Biochem. Biophys. Res. Commun. 443 (2014) 1136–1140. doi:10.1016/j.bbrc.2013.12.062.

[123] S. Console, C. Marty, C. García-Echeverría, R. Schwendener, K. Ballmer-Hofer, Antennapedia and HIV transactivator of transcription (TAT) “protein transduction domains” promote endocytosis of high molecular weight cargo upon binding to cell surface glycosaminoglycans, J. Biol. Chem. 278 (2003) 35109–35114. doi:10.1074/jbc.M301726200.

[124] A. Joliot, C. Pernelle, H. Deagostini-Bazin, A. Prochiantz, Antennapedia homeobox peptide regulates neural morphogenesis., Proc. Natl. Acad. Sci. 88 (1991) 1864–1868. doi:10.1073/pnas.88.5.1864.

[125] I. Le Roux, a H. Joliot, E. Bloch-Gallego, a Prochiantz, M. Volovitch, Neurotrophic activity of the Antennapedia homeodomain depends on its specific DNA-binding properties., Proc. Natl. Acad. Sci. U. S. A. 90 (1993) 9120–9124. doi:10.1073/pnas.90.19.9120.

[126] G.G. Chikh, S. Kong, M.B. Bally, J.C. Meunier, M.P. Schutze-Redelmeier, Efficient delivery of Antennapedia homeodomain fused to CTL epitope with liposomes into dendritic cells results in the activation of CD8+ T cells., J. Immunol. 167 (2001) 6462–70. doi:10.4049/jimmunol.167.11.6462.

[127] C. Marty, C. Meylan, H. Schott, K. Ballmer-Hofer, R.A. Schwendener, Enhanced heparan sulfate proteoglycan-mediated uptake of cell-penetrating peptide-modified liposomes, C. Cell. Mol. Life Sci. 61 (2004) 1785–1794. doi:10.1007/s00018-004-4166-0.

[128] S. Qian, W.T. Heller, Melittin-induced cholesterol reorganization in lipid bilayer membranes, Biochim. Biophys. Acta - Biomembr. 1848 (2015) 2253–2260. doi:10.1016/j.bbamem.2015.06.012.

[129] A. Pino-Angeles, T. Lazaridis, Effects of Peptide Charge, Orientation, and Concentration on Melittin Transmembrane Pores, Biophys. J. 114 (2018) 2865–2874. doi:10.1016/j.bpj.2018.05.006.

[130] A. Lundquist, P. Wessman, A.R. Rennie, K. Edwards, Melittin-Lipid interaction: A comparative study using liposomes, micelles and bilayerdisks, Biochim. Biophys. Acta - Biomembr. 1778 (2008) 2210–2216. doi:10.1016/j.bbamem.2008.05.009.

[131] S. Stalmans, N. Bracke, E. Wynendaele, B. Gevaert, K. Peremans, C. Burvenich, I. Polis, B. De Spiegeleer, Cell-penetrating peptides selectively cross the blood-brain barrier in vivo, PLoS One. 10 (2015) 1–22. doi:10.1371/journal.pone.0139652.

[132] M.J. Simon, S. Gao, W.H. Kang, S. Banta, B. Morrison, TAT-mediated intracellular protein delivery to primary brain cells is dependent on glycosaminoglycan expression, Biotechnol. Bioeng. 104 (2009) 10–19. doi:10.1002/bit.22377.

[133] J.P. Richard, K. Melikov, H. Brooks, P. Prevot, B. Lebleu, L. V. Chernomordik, Cellular uptake of unconjugated TAT peptide involves clathrin-dependent endocytosis and heparan sulfate receptors, J. Biol. Chem. 280 (2005) 15300–15306. doi:10.1074/jbc.M401604200.

[134] M. Malhotra, C. Tomaro-Duchesneau, S. Prakash, Synthesis of TAT peptide-tagged PEGylated chitosan nanoparticles for siRNA delivery targeting neurodegenerative diseases, Biomaterials. 34 (2013) 1270–1280. doi:10.1016/j.biomaterials.2012.10.013.

[135] Y. Qin, H. Chen, W. Yuan, R. Kuai, Q. Zhang, F. Xie, L. Zhang, Z. Zhang, J. Liu, Q. He, Liposome formulated with TAT-modified cholesterol for enhancing the brain delivery, Int. J. Pharm. 419 (2011) 85–95. doi:10.1016/j.ijpharm.2011.07.021.

[136] K. Melikov, A. Hara, K. Yamoah, E. Zaitseva, E. Zaitsev, L. V. Chernomordik, Efficient entry of cell-penetrating peptide nona-arginine into adherent cells involves a transient

increase in intracellular calcium, Biochem. J. 471 (2015) 221–230. doi:10.1042/BJ20150272.

[137] C. de Coupade, A. Fittipaldi, V. Chagnas, M. Michel, S. Carlier, E. Tasciotti, A. Darmon, D. Ravel, J. Kearsey, M. Giacca, F. Cailler, Novel human-derived cell-penetrating peptides for specific subcellular delivery of therapeutic biomolecules, Biochem. J. 390 (2005) 407–418. doi:10.1042/bj20050401.

[138] G. Tünnemann, G. Ter-Avetisyan, R.M. Martin, M. Stöckl, A. Herrmann, M.C. Cardoso, Live-cell analysis of cell penetration ability and toxicity of oligo-arginines, J. Pept. Sci. 14 (2008) 469–476. doi:10.1002/psc.968.

[139] B.W. Neuman, D. a Stein, A.D. Kroeker, A.D. Paulino, H.M. Moulton, P.L. Iversen, M.J. Buchmeier, Antisense morpholino-oligomers directed against the 5' end of the genome inhibit coronavirus proliferation and growth., J. Virol. 78 (2004) 5891–5899. doi:10.1128/JVI.78.11.5891-5899.2004.

[140] S. Futaki, W. Ohashi, T. Suzuki, M. Niwa, S. Tanaka, K. Ueda, H. Harashima, Y. Sugiura, Stearylated arginine-rich peptides: A new class of transfection systems, Bioconjug. Chem. 12 (2001) 1005–1011. doi:10.1021/bc015508l.

[141] K. Takayama, H. Hirose, G. Tanaka, S. Pujals, S. Katayama, I. Nakase, S. Futaki, Effect of the attachment of a penetration accelerating sequence and the influence of hydrophobicity on octaarginine-mediated intracellular delivery, Mol. Pharm. 9 (2012) 1222–1230. doi:10.1021/mp200518n.

[142] K. Takayama, I. Nakase, H. Michiue, T. Takeuchi, K. Tomizawa, H. Matsui, S. Futaki, Enhanced intracellular delivery using arginine-rich peptides by the addition of penetration

accelerating sequences (Pas), J. Control. Release. 138 (2009) 128–133. doi:10.1016/j.jconrel.2009.05.019.

[143] Y.Z. Lin, S.Y. Yao, J. Hawiger, Role of the nuclear localization sequence in fibroblast growth factor-1-stimulated mitogenic pathways, J. Biol. Chem. 271 (1996) 5305–5308. doi:10.1074/jbc.271.10.5305.

[144] P. Ruzza, B. Biondi, A. Marchiani, N. Antolini, A. Calderan, Cell-penetrating peptides: A comparative study on lipid affinity and cargo delivery properties, Pharmaceuticals. 3 (2010) 1045–1062. doi:10.3390/ph3041045.

[145] A. Bolhassani, B.S. Jafarzade, G. Mardani, In vitro and in vivo delivery of therapeutic proteins using cell penetrating peptides, Peptides. 87 (2017) 50–63. doi:10.1016/j.peptides.2016.11.011.

[146] A. Upadhya, P.C. Sangave, Hydrophobic and electrostatic interactions between cell penetrating peptides and plasmid DNA are important for stable non-covalent complexation and intracellular delivery, J. Pept. Sci. 2 (2016) 647–659. doi:10.1002/psc.2927.

[147] Y.Z. Lin, S. Yao, R.A. Veach, T.R. Torgerson, J. Hawiger, Inhibition of nuclear translocation of transcription factor NF-??B by a synthetic peptide containing a cell membrane-permeable motif and nuclear localization sequence, J. Biol. Chem. 270 (1995) 14255–14258. doi:10.1074/jbc.270.24.14255.

[148] M. Khanna, A. Moutal, L. FranÃ§ois-Moutal, R. Khanna, J.M. Brittain, Differential neuroprotective potential of CRMP2 peptide aptamers conjugated to cationic, hydrophobic, and amphipathic cell penetrating peptides, Front. Cell. Neurosci. 8 (2015) 1–15. doi:10.3389/fncel.2014.00471.

[149] Q. Zhang, J. Wang, H. Zhang, D. Liu, L. Ming, L. Liu, Y. Dong, B. Jian, D. Cai, The anticancer efficacy of paclitaxel liposomes modified with low-toxicity hydrophobic cell-penetrating peptides in breast cancer: An: in vitro and in vivo evaluation, RSC Adv. 8 (2018) 24084–24093. doi:10.1039/c8ra03607a.

[150] A.G. Ziady, J.C. Perales, T. Ferkol, T. Gerken, H. Beegen, D.H. Perlmutter, P.B. Davis, Gene transfer into hepatoma cell lines via the serpin enzyme complex receptor, Am. J. Physiol. Liver Physiol. 273 (2017) G545–G552. doi:10.1152/ajpgi.1997.273.2.g545.

[151] G. Joslin, G.L. Griffin, A.M. August, S. Adams, R.J. Fallon, R.M. Senior, D.H. Perlmutter, The serpin-enzyme complex (SEC) receptor mediates the neutrophil chemotactic effect of alpha-1 antitrypsin-elastase complexes and amyloid-beta peptide., J. Clin. Invest. 90 (1992) 1150–4. doi:10.1172/JCI115934.

[152] J.A. Gomez, V. Gama, T. Yoshida, W. Sun, P. Hayes, K. Leskov, D. Boothman, S. Matsuyama, Bax-inhibiting peptides derived from Ku70 and cell-penetrating pentapeptides, Biochem. Soc. Trans. 35 (2007) 797–801. doi:10.1042/BST0350797.

[153] T. Yoshida, I. Tomioka, T. Nagahara, T. Holyst, M. Sawada, P. Hayes, V. Gama, M. Okuno, Y. Chen, Y. Abe, T. Kanouchi, H. Sasada, D. Wang, T. Yokota, E. Sato, S. Matsuyama, Bax-inhibiting peptide derived from mouse and rat Ku70, Biochem. Biophys. Res. Commun. 321 (2004) 961–966. doi:10.1016/j.bbrc.2004.07.054.

[154] P. Kumar, H. Wu, J.L. McBride, K.E. Jung, M. Hee Kim, B.L. Davidson, S. Kyung Lee, P. Shankar, N. Manjunath, Transvascular delivery of small interfering RNA to the central nervous system, Nature. 448 (2007) 39–43. doi:10.1038/nature05901.

[155] L. Xiang, R. Zhou, A. Fu, X. Xu, Y. Huang, C. Hu, Targeted delivery of large fusion protein into hippocampal neurons by systemic administration, J. Drug Target. 19 (2011) 632–636. doi:10.3109/1061186X.2010.523788.

[156] R. Huey, S. Hawthorne, P. McCarron, The potential use of rabies virus glycoprotein-derived peptides to facilitate drug delivery into the central nervous system: a mini review, J. Drug Target. 25 (2017) 379–385. doi:10.1080/1061186X.2016.1223676.

[157] Y. Liu, R. Huang, L. Han, W. Ke, K. Shao, L. Ye, J. Lou, C. Jiang, Brain-targeting gene delivery and cellular internalization mechanisms for modified rabies virus glycoprotein RVG29 nanoparticles, Biomaterials. 30 (2009) 4195–4202. doi:10.1016/j.biomaterials.2009.02.051.

[158] S. Son, D.W. Hwang, K. Singha, J.H. Jeong, T.G. Park, D.S. Lee, W.J. Kim, RVG peptide tethered bioreducible polyethylenimine for gene delivery to brain, J. Control. Release. 155 (2011) 18–25. doi:10.1016/j.jconrel.2010.08.011.

[159] J.Y. Kim, W. Il Choi, Y.H. Kim, G. Tae, Brain-targeted delivery of protein using chitosan- and RVG peptide-conjugated, pluronic-based nano-carrier, Biomaterials. 34 (2013) 1170–1178. doi:10.1016/j.biomaterials.2012.09.047.

[160] D.W. Hwang, S. Son, J. Jang, H. Youn, S. Lee, D. Lee, Y.S. Lee, J.M. Jeong, W.J. Kim, D.S. Lee, A brain-targeted rabies virus glycoprotein-disulfide linked PEI nanocarrier for delivery of neurogenic microRNA, Biomaterials. 32 (2011) 4968–4975. doi:10.1016/j.biomaterials.2011.03.047.

[161] Y. Gao, Z.Y. Wang, J. Zhang, Y. Zhang, H. Huo, T. Wang, T. Jiang, S. Wang, RVG-peptide-linked trimethylated chitosan for delivery of siRNA to the brain, Biomacromolecules. 15 (2014) 1010–1018. doi:10.1021/bm401906p.

[162] M. Qu, Q. Lin, S. He, L. Wang, Y. Fu, Z. Zhang, L. Zhang, A brain targeting functionalized liposomes of the dopamine derivative N-3,4-bis(pivaloyloxy)-dopamine for treatment of Parkinson's disease, J. Control. Release. 277 (2018) 173–182. doi:10.1016/j.jconrel.2018.03.019.

[163] M. Riley, W. Vermerris, Recent Advances in Nanomaterials for Gene Delivery—A Review, Nanomaterials. 7 (2017) 94. doi:10.3390/nano7050094.

[164] S. Nakagawa, M.A. Deli, H. Kawaguchi, T. Shimizudani, T. Shimono, Á. Kittel, K. Tanaka, M. Niwa, A new blood-brain barrier model using primary rat brain endothelial cells, pericytes and astrocytes, Neurochem. Int. 54 (2009) 253–263. doi:10.1016/j.neuint.2008.12.002.

[165] H.C. Helms, N.J. Abbott, M. Burek, R. Cecchelli, P.-O. Couraud, M.A. Deli, C. Förster, H.J. Galla, I.A. Romero, E. V Shusta, M.J. Stebbins, E. Vandenhaute, B. Weksler, B. Brodin, In vitro models of the blood–brain barrier: An overview of commonly used brain endothelial cell culture models and guidelines for their use, J. Cereb. Blood Flow Metab. 36 (2016) 862–890. doi:10.1177/0271678X16630991.

[166] B. dos Santos Rodrigues, A. Banerjee, T. Kanekiyo, J. Singh, Functionalized liposomal nanoparticles for efficient gene delivery system to neuronal cell transfection, Int. J. Pharm. 566 (2019) 717–730. doi:10.1016/j.ijpharm.2019.06.026.

[167] G. Sharma, A. Modgil, C. Sun, J. Singh, Grafting of cell-penetrating peptide to receptor-targeted liposomes improves their transfection efficiency and transport across blood-brain barrier model., J. Pharm. Sci. 101 (2012) 2468–78. doi:10.1002/jps.23152.

[168] B. Layek, J. Singh, Amino acid grafted chitosan for high performance gene delivery: Comparison of amino acid hydrophobicity on vector and polyplex characteristics, Biomacromolecules. (2013). doi:10.1021/bm301720g.

[169] K. Ciftci, R.J. Levy, Enhanced plasmid DNA transfection with lysosomotropic agents in cultured fibroblasts, Int. J. Pharm. 218 (2001) 81–92. doi:10.1016/S0378-5173(01)00623-8.

[170] B. Layek, M.K. Haldar, G. Sharma, L. Lipp, S. Mallik, J. Singh, Hexanoic acid and polyethylene glycol double grafted amphiphilic chitosan for enhanced gene delivery: Influence of hydrophobic and hydrophilic substitution degree, Mol. Pharm. 11 (2014) 982–994. doi:10.1021/mp400633r.

[171] M. Shinohara, R.C. Petersen, D.W. Dickson, G. Bu, Brain regional correlation of amyloid-β with synapses and apolipoprotein e in non-demented individuals: Potential mechanisms underlying regional vulnerability to amyloid-β accumulation, Acta Neuropathol. 125 (2013) 535–547. doi:10.1007/s00401-013-1086-9.

[172] M. Danaei, M. Dehghankhold, S. Ataei, F. Hasanzadeh Davarani, R. Javanmard, A. Dokhani, S. Khorasani, M.R. Mozafari, Impact of particle size and polydispersity index on the clinical applications of lipidic nanocarrier systems, Pharmaceutics. 10 (2018) 1–17. doi:10.3390/pharmaceutics10020057.

[173] C. Madeira, L.M.S. Loura, M.R. Aires-Barros, M. Prieto, Fluorescence methods for lipoplex characterization, Biochim. Biophys. Acta - Biomembr. 1808 (2011) 2694–2705. doi:10.1016/j.bbamem.2011.07.020.

[174] J.P. Pratt, D.J. Ravnic, H.T. Huss, X. Jiang, B.S. Orozco, S.J. Mentzer, Melittin-induced membrane permeability: A nonosmotic mechanism of cell death, Vitr. Cell. Dev. Biol. - Anim. 41 (2005) 349–355. doi:10.1007/s11626-005-0007-1.

[175] Y.J. Lee, S.J. Kang, B.M. Kim, Y.J. Kim, H.D. Woo, H.W. Chung, Cytotoxicity of honeybee (Apis mellifera) venom in normal human lymphocytes and HL-60 cells, Chem. Biol. Interact. 169 (2007) 189–197. doi:10.1016/j.cbi.2007.06.036.

[176] K. Veltman, A.J. Hendriks, A. van Wezel, K. Kettler, D. van de Meent, Cellular uptake of nanoparticles as determined by particle properties, experimental conditions, and cell type, Environ. Toxicol. Chem. 33 (2013) 481–492. doi:10.1002/etc.2470.

[177] S. Behzadi, V. Serpooshan, W. Tao, M.A. Hamaly, M.Y. Alkawareek, E.C. Dreaden, D. Brown, A.M. Alkilany, O.C. Farokhzad, M. Mahmoudi, Cellular uptake of nanoparticles: Journey inside the cell, Chem. Soc. Rev. 46 (2017) 4218–4244. doi:10.1039/c6cs00636a.

[178] M. Voinea, E. Dragomir, I. Manduteanu, M. Simionescu, Binding and uptake of transferrin-bound liposomes targeted to transferrin receptors of endothelial cells, Vascul. Pharmacol. 39 (2002) 13–20. doi:10.1016/S1537-1891(02)00165-9.

[179] S. Anabousi, U. Bakowsky, M. Schneider, H. Huwer, C.M. Lehr, C. Ehrhardt, In vitro assessment of transferrin-conjugated liposomes as drug delivery systems for inhalation therapy of lung cancer, Eur. J. Pharm. Sci. 29 (2006) 367–374. doi:10.1016/j.ejps.2006.07.004.

[180] K.B. Johnsen, A. Burkhart, F. Melander, P.J. Kempen, J.B. Vejlebo, P. Siupka, M.S. Nielsen, T.L. Andresen, T. Moos, Targeting transferrin receptors at the blood-brain barrier improves the uptake of immunoliposomes and subsequent cargo transport into the brain parenchyma, Sci. Rep. 7 (2017) 1–13. doi:10.1038/s41598-017-11220-1.

[181] C. Liu, X.N. Liu, G.L. Wang, Y. Hei, S. Meng, L.F. Yang, L. Yuan, Y. Xie, A dual-mediated liposomal drug delivery system targeting the brain: Rational construction, integrity evaluation across the blood–brain barrier, and the transporting mechanism to glioma cells, Int. J. Nanomedicine. 12 (2017) 2407–2425. doi:10.2147/IJN.S131367.

[182] Y.-L. Tseng, J.-J. Liu, R.-L. Hong, Translocation of liposomes into cancer cells by cell-penetrating peptides penetratin and tat: a kinetic and efficacy study., Mol. Pharmacol. 62 (2002) 864–72. doi:10.1124/mol.62.4.864.

[183] A. Gräslund, F. Madani, S. Lindberg, Ü. Langel, S. Futaki, Mechanisms of cellular uptake of cell-penetrating peptides, J. Biophys. 2011 (2011). doi:10.1155/2011/414729.

[184] J.M. Meissner, M. Toporkiewicz, A. Czogalla, L. Matusewicz, K. Kuliczkowski, A.F. Sikorski, Novel antisense therapeutics delivery systems: In vitro and in vivo studies of liposomes targeted with anti-CD20 antibody, J. Control. Release. 220 (2015) 515–528. doi:10.1016/j.jconrel.2015.11.015.

[185] L.L. Zou, L. Huang, R.L. Hayes, C. Black, Y.H. Qiu, J.R. Perez-Polo, W. Le, G.L. Clifton, K. Yang, Liposome-mediated NGF gene transfection following neuronal injury: potential therapeutic applications, Gene Ther. 6 (1999) 994–1005. doi:10.1038/sj.gt.3300936.

[186] P.-W. Cheng, Receptor Ligand-Facilitated Gene Transfer: Enhancement of Liposome-Mediated Gene Transfer and Expression by Transferrin, Hum. Gene Ther. 7 (1996) 275–282. doi:10.1089/hum.1996.7.3-275.

[187] M.T. Girão Da Cruz, S. Simões, M.C. Pedroso De Lima, Improving lipoplex-mediated gene transfer into C6 glioma cells and primary neurons, Exp. Neurol. 187 (2004) 65–75. doi:10.1016/j.expneurol.2003.12.013.

[188] J. Pozueta, R. Lefort, M.L. Shelanski, Synaptic changes in Alzheimer's disease and its models, Neuroscience. 251 (2013) 51–65. doi:10.1016/j.neuroscience.2012.05.050.

[189] P.L. McClean, C. Hölscher, Liraglutide can reverse memory impairment, synaptic loss and reduce plaque load in aged APP/PS1 mice, a model of Alzheimer's disease, Neuropharmacology. 76 (2014) 57–67. doi:10.1016/j.neuropharm.2013.08.005.

[190] L. Wei, S. Lv, Q. Huang, J. Wei, S. Zhang, R. Huang, Z. Lu, X. Lin, Pratensein attenuates Aβ-induced cognitive deficits in rats: Enhancement of synaptic plasticity and cholinergic function, Fitoterapia. 101 (2015) 208–217. doi:10.1016/j.fitote.2015.01.017.

[191] D. Tampellini, E. Capetillo-Zarate, M. Dumont, Z. Huang, F. Yu, M.T. Lin, G.K. Gouras, Effects of Synaptic Modulation on -Amyloid, Synaptophysin, and Memory Performance in Alzheimer's Disease Transgenic Mice, J. Neurosci. 30 (2010) 14299–14304. doi:10.1523/jneurosci.3383-10.2010.

[192] C.-I. SZE, J.C. TRONCOSO, C. KAWAS, P. MOUTION, D.L. PRICE, L.J. MARTIN, Loss of the Presynaptic Vesicle Protein Synaptophysin in Hippocampus Correlates with Cognitive Decline in Alzheimer Disease, J. Neuropathol. Exp. Neurol. 56 (1997) 933–944. doi:10.1097/00005072-199708000-00011.

[193] K. Hatherell, P.O. Couraud, I.A. Romero, B. Weksler, G.J. Pilkington, Development of a three-dimensional, all-human in vitro model of the blood-brain barrier using mono-, co-, and tri-cultivation Transwell models, J. Neurosci. Methods. 199 (2011) 223–229. doi:10.1016/j.jneumeth.2011.05.012.

[194] I. Wilhelm, I.A. Krizbai, In vitro models of the blood-brain barrier for the study of drug delivery to the brain, Mol. Pharm. 11 (2014) 1949–1963. doi:10.1021/mp500046f.

[195] J.F. Popplewell, M.J. Swann, N.J. Freeman, C. McDonnell, R.C. Ford, Quantifying the effects of melittin on liposomes, Biochim. Biophys. Acta - Biomembr. 1768 (2007) 13–20. doi:10.1016/j.bbamem.2006.05.016.

[196] S.F. 1. B.T.M. Committee F04 Medical and Surgical Materials and Devices, Standard practice for assessment of hemolytic properties of materials., Annu. B. ASTM Stand. (2009) 1–5.

[197] E. Hudry, J. Dashkoff, A.D. Roe, S. Takeda, R.M. Koffie, T. Hashimoto, M. Scheel, T. Spires-Jones, M. Arbel-Ornath, R. Betensky, B.L. Davidson, B.T. Hyman, Gene Transfer of Human Apoe Isoforms Results in Differential Modulation of Amyloid Deposition and Neurotoxicity in Mouse Brain, Sci. Transl. Med. 5 (2013) 212ra161-212ra161. doi:10.1126/scitranslmed.3007000.

[198] J.-C. Dodart, R.A. Marr, M. Koistinaho, B.M. Gregersen, S. Malkani, I.M. Verma, S.M. Paul, Gene delivery of human apolipoprotein E alters brain Abeta burden in a mouse model of Alzheimer's disease., Proc. Natl. Acad. Sci. U. S. A. 102 (2005) 1211–6. doi:10.1073/pnas.0409072102.

[199] J. Hu, C.C. Liu, X.F. Chen, Y.W. Zhang, H. Xu, G. Bu, Opposing effects of viral mediated brain expression of apolipoprotein E2 (apoE2) and apoE4 on apoE lipidation and Aβ metabolism in apoE4-targeted replacement mice, Mol. Neurodegener. 10 (2015) 1–11. doi:10.1186/s13024-015-0001-3.

[200] K.B. Knudsen, H. Northeved, E.K. Pramod Kumar, A. Permin, T. Gjetting, T.L. Andresen, S. Larsen, K.M. Wegener, J. Lykkesfeldt, K. Jantzen, S. Loft, P. Møller, M. Roursgaard, In vivo toxicity of cationic micelles and liposomes, Nanomedicine Nanotechnology, Biol. Med. 11 (2015) 467–477. doi:10.1016/j.nano.2014.08.004.

[201] H.H.J. Gerets, E. Hanon, M. Cornet, S. Dhalluin, O. Depelchin, M. Canning, F.A. Atienzar, Selection of cytotoxicity markers for the screening of new chemical entities in a pharmaceutical context: A preliminary study using a multiplexing approach, Toxicol. Vitr. 23 (2009) 319–332. doi:10.1016/j.tiv.2008.11.012.

[202] S. Campion, J. Aubrecht, K. Boekelheide, D.W. Brewster, V.S. Vaidya, L. Anderson, D. Burt, E. Dere, K. Hwang, S. Pacheco, J. Saikumar, S. Schomaker, M. Sigman, F. Goodsaid, The current status of biomarkers for predicting toxicity., Expert Opin. Drug Metab. Toxicol. 9 (2013) 1391–408. doi:10.1517/17425255.2013.827170.

[203] N.J. Siddiqi, M.A.K. Abdelhalim, A.K. El-Ansary, A.S. Alhomida, W.Y. Ong, Identification of potential biomarkers of gold nanoparticle toxicity in rat brains, J. Neuroinflammation. 9 (2012) 656. doi:10.1186/1742-2094-9-123.

[204] K. Kawata, C.Y. Liu, S.F. Merkel, S.H. Ramirez, T. Ryan, D. Langford, L. Angeles, Neurosci Biobeha HHS Public Access Author manuscript Published in final edited form as: Blood biomarkers for brain injury: What are we measuring?, Neurosci. Biobehav. Rev. 68 (2016) 460–473. doi:10.1016/j.neubiorev.2016.05.009.Blood.

[205] T. Qiu, Q. Liu, Y.X. Chen, Y.F. Zhao, Y.M. Li, Aβ42 and Aβ40: similarities and differences, J. Pept. Sci. 21 (2015) 522–529. doi:10.1002/psc.2789.

[206] R.D. Terry, E. Masliah, D.P. Salmon, N. Butters, R. DeTeresa, R. Hill, L.A. Hansen, R. Katzman, Physical basis of cognitive alterations in alzheimer's disease: Synapse loss is the major correlate of cognitive impairment, Ann. Neurol. 30 (1991) 572–580. doi:10.1002/ana.410300410.

[207] G.K. Gouras, D. Tampellini, R.H. Takahashi, E. Capetillo-Zarate, Intraneuronal β-amyloid accumulation and synapse pathology in Alzheimer's disease, Acta Neuropathol. 119 (2010) 523–541. doi:10.1007/s00401-010-0679-9.

[208] E. Masliah, M. Mallory, M. Alford, R. DeTeresa, L.A. Hansen, D.W. McKeel, J.C. Morris, Altered expression of synaptic proteins occurs early during progression of Alzheimer's disease., Neurology. 56 (2001) 127–9. doi:10.1212/wnl.56.1.127.

[209] A. Savioz, G. Leuba, P.G. Vallet, A framework to understand the variations of PSD-95 expression in brain aging and in Alzheimer's disease, Ageing Res. Rev. 18 (2014) 86–94. doi:10.1016/j.arr.2014.09.004.

[210] A.L. Markowska, D. Price, V.E. Koliatsos, Selective effects of nerve growth factor on spatial recent memory as assessed by a delayed nonmatching-to-position task in the water maze., J. Neurosci. 16 (1996) 3541–8. doi:10.1523/JNEUROSCI.16-10-03541.1996.

[211] M.N. Castel-Barthe, F. Jazat-Poindessous, P. Barneoud, E. Vigne, F. Revah, J. Mallet, Y. Lamour, Direct intracerebral nerve growth factor gene transfer using a recombinant adenovirus: Effect on basal forebrain cholinergic neurons during aging, Neurobiol. Dis. 3 (1996) 76–86. doi:10.1006/nbdi.1996.0008.

[212] C.E. Dixon, P. Flinn, J. Bao, R. Venya, R.L. Hayes, Nerve Growth Factor Attenuates Cholinergic Deficits Following Traumatic Brain Injury in Rats, Exp. Neurol. 146 (1997) 479–490. doi:10.1006/exnr.1997.6557.